THE BIOCHEMISTRY OF SIDEROPHORE BIOSYNTHESIS

By

©2007
Kathleen M. Meneely

B.S., University of Kansas, 1999

Submitted to the Department of Molecular Biosciences and the
Faculty of the Graduate School of the University of Kansas
In partial fulfillment of the requirements for the degree of
Doctor of Philosophy

Chairperson – Audrey Lamb

Committee members: Kristi Neufeld

Bill Picking

Mark Richter

Emily Scott

Date defended: 11/14/2007

The Dissertation Committee for Kathleen Meneely certifies
that this is the approved version of the following dissertation:

THE BIOCHEMISTRY OF SIDEROPHORE BIOSYNTHESIS

Committee:

Chairperson – Audrey Lamb

Kristi Neufeld

Bill Picking

Mark Richter

Emily Scott

Date approved: 12/3/2007

Abstract

Pathogenic bacteria are becoming increasingly antibiotic resistant. For this reason, the development of novel antibiotics is extremely important. A potential new target for antimicrobial drugs is the production of siderophores. *Pseudomonas aeruginosa* produces two siderophores under iron-limiting conditions, pyoverdin and pyochelin. Pyoverdin contains ornithine derivatives as part of the peptide backbone important for iron chelation. PvdA, an ornithine hydroxylase, performs the first step in derivation of the ornithine followed with formylation by PvdF, a formyl transferase.

Biochemical characterization of PvdA reveals that PvdA is specific for the coenzymes, FAD and NADPH, as well as for the substrate, L-ornithine. The enzyme follows Michaelis-Menten kinetics measuring NADPH oxidation, but substrate inhibition is detected when measuring the formation of hydroxylated product. Lysine is determined as a nonsubstrate effector and mixed inhibitor of PvdA with respect to ornithine. Chloride is a competitive inhibitor of the enzyme in relation to NADPH while a mixed inhibitor with respect to substrate. A mercurial compound, *p*-chloromercuribenzoate, is also a mixed inhibitor in relation to substrate. Steady state experiments reveal a ternary complex of PvdA:FAD with NADPH and ornithine during catalysis.

PvdA was further characterized with transient state kinetics to develop a catalytic mechanism. The flavin in complex with PvdA can be reduced in the absence of substrate. Oxidation of the reduced flavin in the presence of substrate

indicates the formation of two transient intermediates, hydroperoxyflavin and hydroxyflavin. However, in the absence of substrate, only the hydroxyflavin intermediate is detected and oxidation of the flavin is not through the production of hydrogen peroxide. A biochemical comparison of PvdA to two homologues, *para*-hydroxybenzoate hydroxylase (PHBH from *Pseudomonas fluorescens*) and flavin-containing monooxygenases (FMOs from *Schizosaccharomyces pombe* and hog liver microsomes) indicates that PvdA proceeds by a novel reaction mechanism.

Structural characterization of PvdA and PvdF by x-ray crystallography is underway. Crystallization studies of the NADPH reductases involved in the synthesis of pyochelin from *P. aeruginosa* (PchG) and yersiniabactin from *Yersinia enterocolitica* (Irp3) are also being performed. The structures of these enzymes are a first step towards the rational design of new inhibitors for use as new antimicrobial agents.

Acknowledgements

I would like to thank all of the people who helped in my graduate career. I would like to acknowledge Dr. J. Martin Bollinger and Eric Barr for their help with the transient-state kinetics presented in Chapter 3. Thank you to Dr. Bruce Palfey for all of the informative discussions and to Dr. Christopher Walsh for the original *pchG-His*$_6$ plasmid used in Chapter 4. I would like to acknowledge all of the undergraduate students that helped with crystallization; Heidi Hepp, Ron Nguyen, Katie Ault, Tony Swatek, Stuart Ashley, Ellen Stolle, and Jon Korte. Daniel Shippy was also a great help by beginning work on the PvdA project. I would like to thank all of the past and present members of the Lamb lab, Andy Haith, Qianyi Luo, Dr. Lena Zaitseva, and Jingping Lu.

I would especially like to thank Dr. T. Christopher Gamblin for the use of his equipment. I would like to acknowledge the Protein Structure Laboratory at the University of Kansas for native Irp3 x-ray data collection. A special thank you to the NIH Dynamic Aspects of Chemical Biology training grant for funding.

Thank you to all of my committee members and especially to Drs. Mark Richter and Emily Scott who served as readers. Finally, a special thank you to my advisor, Dr. Audrey Lamb, for her continuous support and guidance through my graduate career.

Table of Contents

	Page
Abstract	iii
Acknowledgements	v
List of Figures	ix
List of Tables	xi
Chapter 1. Introduction	1
A. Bacterial pathogens	1
B. Current antimicrobials	3
C. Iron utilization	4
D. Ferrous iron uptake	5
E. Heme utilization	7
F. Uptake of iron from iron-binding proteins	7
G. Production of siderophores	8
1. Siderophore regulation	9
2. Siderophore secretion	12
H. Ferric-siderophore uptake	12
I. Classes of siderophores	14
1. Hydroxymate siderophores	14
2. Phenol-catecholate siderophores	18
3. Other Classes of Siderophores	20
J. Siderophore Biosynthesis	21
1. Pyoverdin biosynthesis	25
2. Pyochelin Biosynthesis	27
3. Yersiniabactin Biosynthesis	29
K. Siderophore Biosynthesis Implications for Drug Discovery	33
L. References	34
Chapter 2. Biochemical Characterization of PvdA, the Ornithine Hydroxylase of *Pseudomonas aeruginosa*	45
A. Introduction	45
B. Materials and Methods	48
1. Cloning of PvdA	48
2. PvdA Protein Overproduction and Purification	48
3. Oligomerization Studies	49
4. NADPH Oxidation Assay	50
5. Hydroxylation Assay	50
6. Determination of Enzyme Specificity and Kinetic Parameters	51
7. Determination of FAD Dissociation Constant	52
8. Steady-State Kinetics	52
9. Inhibition Assays	53
10. PvdA Flavin Reduction and Reoxidation	53
C. Results	54
1. PvdA Protein Production and Purification	54

        2. Oligomerization Studies 54
        3. pH Optimum for Catalytic Activity 56
        4. Coenzyme Specificity 56
        5. FAD Dissociation Constant 56
        6. Flavin Re-oxidation 60
        7. Substrate Specificity 60
        8. Determination of Kinetic Constants 63
        9. Ternary Complex Formation 63
        10. Lysine Inhibition 63
        11. Chloride Inhibition 67
        12. Mercurial Inhibition 67
    D. Discussion 72
    E. References 80
Chapter 3. Determination of the PvdA Reaction Mechanism by Stopped-Flow Techniques 83
    A. Introduction 83
    B. Materials and Methods 87
        1. PvdA Purification 87
        2. Stopped-Flow Experiments 87
        3. PvdA Reduction Experiments 87
        4. PvdA Oxidation Experiments 88
        5. NADPH Oxidation Studies 88
        6. Hydrogen Peroxide Formation Assay 88
        7. Data Analysis 89
    C. Results 89
        1. PvdA Flavin Reduction 89
        2. FAD Binding Rate 91
        3. PvdA Flavin Oxidation with Ornithine 91
        4. PvdA Oxidation in the Absence of Ornithine 99
        5. Hydrogen Peroxide Formation in PvdA 101
    D. Discussion 105
    E. References 110
Chapter 4. Siderophore Biosynthetic Protein Purification, Crystallization, and X-ray Diffraction Collection 111
    A. Introduction 111
    B. Materials and Methods 122
        1. Standard Cloning Procedure 122
        2. Site-Directed Mutagenesis 122
        3. Cloning of the genes of interest 124
        4. Over-production of Cloned Proteins 126
        5. General Purification Procedures 129
        6. Buffer Optimization for Proteins 134
        7. Limited Proteolysis of PchG-His$_6$ 142
        8. Standard Crystallization Procedure 142

        9. Standard Crystal Optimization 147
        10. Data Collection of Irp3 Crystals 147
        11. Phasing of Irp3 150
    C. Results and Discussion 153
        1. PvdA 153
        2. PvdF 156
            a. PvdF-throm-His$_6$ 156
            b. PvdF-throm 157
            c. PvdF 159
        3. PchG 162
            a. PchG-His$_6$ 162
            b. PchG 164
            c. PchG-throm-His$_6$ 165
            d. PchG-throm 166
            e. ss-PchG 166
            f. PchG-Intein 167
        4. Irp3 168
    D. Conclusions 174
    E. References 178
Chapter 5. Conclusion 180
    A. References 191

List of Figures

Figure **Page**

1-1. Model for iron acquisition in gram-negative bacteria 6
1-2. Mechanism of Fur repression in *P. aeruginosa* 10
1-3. Representative siderophores 15
1-4. Pyoverdin Classes 17
1-5. Pyoverdin Biosynthesis 22
1-6. Pychelin Biosynthesis 28
1-7. Yersiniabactin Biosynthesis 31
2-1. Reaction schemes for the ornithine hydroxylase (PvdA) from *P. aeruginosa*, the lysine hydroxylase (IucD) from *E. coli*, *p*-hydroxybenzoate hydroxylase (PHBH) from *P. fluorescens*, and flavin-containing monooxygenase (FMO) from hog liver microsomes 46
2-2. Hydrodynamic radii for PvdA in 25 mM Tris-HCl, pH 8.0, 500 mM NaCl, 300 mM imidazole or 100 mM potassium phosphate, pH 8.0, and 100 mM sodium citrate as determined by dynamic light scattering 55
2-3. Effect of pH on PvdA activity 57
2-4. PvdA coenzyme specificity 59
2-5. Flavin reoxidation as a function of time 61
2-6. PvdA substrate specificity 62
2-7. Kinetic analysis of PvdA as determined by NADPH oxidation and hydroxyornithine production 64
2-8. Ternary complex formation of FAD loaded PvdA with NADPH and ornithine 66
2-9. Mixed inhibition of PvdA by L-lysine as determined by the hydroxylation assay 68
2-10. Effect of NaCl on PvdA activity 69
2-11. Inhibition of PvdA by chloride as determined by the NADPH oxidation assay 70
2-12. Mixed inhibition of PvdA by *p*-chloromercuibenzoate (PCMB) as determined by the NADPH oxidation assay 71
2-13. PvdA biochemical characterization in comparison to the functional homologues; PHBH from *P. fluorescens*, IucD from *E. coli*, and FMO from hog liver microsomes 78
3-1. Common flavin oxidation states of hydroxylase enzymes including PHBH and FMO 84
3-2. The reaction mechanisms for p-hydroxybenzoate hydroxylase (PHBH) and flavin monooxygenase (FMO) 86
3-3. Flavin reduction in PvdA 90
3-4. The binding of flavin to PvdA monitored as an increase in fluorescence 93
3-5. Flavin oxidation in PvdA in the presence of substrate 95
3-6. Oxygen dependence for the formation of hydroperoxyflavin in PvdA 97

3-7. PvdA excitation scan monitoring fluorescence above 515 nm 98
3-8. Flavin oxidation in PvdA in the absence of substrate 100
3-9. Oxygen dependence of the intermediate formation in PvdA in the absence of substrate 102
3-10. PvdA NADPH oxidation and hydrogen peroxide formation in the presence and absence of substrates 103
3-11. PvdA reaction mechanism 108
4-1. Crystallization vapor diffusion drop geometries in sealed wells using a 1:1 ratio of protein to precipitant solution suspended above a well of precipitant solution 113
4-2. Optional crystal optimization techniques 116
4-3. PvdA Buffer Optimization Screen 155
4-4. PvdF crystal images 158
4-5. Irp3 protein crystals grown with PEG 8000, PEG 10,000, and PEG 20,000 as the precipitant 170
4-6. Irp3 crystal diffraction image 172
5-1. Proteins containing sequence homology to PvdA, *p*-hydroxybenzoate hydroxylase (PHBH) from *Pseudomonas fluorescens* (PDB number 1PBE) and flavin monooxygenase (FMO) from *Schizosaccharomyces pombe* (PDB number 1VQW) 182
5-2. Structure and binding motif based sequence alignment of PvdA with IucD (*E. coli*) and PHBH (*P. fluorescens*, PDB accession code: 1PBE) 185
5-3. The structure of the PvdF homologue glycinamide ribonucleotide transformylase (GART) from *Escherichia coli* (PDB number 1CDE) 188

List of Tables

Table **Page**

2-1. Summary of the PvdA Coenzymes and Substrate Specificities 58
2-2. Summary of the PvdA Kinetic Parameters 65
3-1. PvdA flavin reduction rate constants 92
3-2. FAD binding rate to PvdA 94
3-3. PvdA hydrogen peroxide formation after 45 seconds 104
4-1. Cloning primers 123
4-2. Protein over-production procedures 127
4-3. ss-PchG-His$_6$ over-production procedures 128
4-4A. PvdA, PvdF, PchG-His$_6$, and PchG-throm-His$_6$ protein purification procedures 130
4-4B. PchG protein purification procedures 131
4-4C. PchG-throm and Irp3 protein purification procedures 132
4-5A. PvdA initial buffer screen for solubility 135
4-5B. PvdA final buffer screens for solubility 136
4-5C. PvdF-throm-His$_6$ Protein buffer screen for solubility 137
4-5D. PvdF-throm and PvdF buffer screen for solubility 138
4-5E. PchG-His$_6$ buffer screen for solubility 139
4-5F. PchG-throm-His$_6$ and PchG-throm buffer screen for solubility 140
4-5G. Irp3 buffer screen for solubility 141
4-6A. PvdA crystallization screens 143
4-6B. PvdF-throm-His$_6$ crystallization screens 144
4-6C. PvdF-throm crystallization screens 145
4-6D. PvdF, PchG, and Irp3 crystallization screens 146
4-7. Crystal Optimization 148
4-8. Crystallization Additives 149
4-9. Irp3 Data Collection Statistics 151
4-10. Heavy metals used for Irp3 MIR studies 152
4-11. Crystal conditions which formed PvdF needles and plates 160
4-12. Irp3 Optimal Crystallization Conditions 169
4-13. Irp3 heavy metal diffraction collection for MIR phasing 175
4-14. Current progress made on siderophore biosynthetic proteins 176

Chapter 1

Introduction

Bacterial pathogens

Bacteria with the ability to cause infections in host organisms such as humans, other animals, or plants are considered bacterial pathogens. This thesis will concentrate on three pathogens, *Pseudomonas aeruginosa*, *Yersinia pestis*, and *Yersinia enterocolitica,* which cause a variety of diseases in humans.

P. aeruginosa is an opportunistic pathogen, which does not normally infect healthy individuals but can cause serious infections in immunocompromised individuals. *P. aeruginosa* can cause a variety of infections from bacteremia or sepsis to cardiovascular infections, respiratory infections and meningitis (*1*). Less severe infections include bone, joint, eye, ear, gastrointestinal, and urinary infections. Secondary infections by *P. aeruginosa* have been reported in AIDS patient, burn victims, and individuals with cystic fibrosis. Cystic fibrosis is an inheritable genetic disorder of the mucosal membranes causing thick mucus, which affects 30,000 children and adults in the United States and 70,000 individuals worldwide (*2*). The median life expectancy for cystic fibrosis patients as of 2006 is 37 years. The leading cause of death of patients with cystic fibrosis is secondary bacterial infections in the lungs primarily by *P. aeruginosa* and *Burkholderia cenocepacia*.

According to the Center for Disease Control, in 2002 there were a reported 1.7 million nosocomial-acquired infections with 99,000 associated deaths (*3*). Many of these infections were caused by *P. aeruginosa*. Infections by *P. aeruginosa* are associated with high mortality. Death from pneumonia typically occurs 3 – 4 days after the onset of initial symptoms and bacteremia has a greater than 50% mortality rate, higher than bacteremia infections by other gram-negative bacteria (*1*). *P. aeruginosa* is notoriously antibiotic resistant, making treatment of reoccurring infections difficult.

Y. enterocolitica causes intestinal symptoms usually in young children including fever, abdominal pain, and diarrhea (*3*). Symptoms normally begin 4 – 7 days after infection and can last more than 1 – 3 weeks. Infection occurs from contaminated food, usually meat or milk, and treatment is not required for uncomplicated cases. If severe or complicated infections exist, antibiotic treatment is administered. *Y. enterocolitica* infections in the United States occur in one out of every 10,000 individuals each year (*4*).

Y. pestis is the causative agent of plague of which there are three types; bubonic, septicemic, and pneumonic (*3*). *Y. pestis* is transmitted by fleas from infected rodents to humans or from the respiratory droplets from pneumonic plague patients. The mortality rate for plague is 50 – 90% if left untreated and is lowered to 15% with antibiotic treatment. The last United States urban epidemic of the plague was in Los Angeles, CA in 1924-1925. Currently, there have been 1 – 40 cases of plague reported annually from 1971 – 1995 and 2,861 cases reported from 10 countries in 1995.

Current antimicrobials

Antimicrobial treatments for bacterial infections consist of five main classes according to the pathways inhibited (*5*). The first class of antibiotics inhibits cell wall synthesis. Penicillins, cephalosporin, vancomycin, and bacitracin are members of this class on antibiotic. A second class of antibiotics inhibits protein synthesis usually by inhibiting bacterial ribosomes. Aminoglycosides such as kanamycin, neomycin, and streptomycin, as well as tetracyclines, macrolides, lincosamides, and chloramphenicols are good examples of protein synthesis inhibitors. A third class of antimicrobials inhibits nucleic acid synthesis with members of this class including quinilones and rifampicin. Disruption of the bacterial membrane or structure is the fourth class of antibiotics. Polymyxin B is a member of this class. Finally, antibiotics can inhibit enzymes involved in essential metabolic pathways such as sulfonamides, which inhibit folic acid synthesis.

While the current antibiotics inhibit a wide range of bacterial targets, many bacteria have developed methods of acquiring drug resistance. *P. aeruginosa* in particular, has multiple systems used for antibiotic resistance (*6*). The bacteria contain multiple efflux pumps, which export antibiotics very quickly. These pumps keep the levels of antibiotic inside the bacterium at a low concentration. Therefore, the antibiotics cannot effectively inhibit their target enzymes. *P. aeruginosa* and other bacteria contain enzymes that are β-lactamases, which open the β-lactam ring of antibiotics such as penicillins. Bacteria can also obtain antibiotic resistance by horizontal gene transfer of the resistance genes developed by related bacteria. This is a very effective way for bacteria to become resistant to antibiotics very quickly.

Bacterial drug resistance has been documented for almost all of the current antibiotics of the market. Therefore, finding new, potent antibiotics is a constant struggle and inhibiting enzymes in pathways distinct from those already inhibited by current antibiotics is needed. An essential process not inhibited by current antibiotics is the acquisition of iron by the bacterium.

Iron utilization

Iron is a vital nutrient for most organisms. Ferrous iron (Fe(II)) is highly soluble up to a concentration of 100 mM at pH 7. However, the ferric form of iron (Fe(III)), which is needed for growth by organisms, is soluble at biological pH only to a concentration of 10^{-9} M making the bioavailability of iron very low (*7*). Animals obtain iron through the food that they eat. Most of the iron ingested is used in heme-containing proteins such as hemoglobin, myoglobin, or in nonheme-containing enzymes. The remainder of the iron is bound to storage and transport proteins such as lactoferrin, ferritin, and transferrin (*8-11*). The concentration of unbound iron in eukaryotes is very low at 10^{-18} – 10^{-24} M (*7, 10, 12*). This level is decreased further in response to infection by a process known as hypoferremia, which stimulates an increase in ferritin synthesis and the release of lactoferrin from neutrophils (*10, 11,* *13*). Lactoferrin has a higher affinity for iron than transferrin and will bind iron normally bound by transferrin. The lactoferrin is removed from circulation by macrophages, thus decreasing the amount of iron in the plasma.

Most microorganisms, such as bacteria and fungi, require at least 10^{-6} M iron for growth and development (*11*). One of the few exceptions are lactobacilli, which do not contain heme compounds and replace iron with cobalt in metal-binding enzymes (*14*). In order to obtain the iron needed for survival, iron-dependent microorganisms scavenge the metal from their environment. Pathogenic bacteria use a variety of methods to obtain iron when invading a host organism including: ferrous iron uptake, heme utilization, transferrin and lactoferrin uptake, and siderophore production (Figure 1-1).

Ferrous iron uptake

The uptake of ferrous iron has been observed in many species of bacteria (*8, 14, 15*). Ferrous iron diffuses easily through porins and does not require specific outer membrane receptors for iron uptake. The iron is transported across the cytoplasmic membrane by conserved ABC transporters (Figure 1-1A). However, the amount of iron needed to support bacterial growth is not attainable solely through the uptake of ferrous iron. Therefore, most bacteria use other iron uptake methods for obtaining this valuable nutrient.

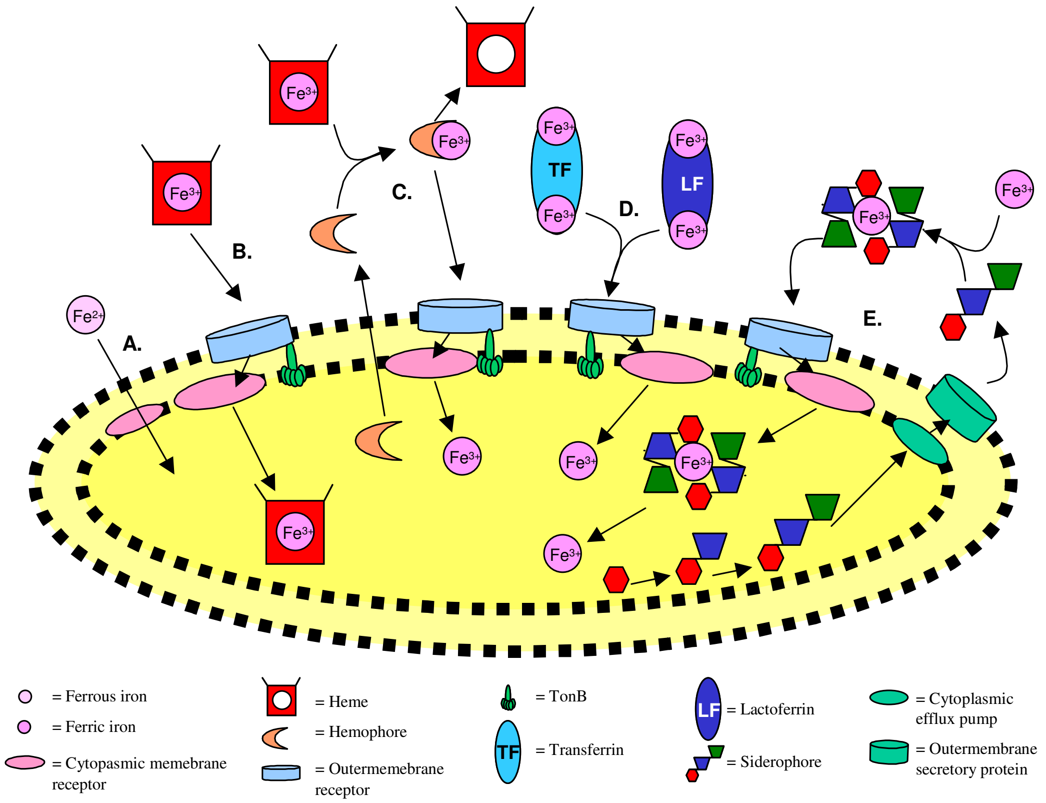
A.
B.
C.
D.
E.
Fe2+
Fe3+
TF
LF
= Ferrous iron
= Ferric iron
= Cytopasmic memebrane receptor
= Heme
= Hemophore
= Outermemebrane receptor
= TonB
= Transferrin
= Lactoferrin
= Siderophore
= Cytoplasmic efflux pump
= Outermembrane secretory protein

Figure 1-1: Model for iron acquisition in gram-negative bacteria. *A.* Ferrous iron import system through cytoplasmic membrane receptor. *B.* Heme binding and incorporation. *C.* Hemophore production for iron removal from heme. *D.* Transferrin and/or lactoferrin binding and iron removal. *E.* Siderophore production, secretion, and ferric-siderophore uptake. All ferric iron uptake methods are TonB-dependent and require specific outer membrane receptors.

Heme utilization

In a host organism, heme is released from cells by the sloughing of epithelial cells or by hemolysis (*10*). Several bacterial organisms have been observed to utilize heme obtained from the environment as free heme or hemoglobin. *P. aeruginosa* contains two distinct systems for heme usage (*7*). The first system is encoded by the *phu* locus containing genes for heme translocation, including an outer membrane receptor for heme and an ABC transporter (Figure 1-1B). The second system for heme utilization by *P. aeruginosa* is encoded by the *has* locus, which contains genes for a heme receptor and a specialized extracellular protein, a hemophore, for binding heme to selectively import the iron (Figure 1-1C) (*7, 15*). *Vibrio cholerae*, the causative agent of cholera, synthesizes hemolysins to lyse erythrocytes and release heme (*16*). The production and secretion of hemolysins are regulated by the iron concentration in the environment. *Hemophilus influenzae* has a strict requirement for heme during infections under aerobic conditions (*10*). *Staphylococcus aureus*, *Y. entrocolitica*, *Y. pestis*, *Shigella dysenteriae*, *Serratia marcescens*, *Neisseria gonorrhoeae*, *Neisseria meningitidis*, and *Escherichia coli* O157 have also been shown to utilize heme (*9, 10, 17-19*).

Uptake of iron from iron-binding proteins

Another direct method of obtaining iron from the environment is from iron-binding proteins such as transferrin and lactoferrin. Transferrin binds to iron in serum and lymph, whereas lactoferrin is found in phagocytic cells and mucosal secretions.

Specific iron uptake systems consisting of one or both of these iron-binding proteins have been observed in a variety of pathogenic bacteria. *N. gonorrhoeae* and *N. meningitidis* contain both transferrin and lactoferrin iron uptake systems, and translocate only the iron but not the proteins (*9, 10, 15*). However, the receptor used for iron uptake and the mechanism of the translocation are unknown. *Bordetella pertussis* has been shown to utilize both transferrin and lactoferrin as iron sources with both binding to the same receptor (Figure 1-1D) (*10*). Some bacteria utilize only transferrin (*S. aureus* and *H. influenzae*), whereas others (*Mycoplasma pneumoniae* and *Tichomonas vaginalis*) have receptors only for lactoferrin and do not uptake iron bound to transferrin (*9, 10, 15, 18*). *Listeria monocytogenes* produces a soluble, extracellular reductase to reduce the iron bound to transferrin from Fe(III) to Fe(II) and stimulate dissociation of the iron-transferrin complex for iron uptake (*10*). No matter the method, iron uptake from iron-binding proteins, the utilization of heme, transferrin, and lactoferrin by bacteria limits the tissues that the pathogen can invade and colonize (*12*).

Production of siderophores

Many bacteria do not contain iron transport systems to take up iron from iron-binding proteins. Therefore, to infect a wider range of host environments, bacteria use an indirect method of obtaining iron by producing siderophores. The production, secretion, and selective uptake of siderophores, low molecular weight, high-affinity, iron chelators, allow bacteria a wider range of colonization territory (Figure 1-1E)

(*12*). A variety of aerobic and facultative anaerobic bacteria, fungi, and plants produce siderophores as their dominant iron acquisition system (*12, 20, 21*). The production of siderophores has been shown to be a virulence factor in many pathogenic bacteria including *E. coli*, *Salmonella typhimurium*, *Vibrio anguillarum*, *N. gonorrhoeae*, and *P. aeruginosa* (*22-29*). Siderophores have a very high affinity for ferric iron with a dissociation constant of 10^{-30} M or lower (*14*). For example, enterobactin has a dissociation constant of 10^{-52} M (*10*). The basic scaffold for siderophore molecules is 500 – 1000 Da and contains six coordination sites to the iron (*14, 20*). This dissertation is concerned with siderophore biosynthetic proteins in *P. aeruginosa*. Therefore, I will describe siderophore production as it pertains to this organism.

Siderophore regulation

Siderophore production is iron-regulated by a repressor which is termed the Fur repressor in *E. coli* (*10, 30-36*). Most bacterial species that produce siderophores contain a Fur homologue for the regulation of siderophore biosynthesis genes. In high iron environments, the Fur protein binds to its cofactor, Fe(II), and will bind DNA in the promoter region of genes containing a Fur box. Fur bound at the Fur box represses expression of genes such as siderophore biosynthetic and ferric-siderophore uptake genes (Figure 1-2A). In contrast, in low iron environments the concentration of iron will drop in the cell and Fur will not bind Fe(II). Apo-Fur, the iron-free form

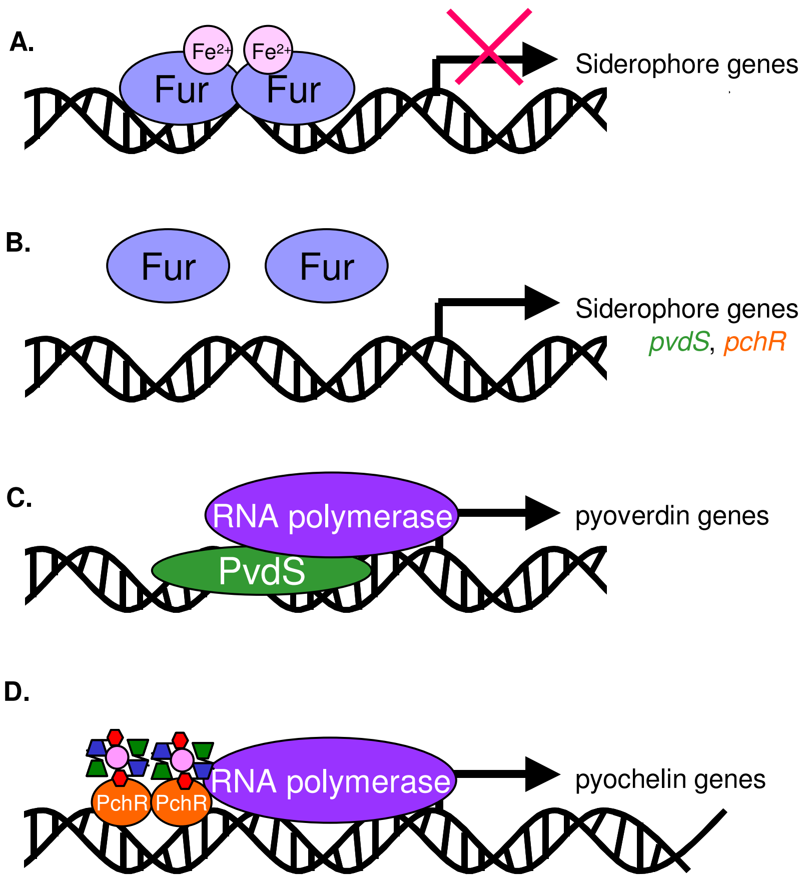
A.
Fe2+
Fe2+
Fur
Fur
Siderophore genes
B.
Fur
Fur
Siderophore genes
pvdS, pchR
C.
RNA polymerase
PvdS
pyoverdin genes
D.
PchR
PchR
RNA polymerase
pyochelin genes

Figure 1-2: Mechanism of Fur repression in *P. aeruginosa*. *A*. In high iron environments, Fur (blue oval) binds Fe(II) (pink circle), dimerizes, and binds to the promoter regions of genes containing a Fur box to repress transcription. *B*. In low iron environments, Fur cannot bind Fe(II) and does not bind to the DNA. Siderophore related genes are transcribed including *pvdS* and *pchR*. *C*. After activation by the pyoverdin outer membrane receptor, PvdS (green oval) recruits RNA polymerase (purple oval) to the promoter regions of pyoverdin related genes for transcription. *D*. PchR (orange oval) acts as a coactivator of pyochelin related genes after binding to Fe-pyochelin ( ) and dimerizing in the bacteria.

of Fur, cannot bind DNA and is unable to repress genes allowing gene expression (Figure 1-2B). In bacteria with multiple siderophore systems, additional regulation methods are employed to control the expression of genes for each system independently. Many bacteria use alternative sigma factors or activators for additional regulation.

P. aeruginosa produces two siderophores, pyoverdin and pyochelin, and regulates the expression of both systems using a combination of alternative sigma factors and activators. Fur repression occurs only for a subset of the siderophore genes, including *pvdS* and *pchR*, but not for siderophore synthesis and uptake genes directly (*37-39*). Instead, PvdS and PchR, once produced, assist in the upregulation of siderophore genes. During iron starvation, the repression by Fur is released allowing transcription of *pvdS* and *pchR* (Figure 1-2B). Newly translated PvdS is in an inactive form and requires the binding of Fe-pyoverdin to its outer membrane receptor for activation (*40*). PvdS has been shown to be an alternative sigma factor that recruits RNA polymerase to the pyoverdin synthesis and uptake genes (Figure 1-2C) (*34, 41-44*). PchR is a coactivator, which mediates the regulation of the pyochelin pathway. PchR, a member of the AraC family of regulators, is activated by Fe-pyochelin in the cell, activates pyochelin synthesis and uptake genes and has been shown to repress its own expression (Figure 1-2D). Once the genes for siderophore synthesis and uptake are transcribed and the message translated, the siderophore is assembled in a multi-step process that will be discussed in detail later.

Siderophore secretion

The completed siderophore is secreted from the bacterium using a system of efflux pumps that are separated into three superfamilies: the major facilitator superfamily (MFS), the resistance, nodulation, and cell division (RND) superfamily, and the ATP-binding cassette (ABC) superfamily (*12, 45*). An RND superfamily efflux pump has been reported to secrete pyoverdin in *P. aeruginosa* (*46-48*). The efflux system consists of three proteins, MexA, MexB, and OprK, which form a complex and secrete pyoverdin into the periplasm using energy from a transmembrane proton gradient. All the members from the RND superfamily work as substrate:proton antiporters to import a proton as the siderophore is secreted into the environment (*45*).

Ferric-siderophore uptake

Once the secreted siderophore encounters and binds iron, the ferric-siderophore must be selectively imported into the bacterium. Due to the large size and low concentration of the ferric-siderophore in the environment, uptake of the iron-chelator complex through outer membrane porins is not feasible (*49*). Therefore, import of the complex requires a specific, high-affinity, outer membrane receptor (Figure 1-1E) (*50*).

The ferrichrome-iron receptor in *E. coli*, FhuA, was the first receptor to be structurally characterized and the work was completed independently by two groups

(*51, 52*). FhuA contains two domains; a 22 stranded β-barrel and an N-terminal mixed four-stranded β-sheet domain, which forms an internal cork to the barrel. Upon ferric-siderophore binding to the receptor, the cork domain undergoes dramatic rearrangement on the periplasmic face of the receptor. This conformational change allows the cork domain to interact with TonB, a cytoplasmic membrane-associated protein involved in transfer of energy from the cytoplasmic membrane to the outer membrane for selective import (*51-53*). The interaction of the outer membrane receptor with TonB only occurs when the receptor has bound the ferric-siderophore (*50, 54, 55*). The bound TonB, in complex with ExoB and ExoD which are accessory proteins to TonB that aid in energy transfer, and which bind in a 1:7:2 ratio, transduces energy to the receptor causing further unfolding of the cork domain and subsequent translocation of the ferric-siderophore (*53, 56-60*). The translocated ferric-siderophore binds to a periplasmic-binding protein and is shuttled through the cytoplasmic membrane by a TonB-dependent ABC transporter system (*61-66*). Crystal structures of the outer membrane receptors for pyochelin (FptA), and pyoverdin (FpvA) have been determined and they appear to be structural and functional homologues to FhuA (*67-70*). Once the ferric-siderophore enters the bacterium, the iron is dissociated from the siderophore by reduction of the ferric iron to ferrous iron by a reductase, ester cleavage of the siderophore (seen with enterochelin in *E. coli*), or siderophore hydrolysis (seen with bacillibactin in *Bacillus subtilis*) (*8, 12, 71*). Specific reductases for ferripyochelin and ferripyoverdin have been determined (*72-74*).

Classes of siderophores

Siderophores are separated into classes based upon the chemical groups involved in iron chelation within the siderophore. The two most common classes of siderophores are hydroxymates and phenolate-catecholates. However, several siderophores use multiple functional groups to chelate the iron and are considered mixed siderophores (Figure 1-3) (*12*).

Hydroxymate siderophores

The hydroxymate siderophores are seen predominantly in fungi but are also produced by some bacteria. The iron chelation is provided by a hydroxymate group (-CO-N(O^-)-) formed from aceylated or formylated hydroxylamines usually derived from lysine or ornithine (Figure 1-3A) (*12*). Lysine derivatives are used for the synthesis of aerobactin (*E. coli*) and mycobactin (*Mycobacterium* spp.) (*12, 75*). Ornithine derivatives are used in the synthesis of pyoverdin (*P. aeruginosa*), exochelin (*Mycobacterium* spp.), ornibactin (strains of pseudomonads), ferrichrome, fusarinine, and coprogens (variety of fungi) (*12, 14, 75*). Histamine derivatives have also been found in anguibactin, the siderophore produced by *Vibrio anguillarum,* a fish pathogen (*75*).

The hydroxymate group is assembled in a two-step process, beginning with hydroxylation of the primary side-chain amine of ornithine or lysine by a flavin

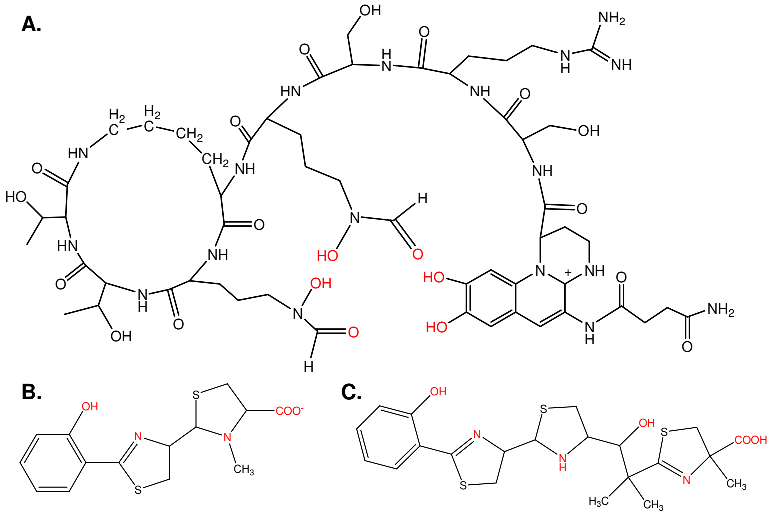
A.
B.
C.
OH
NH$_2$
NH
HO
HO
HO
OH
COO$^-$
COOH
CH$_3$
H$_3$C
N
S

Figure 1-3: Representative siderophores. *A*. Pyoverdin, a hydroxymate siderophore, produced by PAO1 *Pseudomonas aeruginosa*. *B*. Pyochelin, a catecholate siderophore, produced by *Pseudomonas aeruginosa*. *C*. Yersiniabactin, a catecholate siderophore, produced by pathogenic strains of *Yersinia* spp. Iron chelating functional groups are labeled in red.

adenosine dinucleotide-dependent monooxygenase (*76*). The second step involves formylation by a methyl transferase, for pyoverdin and ornibactin, or acetylation by an acetylase, for all other hydroxymate siderophores (*12*).

Pyoverdin in *P. aeruginosa* is an example of a hydroxymate siderophore. Pyoverdin is water soluble and consists of 6 – 12 amino acids, depending on the strain, with a dihydroxyquinoline fluorescent chromophore and a small dicarboxylic acid (Figure 1-3A) (*7, 77-79*). Pyoverdin has a very high affinity for ferric iron with a dissociation constant of $10^{-30.8}$ M and has been shown to chelate iron from transferrin (*25, 28, 80, 81*). The virulence of *P. aeruginosa* is enhanced by the production of pyoverdin (*82*). The pyoverdin locus in the *Pseudomonas* genome is the most divergent region, resulting in highly variable pyoverdin molecules that differ in almost every strain of *Pseudomonas (83)*. The pyoverdin molecules are separated into three main classes: type I, containing two formyl-hydroxyornithines; type II, which contains one formyl-hydroxyornithine and a terminal cyclized hydroxyornithine; and type III, also containing two formyl-hydroxyornithines in a different arrangement from type I (Figure 1-4) (*7, 84*). The laboratory strain PAO1 *P. aeruginosa* produces a type I pyoverdin.

The outer membrane receptor for pyoverdin is FpvA. Originally, there was thought to be two distinct receptors for pyoverdin, one was 80 kDa (*85*) and the other was 90 kDa (*86*). Later, the two receptors were determined to be the same protein (*87*). FpvA is an unusual receptor, in that it can bind the iron-free form of pyoverdin

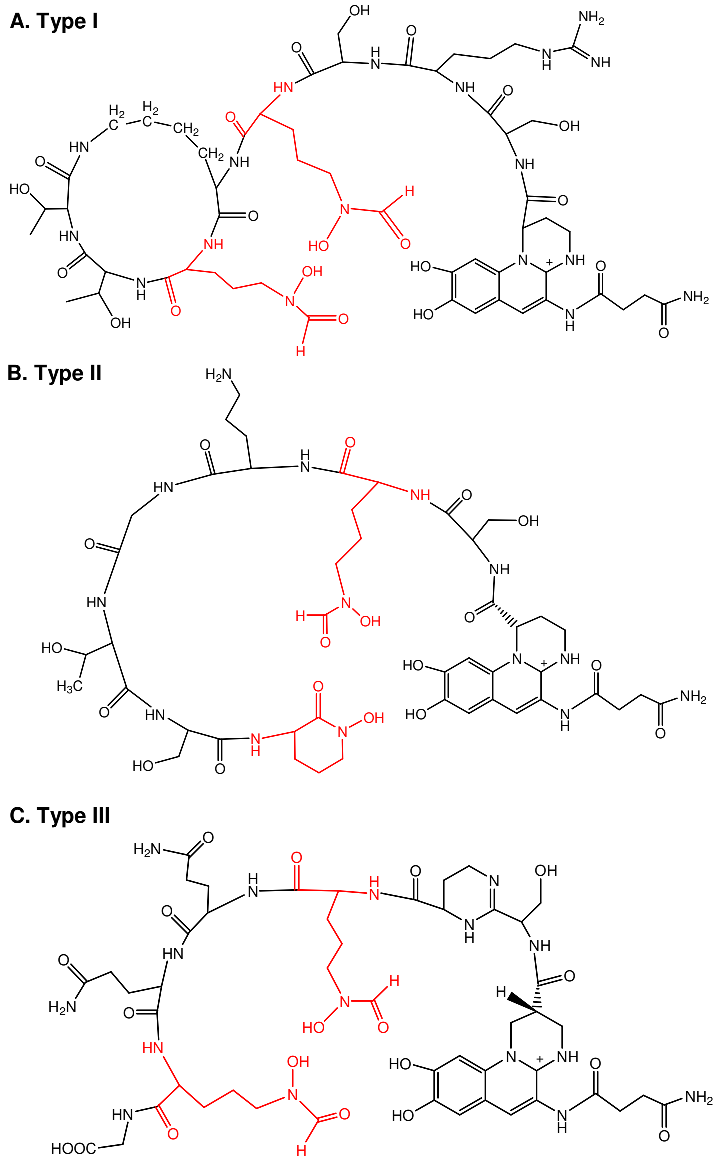

Figure 1-4: Pyoverdin Classes. *A.* Type I, contains two formyl-hydroxyornithine groups and a cyclized peptide structure. *B.* Type II, contains one formyl-hydroxyornithine and a cyclized hydroxyornithine. *C.* Type III, contains two formyl-hydroxyornithines similar to Type I but lacks the cyclized peptide. The ornithine derivatives are labeled in red.

(*69*). FpvA is normally bound to iron-free pyoverdin. When iron-pyoverdin encounters the receptor, it will displace the iron-free pyoverdin. Only the iron-pyoverdin enters the cell indicating that the FpvA binding site is conformer specific (*7, 88-90*). The imported ferric-pyoverdin is reduced to ferrous-pyoverdin. The binding affinity for ferrous iron is lowered, the iron is released, and the pyoverdin is re-secreted into the environment (*7, 90, 91*). Recycling saves cellular energy by not continuously synthesizing new pyoverdin molecules. This makes pyoverdin a highly effective siderophore.

Phenol-catecholate siderophores

The second most common siderophore class is the phenol-catecholates, which contain a mono- or dihydroxybenzoic acid group to chelate the iron (Figure 1-3 B and C) (*14*). This class of siderophores has only been observed in bacteria. The catecholate group is derived from salicylate or dihydroxybenzoic acid and the siderophores have iron binding affinities that range from very tight binding for enterobactin from *E. coli* ($K_d = 10^{-52}$ M) to fairly weak binding seen in pyochelin from *P. aeruginosa* ($K_d = 5 \times 10^{-5}$ M) (*14, 92*).

Pyochelin, one of the two siderophores produced by *P. aeruginosa*, is a 324 Da peptide composed of salicylate and two cysteines forming a thiazoline and a thiozolidine heterocyclic ring (Figure 1-3B) (*92-94*). Pyochelin has been shown to bind several other metals besides iron including Zn(II), Mo(IV), Ni(II), and Co(II) (*7,* *95*). Unlike pyoverdin that is highly divergent among strains of *P. aeruginosa*, the same pyochelin molecule is produced by a wide variety of *Pseudomonas* species and in some *Burkholderia cenocepacia* strains (*7*). The production of pyochelin by *P. aeruginosa* increases the lethality of virulent strains but not in nonvirulent strains, indicating that although involved in the acquisition of iron, pyochelin is not a required virulence factor (*26*).

The mechanism for secretion of pyochelin into the environment has been suggested to be similar to that for pyoverdin, using the RND efflux pump system. However, the cytoplasmic components required for secretion are not known (*96*). Once secreted, pyochelin binds iron in an asymmetric manner with one pyochelin molecule binding to four of the six iron coordination sites. Depending on the siderophore concentration, either a second molecule of pyochelin or two water molecules coordinate the remaining two sites (*97*). This asymmetric binding is a change from the original notion of a strict 2:1 ratio of pyochelin binding (*93*). Once bound to iron, the ferric-pyochelin is imported into the bacterium. Two outer membrane receptors involved in ferric-pyochelin uptake have been identified; a 14 kDa ferripyochelin-binding protein (FBP), and the 75 kDa outer membrane receptor (FptA) (*27, 67, 98, 99*). The structure of FptA has been solved with ferric-pyochelin bound in a 1:1 ratio of siderophore to iron (*68*). However, the method of FBP involvement in siderophore uptake is not known.

Another phenolate-catecholate siderophore that has been intensely studied is yersiniabactin produced by pathogenic strains of *Yersinia pestis*, *Yersinia enterocolitica*, and *Yersinia pseudotuberculosis (100-103).* Yersiniabactin has a similar structure to pyochelin with a salicylate and two cysteines forming a thiazoline and a thiozolidine heterocyclic ring (Figure 1-3C). However, yersiniabactin contains an additional malonyl and cyclized cysteine residue increasing the molecular mass to 482 Da. This additional thiazoline ring decreases the dissociation constant of yersiniabactin to 4×10^{-36} M, which is much higher than that for pyochelin (*102*). The outer membrane receptor for yersiniabactin is FyuA, and the cytoplasmic transporters required for siderophore import are Irp6 and Irp7 in *Y. enterocolitica* (YbtP and YbtQ in *Y. pestis*) (*104, 105*).

Other Classes of Siderophores

Several other classes of siderophores are recognized. Citrate-hydroxymate siderophores are a mixed class of bacterial siderophores (*14*). The siderophores contain derivatives of citric acid in which the distal carboxyl group has been substituted with hydroxymate groups. Another unusual class of siderophores is the mycobactins produced by *Mycobacterium* spp. of bacteria (*14*). Mycobactins are a hybrid of hydroxymate and phenol-catecholate classes and are highly lipid soluble. This class of siderophores is believed to reside in the outer membrane of *Mycobacerium* spp. and work in conjunction with water-soluble chelating agents (exochelins) for iron acquisition. A variety of other classes of siderophores are known that contain various hydroxymate, catecholate, and phenolate groups and are too numerous to describe here (*14*).

Siderophore Biosynthesis

Siderophores are assembled using two different pathways. One pathway involves assembling amino acids into peptides by forming peptide bonds and does not require an RNA template. This process uses large, multi-domain, multi-functional proteins known as nonribosomal peptide synthetases (NRPSs) for assembly (*75*). The other pathway, the NRPS-independent pathway, involves linking dicarboxylic acid and diamine or amino alcohol building blocks that are linked together by amide or ester bonds (*76*). The NRPS-independent pathway is used for the assembly of hydroxymate and carboxylate siderophores such as aerobactin, alcaligin, stephlobactin, and petrobactin (*12, 76*).

The NRPS-dependent pathway is used for the biosynthesis of enterobactin, yersiniabactin, pyochelin, pyoverdin, vibriobactin, and mycobactin (*75, 106-108*). Because the pathway does not use RNA as a template for assembly, the sequence is determined by the order of the domains (*75*). Three functional domains are required for the incorporation of one amino acid into the growing peptide chain and form a single module, consisting of condensation (C), adenylation (A), and peptidyl-carrier (P) domains (Figure 1-5A) (*75, 109*).

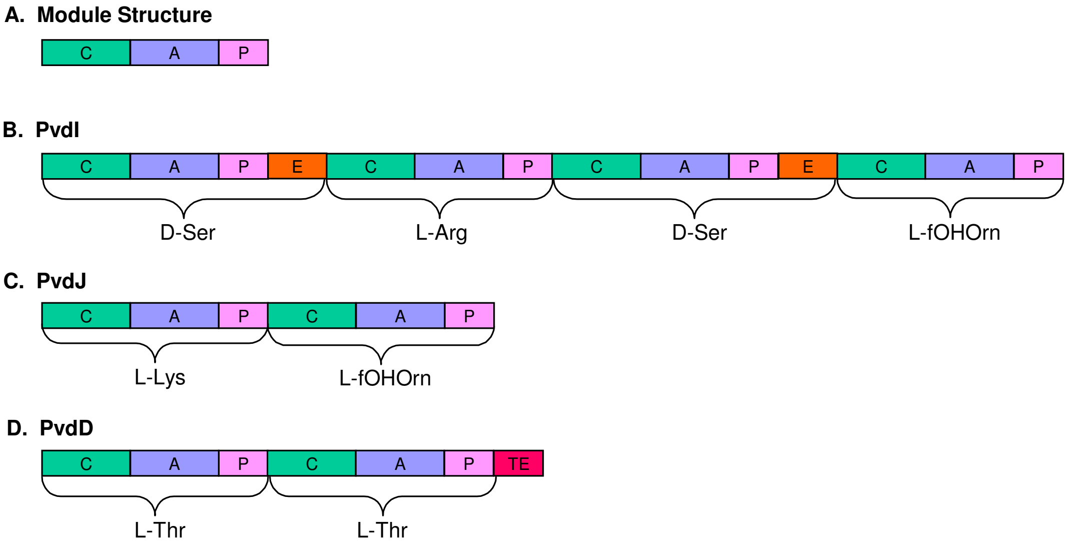
A. Module Structure
C
A
P
B. PvdI
C
A
P
E
C
A
P
C
A
P
E
C
A
P
D-Ser
L-Arg
D-Ser
L-fOHOrn
C. PvdJ
C
A
P
C
A
P
L-Lys
L-fOHOrn
D. PvdD
C
A
P
C
A
P
TE
L-Thr
L-Thr

Figure 1-5: Pyoverdin Biosynthesis. *A.* NRPS module structure containing condensation (green), adenylation (blue), and peptidyl carrier (pink) domains. *B.* PvdI is hypothesized to incorporate two D-Serines, one L-Arg, and one L-formyl-hydroxyornithine (L-fOHOrn) molecule into the growing pyoverdin peptide due to the inclusion of two epimerase (orange) domains. The epimerase domain converts L amino acids into D amino acids. *C.* PvdJ is hypothesized to incorporate the next two amino acids into the growing peptide, L-lys and the second L-fOHOrn. *D.* PvdD incorporates the final two amino acids into pyoverdin, two molecules of L-Thr. The completed pyoverdin molecule is released from the NRPS by the thioesterase (red) domain.

The 50 kDa condensation domain catalyzes the peptide bond formation for chain elongation (*75*). The first structure of a condensation domain determined was VibH, which is involved in vibriobactin biosynthesis in *Vibrio cholera* (*110*). The C functional domain is composed of two structural domains each containing an α-β-α sandwich. A functional modification of the condensation domain is the cyclization (Cy) domain (*75*). The cyclization domain catalyzes the peptide bond formation similar to condensation domains but additionally cyclizes cysteine, serine, or threonine to form a five-membered ring. The ring structure is then dehydrated to yield a thiazoline (Cys) or oxazoline (Ser, Thr) ring.

The next functional domain in the module is the 50 kDa adenylation domain, which selects and activates the amino or aryl acid to be incorporated into the peptide in an ATP-dependent manner (*75*). This activation forms an aminoacyl-AMP that is transferred to the peptidyl-carrier domain. The structures of PheA, which activates phenylalanine for incorporation into the antibiotic gramicidin, and DhbE, which activates 2,3-dihydroxybenzoate (DHB), an aryl acid found in bacillibactin from *Bacillis subtilis*, have been determined (*111, 112*). The adenylation domains have a similar structure to firefly luciferase and contain two compact structural domains.

The last functional domain in the NRPS module is the peptidyl-carrier domain or the aryl-carrier domain when using aryl acids (*75*). This small domain of 8 – 10 kDa contains a conserved serine residue that must be post-transcriptionally modified by the addition of a phosphopantethionyl (pPant) tail. The phosphopantethionyl tail covalently binds the activated aminoacyl-AMP and acts as a tether for the elongating chain. The tail is attached to the peptidyl-carrier domain by phophopantetheinyl transferase (PPTase) enzymes. PPTases are involved in primary and secondary metabolism and usually there are distinct PPTases for each pathway. The PPTase for siderophore production has been determined in several bacteria such as Sfp in *B. subtilis*, YbtD in *Y. pestis* (*113, 114*). However, *P. aeruginosa* contains only one PPTase (PcpS), which is involved in both primary and secondary metabolism (*115*).

In addition to the three required functional domains in the NRPS module, there are a number of additional domains that modify the elongating peptide, including epimerase (E), methyl transferase (MT), and thioesterase (TE) domains (*75*). Epimerization domains convert L-amino acids into the D-amino acid configuration. Methyltransferase domains methylate the amino acids using s-adenosyl methionine (SAM) as the methyl donor. The thioesterase domains terminate the chain elongation and release the completed siderophore. Some bacteria contain additional accessory proteins to modify the siderophore. *P. aeruginosa* and *Yersinia* spp. use an NADPH-dependent reductase, which converts the second thiazoline ring of pyochelin and yersiniabactin into a thiazolidine ring (*116-118*).

The biosynthesis of pyoverdin and pyochelin in *P. aeruginosa* are NRPS-dependent and illustrate how two very different siderophores are assembled. The formation of yersiniabactin, although very similar to pyochelin, uses a hybrid system of NRPS-dependent and NRPS-independent pathways. These three siderophores encompass most siderophore production and are good examples of siderophore biosynthesis.

Pyoverdin biosynthesis

Pyoverdin is assembled using an NRPS system, which is unusual for hydroxymate siderophores (*12*). The first step in assembly is the formation of the fluorescent chromophore. The proteins PvcA, PvcB, PvcC, and PvcD have been implicated in chromophore production (*119*). However, *pvc*$^{-}$ mutants can make and secrete pyoverdin in some growth media indicating the expression of these four genes is not required for pyoverdin synthesis (*120*). The NRPS protein, PvdL, has also been implicated in production of the chromophore. PvdL is the only NRPS in the pyoverdin locus that begins with an adenylation domain indicative of the initial step of the reaction (Figure1-5) (*107, 120*). All of the other NRPS proteins begin with a condensation domain. PvdL also does not include a thioesterase domain indicating it is not involved in the final steps for pyoverdin production.

After the formation of the chromophore, a series of NRPSs work to add the additional 6 – 12 amino acids required to make the completed siderophore. Most of the experimental work for the elucidation of pyoverdin biosynthesis has been carried out on the PAO1 strain of *P. aeruginosa* that contains 6 amino acids (D-Ser-L-Arg-D-Ser-L-fOHOrn-L-Lys-L-fOHOrn-L-Thr-L-Thr) where fOHOrn is formyl-hydroxyornithine. Three NRPS proteins have been determined to be involved in peptide elongation in type I pyoverdins; PvdI, PvdJ, and PvdD (Figure 1-5). These proteins are not involved in production of type II or type III pyoverdins (*120*). PvdI is hypothesized to incorporate the initial amino acids; D-Ser, L-Arg, D-Ser, and L-fOHOrn (Figure 1-5B) (*120-122*). PvdJ was initially reported as two proteins (PvdJ and PvdK), but the corresponding DNA sequence was later determined to encode only one protein upon resequencing (*120, 121*). PvdJ is hypothesized to encode the next two amino acids in the sequence; L-Lys and L-fOHOrn (Figure 1-5C) (*122*). The specificity of the PvdA adenylation domains have been biochemically determined and this NRPS selectively incorporates the last two amino acids (L-Thr-L-Thr) into the peptide chain (Figure 1-5D) (*108, 121, 123*).

In hydroxymate siderophores, the iron is chelated by modified amino acids. In the case of pyoverdin, the iron is chelated by formyl-hydroxyornithine. This modified amino acid is formed in a two-step process using two proteins, PvdA and PvdF. PvdA is an ornithine hydroxylase that converts ornithine to hydroxyornithine. PvdA was first identified by a mutation screen and was later cloned and sequenced (*38, 124*). The gene encoding PvdA does not show increased expression when pyoverdin is added to the bacterium indicating the gene is not regulated by iron (*125*). The PvdA protein or its homologue, PsbA, is produced in a wide variety of *pseudomonas* species (*126, 127*).

Once the hydroxyornithine is produced it is converted to formyl-hydroxyornithine by PvdF, a hydroxyornithine transformylase (*128*). PvdF has only been detected in *P. aeruginosa* strains that produce type I pyoverdins and has slight homology to glycinamide ribonucleotide transformylase (GART) proteins (*120, 128*). The mechanism of formylation and the cofactor required for activity has not yet been determined. In type II pyoverdins, there is one formyl-hydroxyornithine and a cyclized hydroxyornithine. The cyclized hydroxyornithine is formed by acetylation of hydroxyornithine by PvdY and subsequent cyclization (*84*).

Pyochelin Biosynthesis

The pyochelin biosynthesis genes are contained on two operons in the *P. aeruginosa* genome, *pch*DCBA and *pch*EFGHI. To produce pyochelin, one molecule of salicylate, two cysteines, three ATPs, one molecule of SAM, and one NADPH are required (Figure 1-6). Salicylate is formed by two enzymes in *P. aeruginosa*, PchA and PchB (Figure 1-6A) (*129, 130*). PchA is an isochorismate synthase that converts chorismate into isochorismate. PchA is a monomer in solution and is dependent on Mg^{2+} for activity (*130*). PchB, an isochorismate pyruvate lyase (IPL), converts the isochorismate into salicylate and pyruvate (*129*). However, PchB has a secondary activity as a chorismate mutase (CM) that converts chorismate into prephenate only very inefficiently. PchB is not homologous to other IPL enzymes but shows homology to chorismate mutase enzymes. The structure of PchB has been determined and shows PchB as an intertwined dimer of three α-helices each, very similar to the chorismate mutase from *E. coli* (*131*). PchC is a thioesterase and contains an editing function to remove incorrect products from the assembly line (*132*).

The assembly-line production of pyochelin begins with PchD, a stand-alone adenylation domain, which activates salicylate (Figure 1-6B) (*133*). The activated

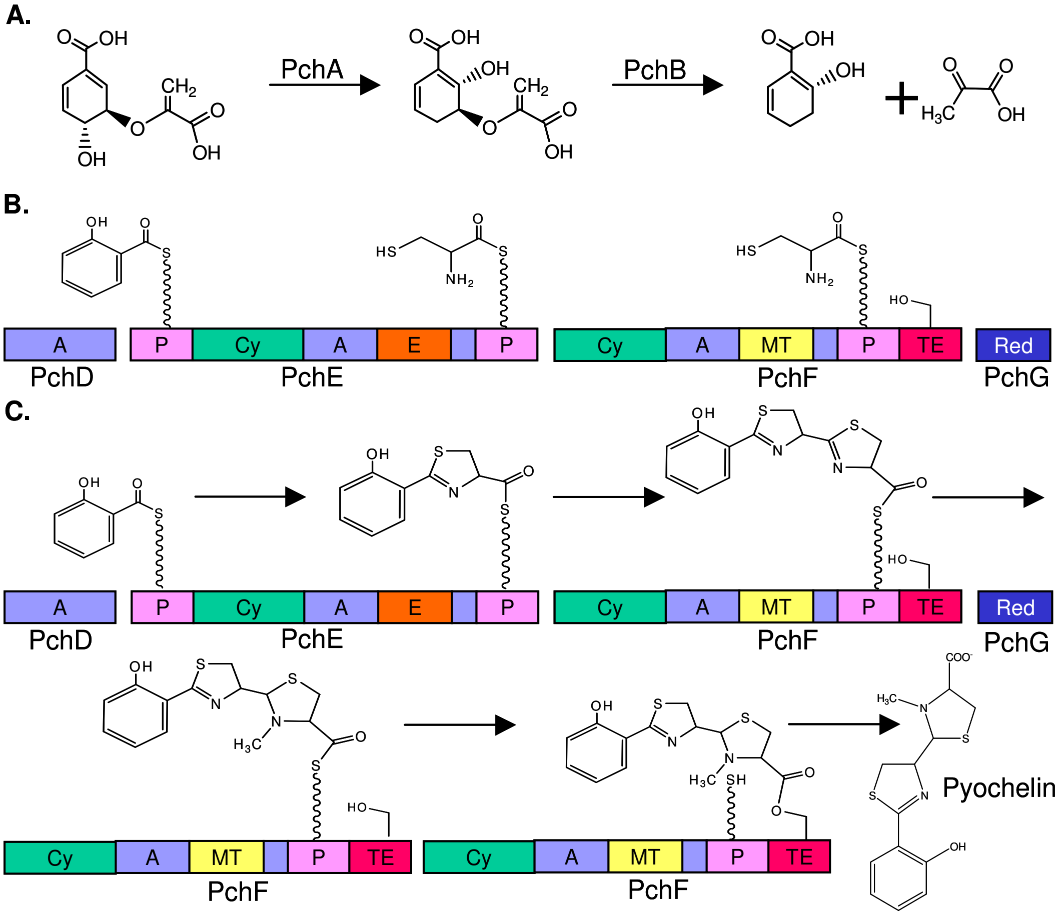
A.
PchA
PchB
B.
A
PchD
P
Cy
A
E
P
PchE
Cy
A
MT
P
TE
PchF
Red
PchG
C.
Pyochelin

Figure 1-6: Pychelin Biosynthesis. *A.* Conversion of chorismate to isochormismate and final production of salicylate using PchA and PchB proteins. *B.* Activation and tethering of salicylate and two cysteines to the peptidyl-carrier domains of PchE and PchF by the adenylation domains of PchD, PchE, and PchF. *C.* Chain elongation with reduction and subsequent methylation of the second cysteine residue in the tethered pyochelin. The completed pyochelin molecule is hydrolyzed for release from PchF. Figure modified from Quadri et al., 1999.

salicylate is transferred to the aryl-carrier domain of PchE. PchE is a 156 kDa, NRPS protein containing one each of aryl-carrier, cyclization, adenylation, epimerization, and peptidyl-carrier domains (*134, 135*). The cyclization domain in PchE condenses the salicylate with the first cysteine and forms the first thiazoline ring, while the epimerase domain converts the L-cysteine to D-cysteine, (Figure 1-6C) (*134*). This peptidyl product is then transferred to the third protein in the assembly line, PchF. PchF is a 197 kDa NRPS protein composed of cyclization, adenylation, methyltransferase, peptidyl-carrier, and thioesterase domains (*134*). The cyclization domain of PchF condenses the product formed by PchE with the second cysteine and subsequently cyclizes the second cysteine. The accessory protein PchG performs the next step in pyochelin formation. PchG is a NADPH-dependent reductase, which reduces the second thiazoline ring into a thiazolidine ring (*116, 117*). The reduction creates a more nucleophilic substrate that facilitates the methylation of the ring by the methyl transferase domain of PchF. PchG has no known homologues except other siderophore-related reductases and no structural information is known. The completed pyochelin molecule is released from PchF through the thioesterase domain and is secreted from the bacterium.

Yersiniabactin Biosynthesis

The genes for the synthesis and uptake of yersiniabactin are contained on a high-pathogenicity island (HPI). This island is seen only in virulent strains of *Yersinia* spp. and contains a higher G+C content than the remainder of the genome

(60% versus 46-50%) (*75, 136*). The island is located beside a gene that encodes asparagine tRNA and contains an integrase gene, both hallmarks of a pathogenicity island (*137*). In *Y. pestis*, the HPI is part of a larger pigmentation (*pgm*) locus encompassing 102 kb of the chromosome (*136-140*). The *pgm* locus is highly unstable, making the loss of the HPI in *Y. pestis* very common. However, the HPI in *Y. enterocolitica* is very stable (*136*).

The yersiniabactin biosynthesis genes are encoded on two operons, *irp*21345, *irp*6789 in *Y. enterocolitica* and *irp*2 *irp*1 *ybt*UTE, *ybt*PQXS in *Y. pestis* (*137*). The homology between the yersiniabactin biosynthetic proteins from *Y. pestis* and *Y. enterocolitica* is very high (~90%) and the proteins can be used interchangeably. Yersiniabactin production was reconstituted *in vitro* using four proteins; Irp5/YbtE, HMWP2 (high molecular weight protein 2, the gene product of irp2), HMWP1 (high molecular weight protein 1, the gene product of irp1), and Irp3/YbtU with one molecule of salicylate, three cysteines, one malonate, five ATPs, three SAMs, and one NADPH per molecule (Figure 1-7) (*141*). The first step in yersiniabactin synthesis is salicylate formation similar to pyochelin formation (Figure 1-7A). However, unlike the two-enzyme system (PchA and PchB) in *P. aeruginosa*, the *Yersinia* spp. requires only one protein, Irp9/YbtS, for salicylate formation. Irp9/YbtS converts chorismate into salicylate with an isochorismate intermediate (*103, 142-144*). The structure of Irp9 has been solved and appears to function as a homodimer (*145*). Irp4/YbtT is thought to have thioesterase activity similar to PchC for removing incorrect molecules from the assembly line (*114, 118*).

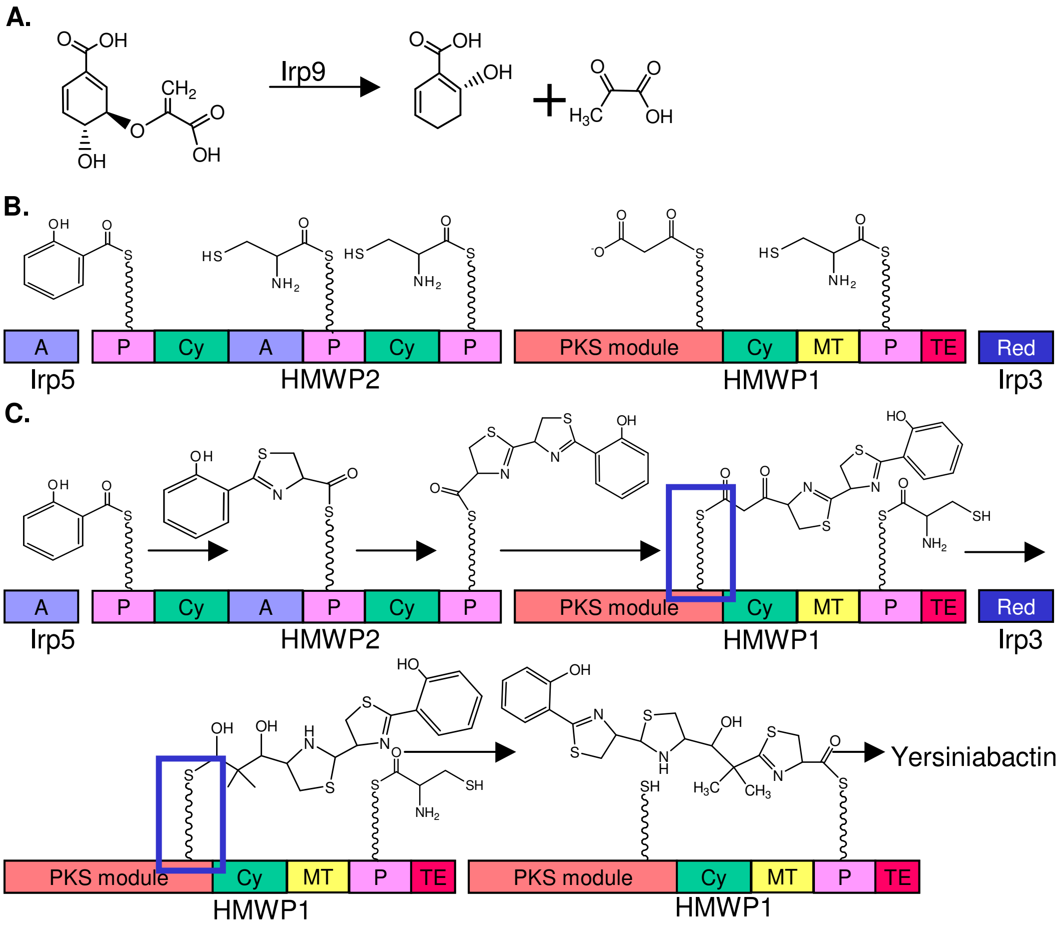
A.
Irp9
B.
A
P
Cy
A
P
Cy
P
PKS module
Cy
MT
P
TE
Red
Irp5
HMWP2
HMWP1
Irp3
C.
Yersiniabactin

Figure 1-7: Yersiniabactin Biosynthesis. *A.* Conversion of chorismate to salicylate using Irp9. *B.* Activation and tethering of salicylate, three cysteines, and a malonyl group to the peptidyl-carrier domains of HMWP2 and by the adenylation domains in Irp5, HMWP2, and HMWP1. *C.* Chain elongation including reduction, double methylation of the malonyl group at the switch site (encompassed by blue square), and incorporation of the third cysteine residue into the tethered yersiniabactin. Lastly, the yersiniabactin intermediate is methylated and the completed Yersiniabactin is hydrolysed for release from HMWP1. Figure modified from Miller et al., 2002.

The first NRPS-mediated steps in yersiniabactin production are similar to pyochelin formation (Figure 1-7B). Salicylate is activated by Irp5/YbtE and transferred to the aryl-carrier domain of HMWP2. The HMWP2 domain sequence is aryl-carrier, cyclization, adenylation, methyltransferase, peptidyl-carrier, cyclization, and peptidyl-carrier (*103, 146-149*). HMWP2 catalyzes the condensation and cyclization of two cysteines with the salicylate (Figure 1-7C).

At this point, the product is transferred to HMWP1. HMWP1 is a hybrid enzyme incorporating NRPS function at the C-terminal half of the protein with polyketide synthesis (PKS) function, an NRPS-independent pathway, at the N-terminal portion (*141*). The PKS module of HMWP1 modifies and loads malonyl onto a carrier domain. A switch point is located between the PKS and NRPS modules in HMWP1, which catalyzes the formation of a C-C bond instead of the normal NRPS C-N bond as the malonyl group in the PKS module is condensed with the product formed by HMWP2 (*146, 150*). At the switch point, reduction of the second thiazoline ring occurs using Irp3/YbtU, a PchG homologue (*118*). Two methyl groups are added to the malonyl group by a methyltransferase domain located in the PKS module. The final NRPS module at the C-terminal of HMWP1 adds and cyclizes the final cysteine into the growing molecule (*141*). The final steps are the methylation of the last thiazoline ring and the release of the yersiniabactin from the protein through the thioesterase domain. The completed yersiniabactin is secreted from the bacterium for iron acquisition.

Siderophore Biosynthesis Implications for Drug Discovery

Most of the enzymes involved in the biosynthesis of siderophores have very little homology to mammalian enzymes. This makes the enzymes very attractive drug targets for the design of new antimicrobials. Inhibitors of the adenylation domains of *P. aeruginosa* (PchD), *Y. pestis* (YbtE), and *M. tuberculosis* (MbtA) have shown growth inhibition of *Y. pestis* and *M. tuberculosis* (*151*). Growth inhibition studies have not been conducted on *P. aeruginosa* due to the dual siderophore pathways. Studies conducted on salicylate synthase enzymes show tight binding of some inhibitors with K_Is ranging from 19 – 43 μM (*152*). Additional accessory proteins such as the enzymes involved in formyl-hydroxyornithine synthesis and the stand-alone reductase also make attractive drug targets.

This dissertation includes biochemical characterization of the pyoverdin accessory protein PvdA, an ornithine hydroxylase from *P. aeruginosa*. Steady-state and transient-state kinetic studies indicate that PvdA proceeds through a novel reaction mechanism. X-ray crystallization studies of PvdA and PvdF, the second enzyme in the ornithine derivitization pathway, as well as the NADPH reductases PchG from *P. aeruginosa* and Irp3 from *Y. enterocolitica* were also conducted. Initial PvdA crystals and plate crystals of PvdF have been obtained. PchG exhibits low solubility although its homologue, Irp3, is soluble and x-ray diffraction data has been collected. This work is a first step towards rational drug design of new inhibitors of the siderophore biosynthetic pathways in these organisms.

References

(1) Qarah, S., Cunha, B. A., Dua, P., and Lessnau, K.-D. (2005) *Pseudomonas aeruginosa* Infections. www.emedicine.com.

(2) (2007) Cystic Fibrosis Foundation. www.cff.org.

(3) (2007) Centers for Disease Control. www.cdc.gov.

(4) Brooks, D. C., Johnston, M. H., and Martin, M. (2005) *Yersinia enterocolitica*. www.emedicine.com.

(5) Silver, L. L., and Bostian, K. A. (1993) Discovery and development of new antibiotics: the problem of antibiotic resistance. *Antimicrob Agents Chemother 37*, 377-83.

(6) Cornelis, P. (2008) *Pseudomonas* Genomics and Molecular Biology, Caister Academic Press, Norfolk, UK.

(7) Poole, K., and McKay, G. A. (2003) Iron acquisition and its control in *Pseudomonas aeruginosa*: many roads lead to Rome. *Front Biosci 8*, d661-86.

(8) Guerinot, M. L. (1994) Microbial iron transport. *Annu Rev Microbiol 48*, 743-72.

(9) Braun, V., and Killmann, H. (1999) Bacterial solutions to the iron-supply problem. *Trends Biochem Sci 24*, 104-9.

(10) Otto, B. R., Verweij-van Vught, A. M., and MacLaren, D. M. (1992) Transferrins and heme-compounds as iron sources for pathogenic bacteria. *Crit Rev Microbiol 18*, 217-33.

(11) Jurado, R. L. (1997) Iron, infections, and anemia of inflammation. *Clin Infect Dis 25*, 888-95.

(12) Miethke, M., and Marahiel, M. A. (2007) Siderophore-Based Iron Acquisition and Pathogen Control. *Microbiol Mol Biol Rev 71*, 413-451.

(13) Wooldridge, K. G., and Williams, P. H. (1993) Iron uptake mechanisms of pathogenic bacteria. *FEMS Microbiol Rev 12*, 325-48.

(14) Neilands, J. B. (1981) Microbial iron compounds. *Annu Rev Biochem 50*, 715-31.

(15) Wandersman, C., and Delepelaire, P. (2004) Bacterial iron sources: from siderophores to hemophores. *Annu Rev Microbiol 58*, 611-47.

(16) Stoebner, J. A., and Payne, S. M. (1988) Iron-regulated hemolysin production and utilization of heme and hemoglobin by *Vibrio cholerae*. *Infect Immun 56*, 2891-5.

(17) Perry, R. D., and Brubaker, R. R. (1979) Accumulation of iron by yersiniae. *J Bacteriol 137*, 1290-8.

(18) Skaar, E. P., Humayun, M., Bae, T., DeBord, K. L., and Schneewind, O. (2004) Iron-source preference of *Staphylococcus aureus* infections. *Science 305*, 1626-8.

(19) Rouault, T. A. (2004) Microbiology. Pathogenic bacteria prefer heme. *Science 305*, 1577-8.

(20) Neilands, J. B. (1993) Siderophores. *Arch Biochem Biophys 302*, 1-3.

(21) Renshaw, J. C., Robson, G. D., Trinci, A. P. J., Weibe, M. G., Livens, F. R., Collison, D., and Taylor, R. J. (2002) Fungal siderophores: structures, functions and applications. *Mycol. Res. 106*, 1123-1142.

(22) Williams, P. H. (1979) Novel iron uptake system specified by *ColV* plasmids: an important component in the virulence of invasive strains of *Escherichia coli*. *Infect Immun 26*, 925-32.

(23) Yancey, R. J., Breeding, S. A., and Lankford, C. E. (1979) Enterochelin (enterobactin): virulence factor for *Salmonella typhimurium*. *Infect Immun 24*, 174-80.

(24) Crosa, J. H. (1980) A plasmid associated with virulence in the marine fish pathogen *Vibrio anguillarum* specifies an iron-sequestering system. *Nature 284*, 566-8.

(25) Ankenbauer, R., Sriyosachati, S., and Cox, C. D. (1985) Effects of siderophores on the growth of *Pseudomonas aeruginosa* in human serum and transferrin. *Infect Immun 49*, 132-40.

(26) Cox, C. D. (1982) Effect of pyochelin on the virulence of *Pseudomonas aeruginosa*. *Infect Immun 36*, 17-23.

(27) Sokol, P. A. (1987) Surface expression of ferripyochelin-binding protein is required for virulence of *Pseudomonas aeruginosa*. *Infect Immun 55*, 2021-5.

(28) Sriyosachati, S., and Cox, C. D. (1986) Siderophore-mediated iron acquisition from transferrin by *Pseudomonas aeruginosa*. *Infect Immun 52*, 885-91.

(29) Finkelstein, R. A., and Yancey, R. J. (1981) Effect of siderophores on virulence of *Neisseria gonorrhoeae*. *Infect Immun 32*, 609-13.

(30) de Lorenzo, V., Giovannini, F., Herrero, M., and Neilands, J. B. (1988) Metal ion regulation of gene expression. Fur repressor-operator interaction at the promoter region of the aerobactin system of *pColV-K30*. *J Mol Biol 203*, 875-84.

(31) Hunt, M. D., Pettis, G. S., and McIntosh, M. A. (1994) Promoter and operator determinants for fur-mediated iron regulation in the bidirectional *fepA-fes* control region of the *Escherichia coli* enterobactin gene system. *J Bacteriol 176*, 3944-55.

(32) O'Sullivan, D. J., and O'Gara, F. (1991) Regulation of iron assimilation: nucleotide sequence analysis of an iron-regulated promoter from a fluorescent pseudomonad. *Mol Gen Genet 228*, 1-8.

(33) Prince, R. W., Cox, C. D., and Vasil, M. L. (1993) Coordinate regulation of siderophore and exotoxin A production: molecular cloning and sequencing of the *Pseudomonas aeruginosa fur* gene. *J Bacteriol 175*, 2589-98.

(34) Venturi, V., Weisbeek, P., and Koster, M. (1995) Gene regulation of siderophore-mediated iron acquisition in Pseudomonas: not only the Fur repressor. *Mol Microbiol 17*, 603-10.

(35) Hantke, K. (2001) Iron and metal regulation in bacteria. *Curr Opin Microbiol 4*, 172-7.

(36) Bagg, A., and Neilands, J. B. (1987) Ferric uptake regulation protein acts as a repressor, employing iron (II) as a cofactor to bind the operator of an iron transport operon in *Escherichia coli*. *Biochemistry 26*, 5471-7.

(37) Rombel, I. T., McMorran, B. J., and Lamont, I. L. (1995) Identification of a DNA sequence motif required for expression of iron-regulated genes in pseudomonads. *Mol Gen Genet 246*, 519-28.

(38) Visca, P., Ciervo, A., and Orsi, N. (1994) Cloning and nucleotide sequence of the *pvdA* gene encoding the pyoverdin biosynthetic enzyme L-ornithine N5-oxygenase in *Pseudomonas aeruginosa*. *J Bacteriol 176*, 1128-40.

(39) Ochsner, U. A., Vasil, A. I., and Vasil, M. L. (1995) Role of the ferric uptake regulator of *Pseudomonas aeruginosa* in the regulation of siderophores and exotoxin A expression: purification and activity on iron-regulated promoters. *J Bacteriol 177*, 7194-201.

(40) Lamont, I. L., Beare, P. A., Ochsner, U., Vasil, A. I., and Vasil, M. L. (2002) Siderophore-mediated signaling regulates virulence factor production in *Pseudomonas aeruginosa*. *Proc Natl Acad Sci U S A 99*, 7072-7.

(41) Cunliffe, H. E., Merriman, T. R., and Lamont, I. L. (1995) Cloning and characterization of *pvdS*, a gene required for pyoverdine synthesis in *Pseudomonas aeruginosa*: PvdS is probably an alternative sigma factor. *J Bacteriol 177*, 2744-50.

(42) Braun, V., Mahren, S., and Ogierman, M. (2003) Regulation of the FecI-type ECF sigma factor by transmembrane signalling. *Curr Opin Microbiol 6*, 173-80.

(43) Miyazaki, H., Kato, H., Nakazawa, T., and Tsuda, M. (1995) A positive regulatory gene, *pvdS*, for expression of pyoverdin biosynthetic genes in *Pseudomonas aeruginosa* PAO. *Mol Gen Genet 248*, 17-24.

(44) Wilson, M. J., McMorran, B. J., and Lamont, I. L. (2001) Analysis of promoters recognized by PvdS, an extracytoplasmic-function sigma factor protein from *Pseudomonas aeruginosa*. *J Bacteriol 183*, 2151-5.

(45) Tseng, T. T., Gratwick, K. S., Kollman, J., Park, D., Nies, D. H., Goffeau, A., and Saier, M. H., Jr. (1999) The RND permease superfamily: an ancient, ubiquitous and diverse family that includes human disease and development proteins. *J Mol Microbiol Biotechnol 1*, 107-25.

(46) Poole, K., Heinrichs, D. E., and Neshat, S. (1993) Cloning and sequence analysis of an EnvCD homologue in *Pseudomonas aeruginosa*: regulation by iron and possible involvement in the secretion of the siderophore pyoverdine. *Mol Microbiol 10*, 529-44.

(47) Poole, K., Krebes, K., McNally, C., and Neshat, S. (1993) Multiple antibiotic resistance in *Pseudomonas aeruginosa*: evidence for involvement of an efflux operon. *J Bacteriol 175*, 7363-72.

(48) Li, X. Z., Nikaido, H., and Poole, K. (1995) Role of *mexA-mexB-oprM* in antibiotic efflux in *Pseudomonas aeruginosa*. *Antimicrob Agents Chemother 39*, 1948-53.

(49) Koebnik, R., Locher, K. P., and Van Gelder, P. (2000) Structure and function of bacterial outer membrane proteins: barrels in a nutshell. *Mol Microbiol 37*, 239-53.

(50) Kadner, R. J. (1990) Vitamin B12 transport in *Escherichia coli*: energy coupling between membranes. *Mol Microbiol 4*, 2027-33.

(51) Locher, K. P., Rees, B., Koebnik, R., Mitschler, A., Moulinier, L., Rosenbusch, J. P., and Moras, D. (1998) Transmembrane signaling across the ligand-gated FhuA receptor: crystal structures of free and ferrichrome-bound states reveal allosteric changes. *Cell 95*, 771-8.

(52) Ferguson, A. D., Hofmann, E., Coulton, J. W., Diederichs, K., and Welte, W. (1998) Siderophore-mediated iron transport: crystal structure of FhuA with bound lipopolysaccharide. *Science 282*, 2215-20.

(53) Pawelek, P. D., Croteau, N., Ng-Thow-Hing, C., Khursigara, C. M., Moiseeva, N., Allaire, M., and Coulton, J. W. (2006) Structure of TonB in complex with FhuA, *E. coli* outer membrane receptor. *Science 312*, 1399-402.

(54) Larsen, R. A., Foster-Hartnett, D., McIntosh, M. A., and Postle, K. (1997) Regions of *Escherichia coli* TonB and FepA proteins essential for *in vivo* physical interactions. *J Bacteriol 179*, 3213-21.

(55) Moeck, G. S., Coulton, J. W., and Postle, K. (1997) Cell envelope signaling in *Escherichia coli*. Ligand binding to the ferrichrome-iron receptor *fhua* promotes interaction with the energy-transducing protein TonB. *J Biol Chem 272*, 28391-7.

(56) Moeck, G. S., and Coulton, J. W. (1998) TonB-dependent iron acquisition: mechanisms of siderophore-mediated active transport. *Mol Microbiol 28*, 675-81.

(57) Bradbeer, C. (1993) The proton motive force drives the outer membrane transport of cobalamin in *Escherichia coli*. *J Bacteriol 175*, 3146-50.

(58) Postle, K. (1993) TonB protein and energy transduction between membranes. *J Bioenerg Biomembr 25*, 591-601.

(59) Braun, V., Killmann, H., and Benz, R. (1994) Energy-coupled transport through the outer membrane of *Escherichia coli* small deletions in the gating loop convert the FhuA transport protein into a diffusion channel. *FEBS Lett 346*, 59-64.

(60) Higgs, P. I., Larsen, R. A., and Postle, K. (2002) Quantification of known components of the *Escherichia coli* TonB energy transduction system: TonB, ExbB, ExbD and FepA. *Mol Microbiol 44*, 271-81.

(61) Stephens, D. L., Choe, M. D., and Earhart, C. F. (1995) *Escherichia coli* periplasmic protein FepB binds ferrienterobactin. *Microbiology 141 (Pt 7)*, 1647-54.

(62) Chenault, S. S., and Earhart, C. F. (1991) Organization of genes encoding membrane proteins of the *Escherichia coli* ferrienterobactin permease. *Mol Microbiol 5*, 1405-13.

(63) Shea, C. M., and McIntosh, M. A. (1991) Nucleotide sequence and genetic organization of the ferric enterobactin transport system: homology to other

periplasmic binding protein-dependent systems in *Escherichia coli*. *Mol Microbiol 5*, 1415-28.

(64) Miethke, M., Klotz, O., Linne, U., May, J. J., Beckering, C. L., and Marahiel, M. A. (2006) Ferri-bacillibactin uptake and hydrolysis in *Bacillus subtilis*. *Mol Microbiol 61*, 1413-27.

(65) Clarke, T. E., Ku, S. Y., Dougan, D. R., Vogel, H. J., and Tari, L. W. (2000) The structure of the ferric siderophore binding protein FhuD complexed with gallichrome. *Nat Struct Biol 7*, 287-91.

(66) Clarke, T. E., Braun, V., Winkelmann, G., Tari, L. W., and Vogel, H. J. (2002) X-ray crystallographic structures of the *Escherichia coli* periplasmic protein FhuD bound to hydroxamate-type siderophores and the antibiotic albomycin. *J Biol Chem 277*, 13966-72.

(67) Ankenbauer, R. G., and Quan, H. N. (1994) FptA, the Fe(III)-pyochelin receptor of *Pseudomonas aeruginosa*: a phenolate siderophore receptor homologous to hydroxamate siderophore receptors. *J Bacteriol 176*, 307-19.

(68) Cobessi, D., Celia, H., and Pattus, F. (2005) Crystal structure at high resolution of ferric-pyochelin and its membrane receptor FptA from *Pseudomonas aeruginosa*. *J Mol Biol 352*, 893-904.

(69) Cobessi, D., Celia, H., Folschweiller, N., Schalk, I. J., Abdallah, M. A., and Pattus, F. (2005) The crystal structure of the pyoverdine outer membrane receptor FpvA from *Pseudomonas aeruginosa* at 3.6 angstroms resolution. *J Mol Biol 347*, 121-34.

(70) Wirth, C., Meyer-Klaucke, W., Pattus, F., and Cobessi, D. (2007) From the periplasmic signaling domain to the extracellular face of an outer membrane signal transducer of *Pseudomonas aeruginosa*: crystal structure of the ferric pyoverdine outer membrane receptor. *J Mol Biol 368*, 398-406.

(71) Langman, L., Young, I. G., Frost, G. E., Rosenberg, H., and Gibson, F. (1972) Enterochelin system of iron transport in *Escherichia coli*: mutations affecting ferric-enterochelin esterase. *J Bacteriol 112*, 1142-9.

(72) Cox, C. D. (1980) Iron reductases from *Pseudomonas aeruginosa*. *J Bacteriol 141*, 199-204.

(73) Halle, F., and Meyer, J. M. (1992) Ferrisiderophore reductases of Pseudomonas. Purification, properties and cellular location of the *Pseudomonas aeruginosa* ferripyoverdine reductase. *Eur J Biochem 209*, 613-20.

(74) Halle, F., and Meyer, J. M. (1992) Iron release from ferrisiderophores. A multi-step mechanism involving a NADH/FMN oxidoreductase and a chemical reduction by FMNH2. *Eur J Biochem 209*, 621-7.

(75) Crosa, J. H., and Walsh, C. T. (2002) Genetics and assembly line enzymology of siderophore biosynthesis in bacteria. *Microbiol Mol Biol Rev 66*, 223-49.

(76) Challis, G. L. (2005) A widely distributed bacterial pathway for siderophore biosynthesis independent of nonribosomal peptide synthetases. *Chembiochem 6*, 601-11.

(77) Wendenbaum, S., Demange, P., Dell, A., Meyer, J. M., and Abdallah, M. A. (1983) The Structure of Pyoverdine Pa, the Siderophore of *Pseudomonas aeruginosa*. *Tetrahedron Letters 24*, 4877-4880.

(78) Cox, C. D., and Adams, P. (1985) Siderophore activity of pyoverdin for *Pseudomonas aeruginosa*. *Infect Immun 48*, 130-8.

(79) Meyer, J. M. (2000) Pyoverdines: pigments, siderophores and potential taxonomic markers of fluorescent *Pseudomonas* species. *Arch Microbiol 174*, 135-42.

(80) Boukhalfa, H., and Crumbliss, A. L. (2002) Chemical aspects of siderophore mediated iron transport. *Biometals 15*, 325-39.

(81) Wolz, C., Hohloch, K., Ocaktan, A., Poole, K., Evans, R. W., Rochel, N., Albrecht-Gary, A. M., Abdallah, M. A., and Doring, G. (1994) Iron release from transferrin by pyoverdin and elastase from *Pseudomonas aeruginosa*. *Infect Immun 62*, 4021-7.

(82) Takase, H., Nitanai, H., Hoshino, K., and Otani, T. (2000) Impact of siderophore production on *Pseudomonas aeruginosa* infections in immunosuppressed mice. *Infect Immun 68*, 1834-9.

(83) Smith, E. E., Sims, E. H., Spencer, D. H., Kaul, R., and Olson, M. V. (2005) Evidence for diversifying selection at the pyoverdine locus of *Pseudomonas aeruginosa*. *J Bacteriol 187*, 2138-47.

(84) Lamont, I. L., Martin, L. W., Sims, T., Scott, A., and Wallace, M. (2006) Characterization of a gene encoding an acetylase required for pyoverdine synthesis in *Pseudomonas aeruginosa*. *J Bacteriol 188*, 3149-52.

(85) Meyer, J. M., Hohnadel, D., Khan, A., and Cornelis, P. (1990) Pyoverdin-facilitated iron uptake in *Pseudomonas aeruginosa*: immunological characterization of the ferripyoverdin receptor. *Mol Microbiol 4*, 1401-5.

(86) Poole, K., Neshat, S., and Heinrichs, D. (1991) Pyoverdine-mediated iron transport in *Pseudomonas aeruginosa*: involvement of a high-molecular-mass outer membrane protein. *FEMS Microbiol Lett 62*, 1-5.

(87) Poole, K., Neshat, S., Krebes, K., and Heinrichs, D. E. (1993) Cloning and nucleotide sequence analysis of the ferripyoverdine receptor gene *fpvA* of *Pseudomonas aeruginosa*. *J Bacteriol 175*, 4597-604.

(88) Schalk, I. J., Kyslik, P., Prome, D., van Dorsselaer, A., Poole, K., Abdallah, M. A., and Pattus, F. (1999) Copurification of the FpvA ferric pyoverdin receptor of *Pseudomonas aeruginosa* with its iron-free ligand: implications for siderophore-mediated iron transport. *Biochemistry 38*, 9357-65.

(89) Schalk, I. J., Hennard, C., Dugave, C., Poole, K., Abdallah, M. A., and Pattus, F. (2001) Iron-free pyoverdin binds to its outer membrane receptor FpvA in *Pseudomonas aeruginosa*: a new mechanism for membrane iron transport. *Mol Microbiol 39*, 351-60.

(90) Schalk, I. J., Abdallah, M. A., and Pattus, F. (2002) Recycling of pyoverdin on the FpvA receptor after ferric pyoverdin uptake and dissociation in *Pseudomonas aeruginosa*. *Biochemistry 41*, 1663-71.

(91) Schalk, I. J., Abdallah, M. A., and Pattus, F. (2002) A new mechanism for membrane iron transport in *Pseudomonas aeruginosa*. *Biochem Soc Trans 30*, 702-5.

(92) Cox, C. D., and Graham, R. (1979) Isolation of an iron-binding compound from *Pseudomonas aeruginosa*. *J Bacteriol 137*, 357-64.

(93) Cox, C. D., Rinehart, K. L., Jr., Moore, M. L., and Cook, J. C., Jr. (1981) Pyochelin: novel structure of an iron-chelating growth promoter for *Pseudomonas aeruginosa*. *Proc Natl Acad Sci U S A 78*, 4256-60.

(94) Ankenbauer, R. G., Toyokuni, T., Staley, A., Rinehart, K. L., Jr., and Cox, C. D. (1988) Synthesis and biological activity of pyochelin, a siderophore of *Pseudomonas aeruginosa*. *J Bacteriol 170*, 5344-51.

(95) Namiranian, S., Richardson, D. J., Russell, D. A., and Sodeau, J. R. (1997) Excited state properties of the siderophore pyochelin and its complex with zinc ions. *Photochem Photobiol 65*, 777-82.

(96) Hamzehpour, M. M., Pechere, J. C., Plesiat, P., and Kohler, T. (1995) OprK and OprM define two genetically distinct multidrug efflux systems in *Pseudomonas aeruginosa*. *Antimicrob Agents Chemother 39*, 2392-6.

(97) Tseng, C. F., Burger, A., Mislin, G. L., Schalk, I. J., Yu, S. S., Chan, S. I., and Abdallah, M. A. (2006) Bacterial siderophores: the solution stoichiometry and coordination of the Fe(III) complexes of pyochelin and related compounds. *J Biol Inorg Chem 11*, 419-32.

(98) Sokol, P. A., and Woods, D. E. (1983) Demonstration of an iron-siderophore-binding protein in the outer membrane of *Pseudomonas aeruginosa*. *Infect Immun 40*, 665-9.

(99) Heinrichs, D. E., Young, L., and Poole, K. (1991) Pyochelin-mediated iron transport in *Pseudomonas aeruginosa*: involvement of a high-molecular-mass outer membrane protein. *Infect Immun 59*, 3680-4.

(100) Chambers, C. E., McIntyre, D. D., Mouck, M., and Sokol, P. A. (1996) Physical and structural characterization of yersiniophore, a siderophore produced by clinical isolates of *Yersinia enterocolitica*. *Biometals 9*, 157-67.

(101) Haag, H., Hantke, K., Drechsel, H., Stojiljkovic, I., Jung, G., and Zahner, H. (1993) Purification of yersiniabactin: a siderophore and possible virulence factor of *Yersinia enterocolitica*. *J Gen Microbiol 139*, 2159-65.

(102) Perry, R. D., Balbo, P. B., Jones, H. A., Fetherston, J. D., and DeMoll, E. (1999) Yersiniabactin from *Yersinia pestis*: biochemical characterization of the siderophore and its role in iron transport and regulation. *Microbiology 145 (Pt 5)*, 1181-90.

(103) Gehring, A. M., DeMoll, E., Fetherston, J. D., Mori, I., Mayhew, G. F., Blattner, F. R., Walsh, C. T., and Perry, R. D. (1998) Iron acquisition in plague: modular logic in enzymatic biogenesis of yersiniabactin by *Yersinia pestis*. *Chem Biol 5*, 573-86.

(104) Fetherston, J. D., Bertolino, V. J., and Perry, R. D. (1999) YbtP and YbtQ: two ABC transporters required for iron uptake in *Yersinia pestis*. *Mol Microbiol 32*, 289-99.

(105) Brem, D., Pelludat, C., Rakin, A., Jacobi, C. A., and Heesemann, J. (2001) Functional analysis of yersiniabactin transport genes of *Yersinia enterocolitica*. *Microbiology 147*, 1115-27.

(106) Quadri, L. E. (2000) Assembly of aryl-capped siderophores by modular peptide synthetases and polyketide synthases. *Mol Microbiol 37*, 1-12.

(107) Mossialos, D., Ochsner, U., Baysse, C., Chablain, P., Pirnay, J. P., Koedam, N., Budzikiewicz, H., Fernandez, D. U., Schafer, M., Ravel, J., and Cornelis, P. (2002) Identification of new, conserved, non-ribosomal peptide synthetases from fluorescent pseudomonads involved in the biosynthesis of the siderophore pyoverdine. *Mol Microbiol 45*, 1673-85.

(108) Ackerley, D. F., Caradoc-Davies, T. T., and Lamont, I. L. (2003) Substrate specificity of the nonribosomal peptide synthetase PvdD from *Pseudomonas aeruginosa*. *J Bacteriol 185*, 2848-55.

(109) Fischbach, M. A., and Walsh, C. T. (2006) Assembly-line enzymology for polyketide and nonribosomal Peptide antibiotics: logic, machinery, and mechanisms. *Chem Rev 106*, 3468-96.

(110) Keating, T. A., Marshall, C. G., Walsh, C. T., and Keating, A. E. (2002) The structure of VibH represents nonribosomal peptide synthetase condensation, cyclization and epimerization domains. *Nat Struct Biol 9*, 522-6.

(111) Conti, E., Stachelhaus, T., Marahiel, M. A., and Brick, P. (1997) Structural basis for the activation of phenylalanine in the non-ribosomal biosynthesis of gramicidin S. *Embo J 16*, 4174-83.

(112) May, J. J., Kessler, N., Marahiel, M. A., and Stubbs, M. T. (2002) Crystal structure of DhbE, an archetype for aryl acid activating domains of modular nonribosomal peptide synthetases. *Proc Natl Acad Sci U S A 99*, 12120-5.

(113) Quadri, L. E., Weinreb, P. H., Lei, M., Nakano, M. M., Zuber, P., and Walsh, C. T. (1998) Characterization of Sfp, a *Bacillus subtilis* phosphopantetheinyl transferase for peptidyl carrier protein domains in peptide synthetases. *Biochemistry 37*, 1585-95.

(114) Bobrov, A. G., Geoffroy, V. A., and Perry, R. D. (2002) Yersiniabactin production requires the thioesterase domain of HMWP2 and YbtD, a putative phosphopantetheinylate transferase. *Infect Immun 70*, 4204-14.

(115) Barekzi, N., Joshi, S., Irwin, S., Ontl, T., and Schweizer, H. P. (2004) Genetic characterization of *pcpS*, encoding the multifunctional phosphopantetheinyl transferase of *Pseudomonas aeruginosa*. *Microbiology 150*, 795-803.

(116) Reimmann, C., Patel, H. M., Serino, L., Barone, M., Walsh, C. T., and Haas, D. (2001) Essential PchG-dependent reduction in pyochelin biosynthesis of *Pseudomonas aeruginosa*. *J Bacteriol 183*, 813-20.

(117) Patel, H. M., and Walsh, C. T. (2001) *In vitro* reconstitution of the *Pseudomonas aeruginosa* nonribosomal peptide synthesis of pyochelin: characterization of backbone tailoring thiazoline reductase and N-methyltransferase activities. *Biochemistry 40*, 9023-31.

(118) Geoffroy, V. A., Fetherston, J. D., and Perry, R. D. (2000) *Yersinia pestis* YbtU and YbtT are involved in synthesis of the siderophore yersiniabactin but have different effects on regulation. *Infect Immun 68*, 4452-61.

(119) Stintzi, A., Johnson, Z., Stonehouse, M., Ochsner, U., Meyer, J. M., Vasil, M. L., and Poole, K. (1999) The *pvc* gene cluster of *Pseudomonas aeruginosa*: role in synthesis of the pyoverdine chromophore and regulation by PtxR and PvdS. *J Bacteriol 181*, 4118-24.

(120) Lamont, I. L., and Martin, L. W. (2003) Identification and characterization of novel pyoverdine synthesis genes in *Pseudomonas aeruginosa*. *Microbiology 149*, 833-42.

(121) Lehoux, D. E., Sanschagrin, F., and Levesque, R. C. (2000) Genomics of the 35-kb *pvd* locus and analysis of novel *pvdIJK* genes implicated in pyoverdine biosynthesis in *Pseudomonas aeruginosa*. *FEMS Microbiol Lett 190*, 141-6.

(122) Ravel, J., and Cornelis, P. (2003) Genomics of pyoverdine-mediated iron uptake in pseudomonads. *Trends Microbiol 11*, 195-200.

(123) Merriman, T. R., Merriman, M. E., and Lamont, I. L. (1995) Nucleotide sequence of *pvdD*, a pyoverdine biosynthetic gene from *Pseudomonas aeruginosa*: PvdD has similarity to peptide synthetases. *J Bacteriol 177*, 252-8.

(124) Visca, P., Serino, L., and Orsi, N. (1992) Isolation and characterization of *Pseudomonas aeruginosa* mutants blocked in the synthesis of pyoverdin. *J Bacteriol 174*, 5727-31.

(125) Ambrosi, C., Leoni, L., and Visca, P. (2002) Different responses of pyoverdine genes to autoinduction in *Pseudomonas aeruginosa* and the group *Pseudomonas fluorescens-Pseudomonas putida*. *Appl Environ Microbiol 68*, 4122-6.

(126) Ambrosi, C., Leoni, L., Putignani, L., Orsi, N., and Visca, P. (2000) Pseudobactin biogenesis in the plant growth-promoting rhizobacterium *Pseudomonas* strain B10: identification and functional analysis of the L-ornithine N(5)-oxygenase (*psbA*) gene. *J Bacteriol 182*, 6233-8.

(127) Putignani, L., Ambrosi, C., Ascenzi, P., and Visca, P. (2004) Expression of L-ornithine Ndelta-oxygenase (PvdA) in fluorescent *Pseudomonas* species: an immunochemical and *in silico* study. *Biochem Biophys Res Commun 313*, 245-57.

(128) McMorran, B. J., Kumara, H. M., Sullivan, K., and Lamont, I. L. (2001) Involvement of a transformylase enzyme in siderophore synthesis in *Pseudomonas aeruginosa*. *Microbiology 147*, 1517-24.

(129) Gaille, C., Kast, P., and Haas, D. (2002) Salicylate biosynthesis in *Pseudomonas aeruginosa*. Purification and characterization of PchB, a novel bifunctional enzyme displaying isochorismate pyruvate-lyase and chorismate mutase activities. *J Biol Chem 277*, 21768-75.

(130) Gaille, C., Reimmann, C., and Haas, D. (2003) Isochorismate synthase (PchA), the first and rate-limiting enzyme in salicylate biosynthesis of *Pseudomonas aeruginosa*. *J Biol Chem 278*, 16893-8.

(131) Zaitseva, J., Lu, J., Olechoski, K. L., and Lamb, A. L. (2006) Two crystal structures of the isochorismate pyruvate lyase from *Pseudomonas aeruginosa*. *J Biol Chem 281*, 33441-9.

(132) Reimmann, C., Patel, H. M., Walsh, C. T., and Haas, D. (2004) PchC thioesterase optimizes nonribosomal biosynthesis of the peptide siderophore pyochelin in *Pseudomonas aeruginosa*. *J Bacteriol 186*, 6367-73.

(133) Quadri, L. E., Keating, T. A., Patel, H. M., and Walsh, C. T. (1999) Assembly of the *Pseudomonas aeruginosa* nonribosomal peptide siderophore pyochelin: *In vitro* reconstitution of aryl-4, 2-bisthiazoline synthetase activity from PchD, PchE, and PchF. *Biochemistry 38*, 14941-54.

(134) Reimmann, C., Serino, L., Beyeler, M., and Haas, D. (1998) Dihydroaeruginoic acid synthetase and pyochelin synthetase, products of the *pchEF* genes, are induced by extracellular pyochelin in *Pseudomonas aeruginosa*. *Microbiology 144 (Pt 11)*, 3135-48.

(135) Patel, H. M., Tao, J., and Walsh, C. T. (2003) Epimerization of an L-cysteinyl to a D-cysteinyl residue during thiazoline ring formation in siderophore chain elongation by pyochelin synthetase from *Pseudomonas aeruginosa*. *Biochemistry 42*, 10514-27.

(136) Carniel, E. (2001) The *Yersinia* high-pathogenicity island: an iron-uptake island. *Microbes Infect 3*, 561-9.

(137) Rakin, A., Noelting, C., Schubert, S., and Heesemann, J. (1999) Common and specific characteristics of the high-pathogenicity island of *Yersinia enterocolitica*. *Infect Immun 67*, 5265-74.

(138) Fetherston, J. D., Schuetze, P., and Perry, R. D. (1992) Loss of the pigmentation phenotype in *Yersinia pestis* is due to the spontaneous deletion of 102 kb of chromosomal DNA which is flanked by a repetitive element. *Mol Microbiol 6*, 2693-704.

(139) Fetherston, J. D., and Perry, R. D. (1994) The pigmentation locus of *Yersinia pestis* KIM6+ is flanked by an insertion sequence and includes the structural genes for pesticin sensitivity and HMWP2. *Mol Microbiol 13*, 697-708.

(140) Bearden, S. W., Fetherston, J. D., and Perry, R. D. (1997) Genetic organization of the yersiniabactin biosynthetic region and construction of avirulent mutants in *Yersinia pestis*. *Infect Immun 65*, 1659-68.

(141) Miller, D. A., Luo, L., Hillson, N., Keating, T. A., and Walsh, C. T. (2002) Yersiniabactin synthetase: a four-protein assembly line producing the nonribosomal peptide/polyketide hybrid siderophore of *Yersinia pestis*. *Chem Biol 9*, 333-44.

(142) Pelludat, C., Brem, D., and Heesemann, J. (2003) Irp9, encoded by the high-pathogenicity island of *Yersinia enterocolitica*, is able to convert chorismate into salicylate, the precursor of the siderophore yersiniabactin. *J Bacteriol 185*, 5648-53.

(143) Kerbarh, O., Bulloch, E. M., Payne, R. J., Sahr, T., Rebeille, F., and Abell, C. (2005) Mechanistic and inhibition studies of chorismate-utilizing enzymes. *Biochem Soc Trans 33*, 763-6.

(144) Kerbarh, O., Ciulli, A., Howard, N. I., and Abell, C. (2005) Salicylate biosynthesis: overexpression, purification, and characterization of Irp9, a bifunctional salicylate synthase from *Yersinia enterocolitica*. *J Bacteriol 187*, 5061-6.

(145) Kerbarh, O., Chirgadze, D. Y., Blundell, T. L., and Abell, C. (2006) Crystal structures of *Yersinia enterocolitica* salicylate synthase and its complex with the reaction products salicylate and pyruvate. *J Mol Biol 357*, 524-34.

(146) Gehring, A. M., Mori, I. I., Perry, R. D., and Walsh, C. T. (1998) The nonribosomal peptide synthetase HMWP2 forms a thiazoline ring during biogenesis of yersiniabactin, an iron-chelating virulence factor of *Yersinia pestis*. *Biochemistry 37*, 17104.

(147) Suo, Z., Walsh, C. T., and Miller, D. A. (1999) Tandem heterocyclization activity of the multidomain 230 kDa HMWP2 subunit of *Yersinia pestis* yersiniabactin synthetase: interaction of the 1-1382 and 1383-2035 fragments. *Biochemistry 38*, 17000.

(148) Keating, T. A., Miller, D. A., and Walsh, C. T. (2000) Expression, purification, and characterization of HMWP2, a 229 kDa, six domain protein subunit of Yersiniabactin synthetase. *Biochemistry 39*, 4729-39.

(149) Miller, D. A., and Walsh, C. T. (2001) Yersiniabactin synthetase: probing the recognition of carrier protein domains by the catalytic heterocyclization domains, Cy1 and Cy2, in the chain-initiating HWMP2 subunit. *Biochemistry 40*, 5313-21.

(150) Suo, Z., Tseng, C. C., and Walsh, C. T. (2001) Purification, priming, and catalytic acylation of carrier protein domains in the polyketide synthase and nonribosomal peptidyl synthetase modules of the HMWP1 subunit of yersiniabactin synthetase. *Proc Natl Acad Sci U S A 98*, 99-104.

(151) Ferreras, J. A., Ryu, J. S., Di Lello, F., Tan, D. S., and Quadri, L. E. (2005) Small-molecule inhibition of siderophore biosynthesis in *Mycobacterium tuberculosis* and *Yersinia pestis*. *Nat Chem Biol 1*, 29-32.

(152) Payne, R. J., Kerbarh, O., Miguel, R. N., Abell, A. D., and Abell, C. (2005) Inhibition studies on salicylate synthase. *Org Biomol Chem 3*, 1825-7.

Chapter 2

Biochemical Characterization of PvdA, the Ornithine Hydroxylase of *Pseudomonas aeruginosa*

Hydroxymate siderophores chelate iron using formyl-hydroxyl amines, derivatives primarily of ornithine or lysine. *Pseudomonas aeruginosa* incorporates an ornithine derivative in pyoverdin (*1*). Ornithine hydroxylase (PvdA) is the first enzyme required for this derivatization. PvdA hydroxylates the side-chain primary amine and is an important initial step for the siderophore synthesis (Figure 2-1A). PvdA is most closely related functionally to the lysine hydroxylase (IucD) of *E. coli* required for aerobactin production (Figure 2-1B). However, PvdA is also functionally related to two other well-studied enzymes, *p*-hydroxybenzoate hydroxylase (PHBH) of *P. fluorescens* important for the degradation of wood (Figure 2-1C) and flavin-containing monooxygenases (FMOs) from a variety of organisms involved in xenobiotic detoxification (Figure 2-1D).

Although the sequence similarity (~40%) and identity (~20%) among IucD, PHBH, and FMO are low, these enzymes share some biochemical properties such as a requirement for FAD and NADPH (*2-4*). Recently, PvdA has been shown to also require FAD and NADPH for activity (*5*). During the reaction, NADPH reduces the FAD, which then covalently binds molecular oxygen (Figure 2-1). One oxygen atom

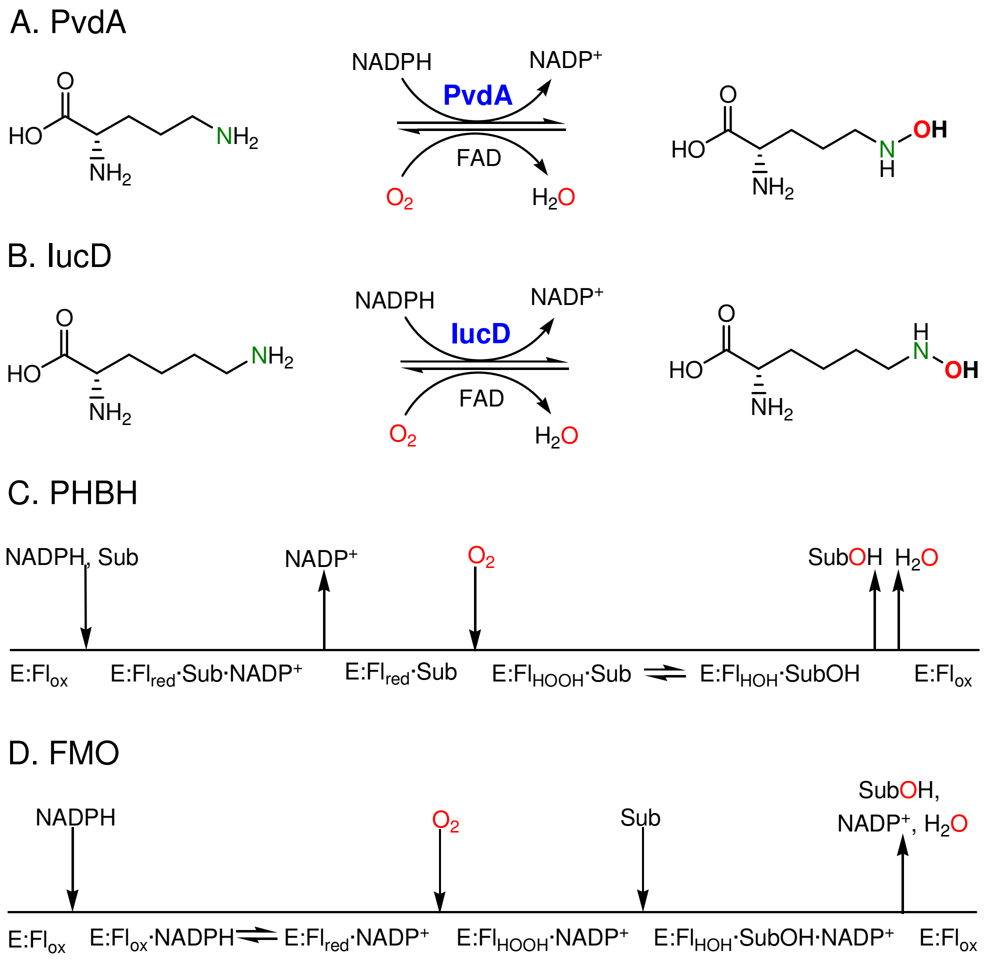
A. PvdA
NADPH
NADP+
PvdA
FAD
O2
H2O
HO
O
NH2
NH2
OH
N
H
B. IucD
NADPH
NADP+
IucD
FAD
O2
H2O
HO
O
NH2
NH2
H
N
OH
C. PHBH
NADPH, Sub
NADP+
O2
SubOH
H2O
E:Flox
E:Flred·Sub·NADP+
E:Flred·Sub
E:FlHOOH·Sub
E:FlHOH·SubOH
E:Flox
D. FMO
NADPH
O2
Sub
SubOH,
NADP+, H2O
E:Flox
E:Flox·NADPH
E:Flred·NADP+
E:FlHOOH·NADP+
E:FlHOH·SubOH·NADP+
E:Flox

Figure 2-1: Reaction schemes for (*A*) the ornithine hydroxylase (PvdA) from *P. aeruginosa*, (*B*) the lysine hydroxylase (IucD) from *E. coli*, (*C*) *p*-hydroxybenzoate hydroxylase (PHBH) from *P. fluorescens*, and (*D*) flavin-containing monooxygenase (FMO) from hog liver microsomes. The hydroxlated amines of PvdA and IucD are labeled in green and the oxygen atoms added to the substrate are labeled in red. The substrate for PHBH (*p*-hydroxybenzoate) and FMO (nucleophilic and some electrophilic compounds) are labeled as Sub and the flavin states are labeled as oxidized (Fl_{ox}), reduced (Fl_{red}), hydroperoxyflavin intermediate (Fl_{HOOH}), and hydroxyflavin intermediate (Fl_{HOH}).

is used for hydroxylation of the primary side-chain of ornithine (PvdA), lysine (IucD), the aromatic ring of *p*-hydroxybenzoate (PHBH), or a variety of nucleophilic and electrophilic substrates (FMO), while the second oxygen atom is released as H_2O (*3, 5-7*).

The reaction mechanism for PvdA and IucD has not been elucidated. In contrast, the reaction mechanisms for PHBH and FMO have been well documented. PHBH and FMO both form a ternary complex between the FAD-loaded enzyme, NADPH, and the substrate during catalysis, although the reaction mechanism differs significantly between the enzymes. PHBH requires substrate to be bound before FAD reduction by NADPH (Figure 2-1C). The $NADP^+$ is released and the enzyme binds molecular oxygen. The reduced flavin passes through two transient intermediate steps before becoming reoxidized and forming the product (3,4-dihydroxybenzoate) and H_2O (*3, 8-10*). In contrast, FMO does not require substrate binding for flavin reduction (Figure 2-1D). The FAD is reduced in the presence of NADPH and upon binding molecular oxygen, forms a stable hydroperoxyflavin intermediate. Once the activated FMO binds substrate, the flavin transitions through an additional intermediate (hydroxyflavin) before becoming reoxidized (*3, 11-13*).

Here we describe the preliminary characterization of PvdA, including the oligomerization state in solution, kinetics of NADPH oxidation and product formation, inhibition by substrate, lysine, chloride, and mercurial compounds, and preliminary rapid order steady-state kinetics. We put these new data together with what is known about IucD, PHBH, and FMO to provide insights into the reaction mechanism for PvdA. This work is the first step toward designing inhibitors for use as novel antimicrobials to reduce the virulence of *P. aeruginosa* and potentially bacteria with related siderophore pathways.

Materials and Methods

Cloning of PvdA. PAO1 *P. aeruginosa* genomic DNA was isolated from a culture kindly provided by Dr. Jeffrey Urbauer. Primers to the *pvdA* gene were designed to include an *Nde*I site (underlined) in the forward primer (5'-GAA TTC CAT ATG ACT CAG GCA ACT GCA ACC-3') and a *Hind*III site (underlined) in the reverse primer (5'-CCC AAG CTT TCA GCT GGC CAG GGC GTG-3'). The *pvdA* gene was amplified by polymerase chain reaction with Herculase polymerase (Stratagene), used for amplification of GC rich sequences. Addition of 10% dimethyl sulfoxide (DMSO) to the reaction mix acted as an adjuvant. The amplified fragment (1329 base pairs) was digested with *Nde*I and *Hind*III enzymes and ligated into the pET28b plasmid (Novagen). The resultant plasmid encodes PvdA with an N-terminal His$_6$ tag. This plasmid was transformed into BL21(DE3) *E. coli* cells (Stratagene) for protein overproduction.

PvdA Protein Overproduction and Purification. The PvdA protein was overproduced in BL21(DE3) *E. coli* containing the transformed *pvdA* expression plasmid. Optimal overproduction used LB medium containing 50 μg/ml kanamycin. The cells were grown at 37 °C with shaking (225 rpm) until an OD_{600} of ~0.8 was reached. PvdA protein production was induced with 0.2 mM isopropyl-β-D-thiogalactopyranoside and the cells were harvested after 3 – 4 hours by centrifugation (6,000 x g, 10 min, 4 °C). The pelleted cells were resuspended in 25 mM potassium phosphate, pH 8.0, 500 mM NaCl, 50 mM sodium citrate, and 5 mM imidazole (buffer A) and lysed by passage through a French pressure cell (35,000 psi). The cellular debris was removed by centrifugation (12,000 x g, 30 min, 4 °C) and the supernatant was applied to a chelating Sepharose fast flow column (Amersham Biosciences) charged with nickel chloride and pre-equilibrated in buffer A for nickel affinity chromatography. A linear gradient of 5 – 500 mM imidazole in buffer A was applied to the column and PvdA protein eluted at approximately 300 mM imidazole. The fractions containing PvdA were pooled and applied to a Superdex 200 size exclusion column (Amersham Biosciences) equilibrated with 100 mM potassium phosphate, pH 8.0, and 100 mM sodium citrate. The fractions containing PvdA were combined and concentrated with an Amicon stirred cell containing a YM-30 membrane to 9 - 13 mg/ml as determined by the Bradford assay. The purified, concentrated protein was stored at -80 °C for use in activity assays.

Oligomerization Studies. The hydrodynamic radius and oligomerization state of PvdA were measured in two buffering conditions with a PD2000DLS$^{\text{Plus}}$ Dynamic Light Scattering detector (Precision Detectors). The buffers used for determination were (1) 25 mM Tris-HCl, pH 8.0, 500 mM NaCl, and 300 mM imidazole or (2) 100 mM potassium phosphate, pH 8.0, and 100 mM sodium citrate at a PvdA concentration of 5 - 8 mg/ml. The hydrodynamic radii were also determined in the presence of excess FAD or excess FAD and ornithine to determine if substrate and coenzyme binding affected the oligomerization state. All experiments were repeated five times.

NADPH Oxidation Assay. The standard activity assay buffer contained 100 mM potassium phosphate, pH 8.0, 0.03 mM FAD, and 0.15 mM NADPH. PvdA (5 μM) was pre-incubated for 2 min at 24 °C in 1 ml assay buffer and the reaction was initiated with 5 mM L-ornithine. The oxidation of NADPH to $NADP^+$ was monitored by a decrease in absorbance at 366 nm ($\varepsilon = 2850\ M^{-1}\ cm^{-1}$) over time with a BioMate 3 spectrometer (Thermo Spectronics) at 24 °C according to the protocol described for IucD (*4*). All experiments were conducted in triplicate.

Hydroxylation Assay. Hydroxylated product formation by PvdA was determined using a variation of the Csaky iodine oxidation reaction (*14-17*). The standard assay buffer was the same as described for the NADPH oxidation assay. The reaction was initiated by the addition of 5 mM L-ornithine to 5 μM enzyme in 1 ml assay buffer at 24 °C. At each time point, 83 μl of the assay mixture was added to 42 μl 0.2 N perchloric acid to terminate the reaction and 50 μl of the reaction mixture was transferred into a well of a glass 96 well plate. The acidic reaction mixture was neutralized with 50 μl 5% (w/v) sodium acetate solution. To each well, 50 μl 1%

(w/v) sulfanilic acid in 25% (v/v) acetic acid and 20 µl 1.3 % (w/v) potassium iodide in glacial acetic acid was added. The reaction was allowed to incubate for 5 min at 25 °C for conversion of the hydroxylamine into nitrite. Excess iodide was removed from the mixture with 20 µl 0.1 N sodium thiosulfate and 20 µl 0.6% (w/v) α-naphthylamine in 30% (v/v) acetic acid was added to react with the nitrite and develop a colorimetric change. After 15 minutes of incubation, the absorbance was read at 562 nm on an Elx800 plate reader (Bio-Tek). A standard curve of known quantities of hydroxylamine hydrochloride was used to calculate the amount of hydroxylated product formed. All experiments were conducted in triplicate.

Determination of Enzyme Specificity and Kinetic Parameters. The standard assay conditions were varied to fully characterize PvdA. The pH optimum for PvdA activity was determined by measuring NADPH oxidation in 0.5 pH unit steps ranging from pH 6.0 – 10.0 in the presence and absence of ornithine. The buffers tested were (1) 100 mM potassium phosphate at pH 6.0 – 8.0, (2) 100 mM Tris-HCl at pH 7.0 – 9.0, (3) 100 mM glycine at pH 9.0 – 10.0, or (4) 33 mM potassium phosphate, 33 mM Tris-SO_4, and 33 mM glycine at pH 6.0 – 10.0. An ionic strength of at least 100 mM promoted protein solubility and stability, and was used consistently for all experiments.

PvdA specificity was determined with the NADPH oxidation and hydroxylation assays. PvdA was assayed for activity after coenzyme and substrate deletion or substitution. For the coenzyme substitution reactions, FAD was replaced with FMN and NADPH with NADH at comparable concentrations. For the substrate substitution reactions, 5 mM L-ornithine was exchanged with 5 mM of a substrate analog: DL-2,3-diaminopropionic acid, DL-2,4-diaminobutyric acid, L-lysine, 5-aminopentanoic acid, 1,4-diaminobutane, D-ornithine, or L-norleucine.

The PvdA Michaelis-Menten kinetics were assayed with L-ornithine concentrations of 0 – 15 mM. All reactions were carried out in triplicate. Data analysis and curve fitting was done with SigmaPlot 8.0®. All curves were fit with the Michaelis-Menten equation, except for substrate inhibition which was fit to the equation: $V_o = V_{max}[\text{Substrate}] / [K_m + [\text{Substrate}] + ([\text{Substrate}]^2/K_I)]$ (17).

Determination of FAD Dissociation Constant. FAD binding to PvdA was monitored as an increase in protein fluorescence upon excitation at 280 nm. The fluorescence emission was detected at 330 nm on a Cary Eclipse Fluorescence Spectrophotometer (Varian) at 24 °C. The PvdA concentration was 2.5 μM in 100 mM potassium phosphate pH 8.0. FAD was titrated into the mixture in concentrations of 0 to 60 μM. The experiment was carried out in triplicate.

Steady-State Kinetics. To determine initial steady state kinetics of PvdA, NADPH oxidation was measured with 5 μM PvdA in 1 ml of the standard assay buffer containing 0.03 mM FAD. The NADPH concentration (0.05 – 0.125 mM) was varied relative to the ornithine concentration (0.5 – 10 mM) and a double reciprocal plot was used to determine whether PvdA used a random, ordered, or ping-pong mechanism.

Inhibition Assays. Lysine inhibition was determined with the hydroxylation assay. The substrate, coenzymes and enzyme were increased in concentration as follows: 25 µM PvdA, 0.15 mM FAD, and 0.75 mM NADPH to increase the signal. L-ornithine concentrations ranged from 0.15 – 2 mM in 1 ml assay buffer containing 100 mM potassium phosphate, pH 8.0. L-lysine concentrations ranged from 0 – 10 mM. Inhibition by chloride was measured with the NADPH oxidation under standard assay conditions with sodium chloride concentrations ranging from 0 to 250 mM. Chloride inhibition was measured with respect to L-ornithine concentration (0.5 – 10 mM) or NADPH concentration (0.05 – 0.125 mM). Mercurial inhibition by *p*-chloromercuribenzoate (PCMB) was characterized by NADPH oxidation under standard assay conditions. The PCMB concentration ranged from 0 to 10 µM with L-ornithine concentrations from 0.075 – 5 mM. All experiments were conducted in triplicate.

PvdA Flavin Reduction and Reoxidation. The rate constants of flavin reduction and reoxidation were measured with a Cary 50 Bio Spectrophotometer (Varian) at 24 °C. PvdA (40 µM) was incubated in 100 mM potassium phosphate pH 8.0 with 20 µM FAD. Upon the addition of 40 µM NADPH, the absorbance from 300 – 800 nm was measured. The change in absorbance measured at 451 nm was used to determine the rate constants. The curves were fit to a sum of exponentials equation.

Results

PvdA Protein Production and Purification. The *pvdA* gene was cloned from PAO1 *P. aeruginosa* genomic DNA to generate an overproduction plasmid. The plasmid was expressed in BL21(DE3) *E. coli* cells to obtain PvdA protein with an N-terminal His_6 tag. PvdA protein was purified by nickel chelating and size exclusion chromatography to yield 20 – 45 mg of protein with ~95% purity per liter of cell culture.

Oligomerization Studies. To determine the hydrodynamic radius of PvdA in solution, the protein was subjected to Dynamic Light Scattering (Figure 2-2). PvdA was initially purified in 25 mM Tris-HCl, pH 8.0, 500 mM NaCl, and 300 mM imidazole. The average hydrodynamic radius for apo-PvdA in the high salt buffer was 4.67 nm with a small percentage of PvdA as larger species suggesting tetramers and large aggregates (Figure 2-2A). The addition of excess FAD yielded a hydrodynamic radius comparable to apo-protein, whereas the addition of excess FAD and excess ornithine to PvdA in the high salt buffer caused the protein to become principally tetrameric, with a hydrodynamic radius of 13.9 nm. However, in this buffer PvdA was not stable and would easily precipitate. In contrast, PvdA purified into 100 mM potassium phosphate, pH 8.0 and 100 mM sodium citrate was very stable and had an average hydrodynamic radius of 4.77 nm that did not vary upon the addition of excess FAD and ornithine (Figure 2-2B).

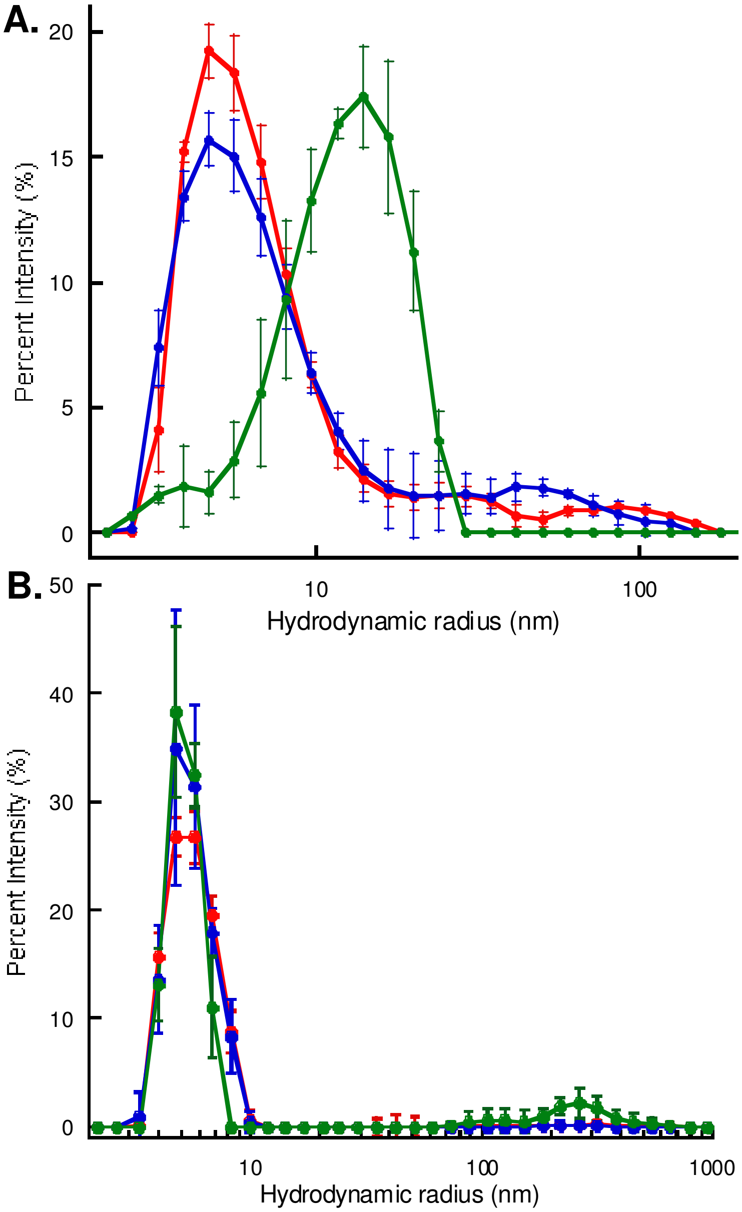

Figure 2-2: Hydrodynamic radii for PvdA in (*A*) 25 mM Tris-HCl, pH 8.0, 500 mM NaCl, 300 mM imidazole or (*B*) 100 mM potassium phosphate, pH 8.0, and 100 mM sodium citrate as determined by dynamic light scattering. The fraction of species with a particular hydrodynamic radius is plotted for apo-PvdA (red), for PvdA with excess FAD (blue), and for PvdA with excess FAD and ornithine (green).

pH Optimum for Catalytic Activity. The initial velocities of NADPH oxidation by PvdA were measured at a pH range of 6.0 to 10.0 (Figure 2-3). The pH with maximal turnover was pH 8.0 – 8.5. Therefore, the 0.1 M potassium phosphate, pH 8.0 buffer system was adopted for all remaining assays. The NADPH oxidation rate in the absence of substrate did not vary over the entire pH range indicating that enzymatic turnover in the absence of substrate, or uncoupling, is not a function of pH.

Coenzyme Specificity. With the NADPH oxidation and the hydroxylation assay, the coenzymes required for PvdA activity were determined. PvdA catalytic activity is very specific for two coenzymes, FAD and NADPH (Table 2-1, Figure 2-4). PvdA was not able to use FMN in place of FAD. NADH was not oxidized when substituted for NADPH but hydroxylated ornithine was produced at 14% of full activity. Substrate independent NADPH oxidation was detected at 2% of full activity.

FAD Dissociation Constant. No absorption peak at 450 nm was observed in the purified PvdA solution indicating that FAD does not copurify with the enzyme, suggesting that the FAD dissociation constant in PvdA is large. A K_d of 26 ± 5 μM was determined by monitoring protein fluorescence. This represents a 2.5-fold decrease from that previously reported (*5*). This difference may be due to the inclusion of chloride in the buffer systems of the previous experiments. We will show that chloride is an inhibitor of PvdA later in this chapter.

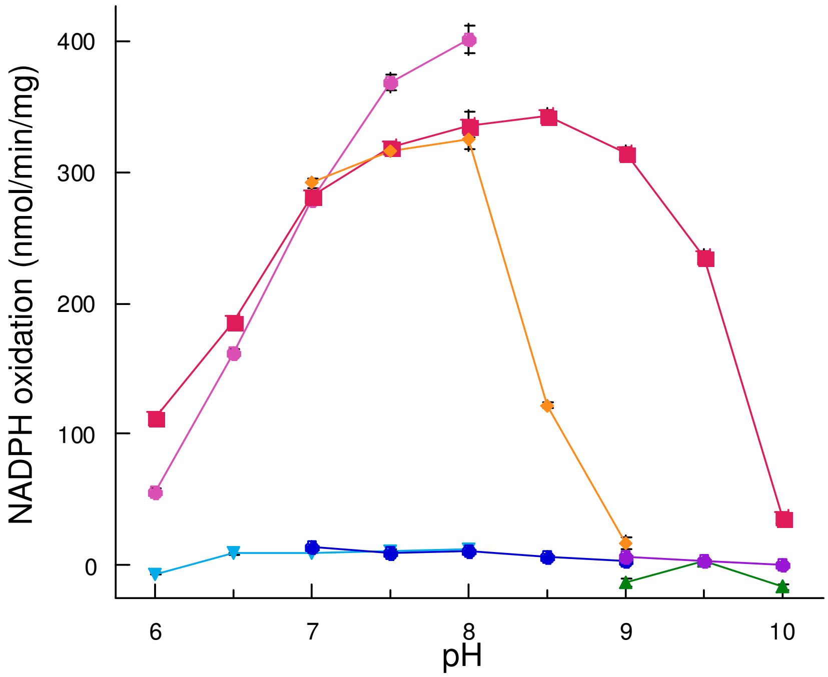

Figure 2-3: Effect of pH on PvdA activity. The rate of NADPH oxidation was measured in the presence of ornithine as a decrease in absorbance at 366 nm in 100 mM potassium phosphate at pH 6.0 – 8.0 (pink circles); 33 mM potassium phosphate, 33 mM Tris-SO_4, and 33 mM glycine at pH 6.0 – 10.0 (red squares); 100 mM Tris-HCl at pH 7.0-9.0 (orange diamonds); and 100 mM glycine at pH 9.0 – 10.0 (green triangles). The rate of NADPH oxidation was measured in the absence of ornithine in 100 mM potassium phosphate at pH 6.0 – 8.0 (cyan triangles), 100 mM Tris-HCl at pH 7.0 – 9.0 (blue circles), and 100 mM glycine at pH 9.0 – 10.0 (purple circles).

Table 2-1: Summary of the PvdA Coenzymes and Substrate Specificities

Test conditions	NADPH oxidation (nmol/min/mg)	Hydroxylated product formation (nmol/min/mg)
Omission Test		
Control	534 ± 14	321 ± 3
- FAD	*	22 ± 12
- NADPH	*	*
- L-ornithine	11 ± 1	*
Specificity		
-FAD		
+ FMN	*	*
- NADPH		
+ NADH	*	46 ± 1
- L-ornithine		
+ DL-2,3-diaminopropionic acid	8 ± 4[#]	*
+ DL-2,4-diaminobutyric acid	*	*
+ L-lysine	428 ± 4	*
+ 5-aminopentanoic acid	*	*
+ 1,4-diaminobutane	21 ± 2	*
+ D-ornithine	5 ± 3[#]	*
+ L-norleucine	*	*

* = below the limits of detection (5 nmol for the hydroxylation assay, and <1 nmol for the NADPH oxidation assay)

[#] = less than substrate independent NADPH oxidation.

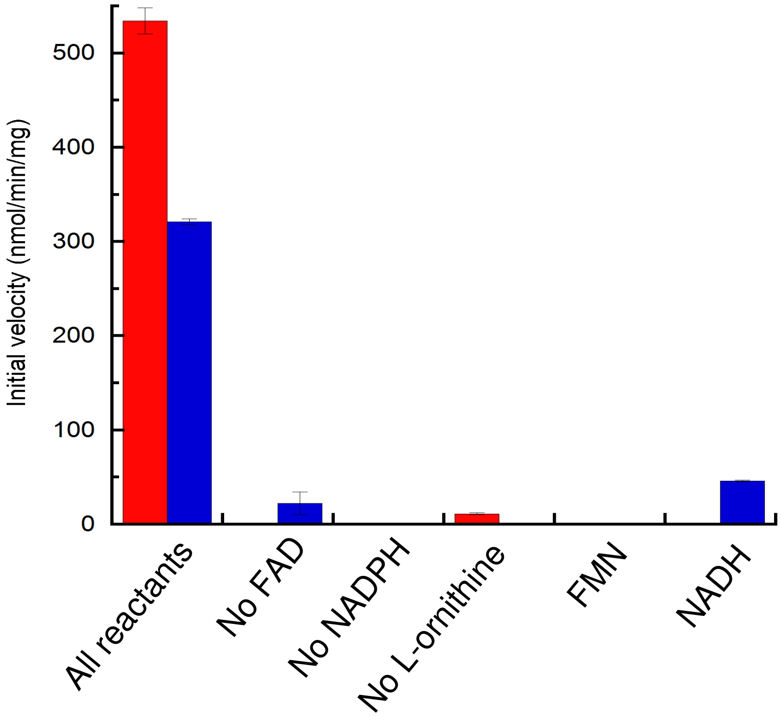

Figure 2-4: PvdA coenzyme specificity. The rate of NADPH oxidation (red bars) and product formation (blue bars) was measured in the absence of coenzyme and substrate and in the presence of coenzyme analogs.

Flavin Re-oxidation. The aerobic reduction of flavin by NADPH in PvdA was monitored as a decrease in absorbance at 451 nm (the peak of oxidized flavin absorbance) with sub-stoichiometric amounts of FAD and stoichiometric amounts of NADPH. The rate constant for flavin reduction was determined to be 0.036 ± 0.007 s^{-1}. No semiquinone intermediates were detected since absorbance peaks were not observed above 600 nm. The aerobic oxidation of the reduced flavin was observed as a reappearance of a peak at 451 nm with a rate constant determined to be 0.019 ± 0.002 s^{-1} (Figure 2-5).

Substrate Specificity. The PvdA active site is very specific for substrate. Shortening of the side chain by one or two methylene groups (DL-2,4-diaminobutyric acid or DL-2,3-diaminopropionic acid, respectively) resulted in no significant activity in either assay (Table 2-1 and Figure 2-6). However, PvdA demonstrated NADPH oxidation at 80% of the full activity using L-lysine as a substrate (extending the side chain by one methylene group) but no hydroxylated product was formed suggesting enzyme uncoupling. D-ornithine showed no activity in either assay (Table 2-1, Figure 2-6 and ref *5*). No NADPH oxidation or hydroxylated product was detected with an ornithine substrate analogue missing the α-carboxyl group (5-aminopentanoic acid). Removal of the α-amino group (1,4-diaminobutane) resulted in little NADPH oxidation (4%) and no hydroxylated product. Therefore, the amino acid backbone

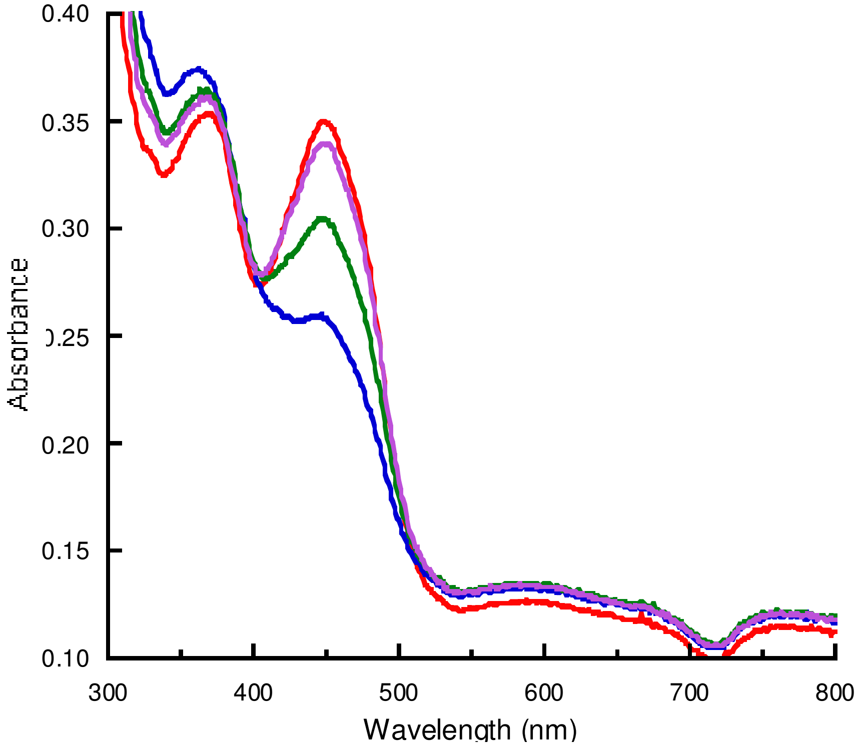

Figure 2-5: Flavin reoxidation as a function of time. Absorbance spectra of PvdA:FAD complex were measured at 300-800 nm. Representative absorbance spectra from three independent experiments of the oxidized flavin (red), the reduced flavin (blue), and at 60 seconds (green) and 120 seconds (purple) after reduction are plotted. The rate constants for flavin reduction and reoxidation were determined by the change in absorbance at 451 nm to be 0.036 ± 0.007 s^{-1} and 0.019 ± 0.002 s^{-1} respectively. The PvdA concentration was 40 µM with an FAD concentration of 20 µM.

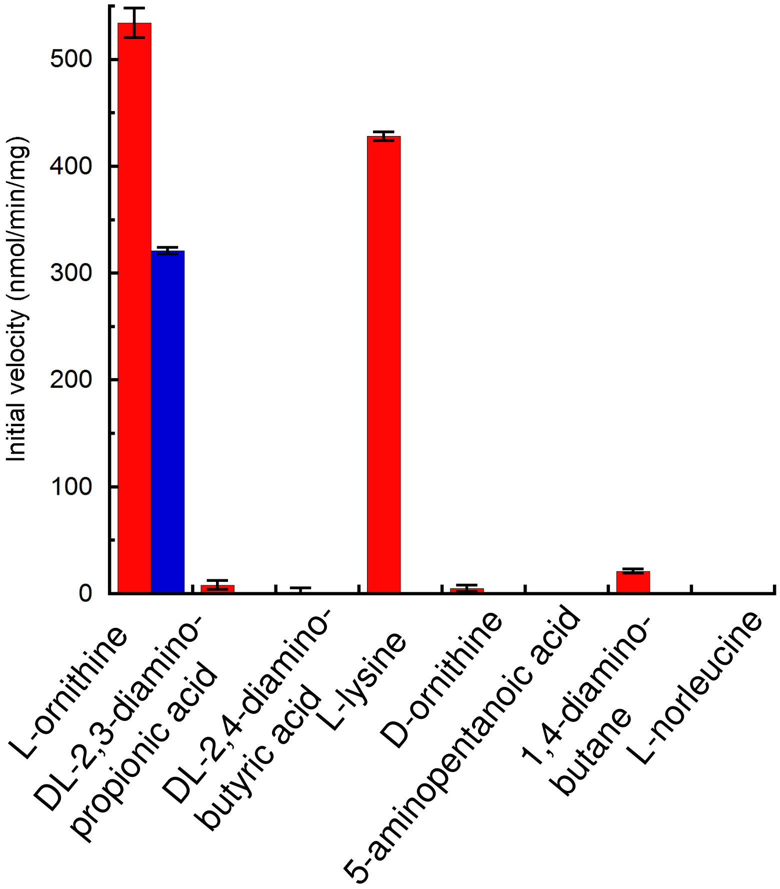

Figure 2-6: PvdA substrate specificity. The rate of NADPH oxidation (red bars) and product formation (blue bars) was measured in the presence of substrate analogs.

groups are required for activity and may be involved in substrate binding. No activity was detected in either assay with the substrate analogue L-norleucine. In this compound, the side chain primary amine is substituted with a methyl group thus removing the amine to be hydroxylated.

Determination of Kinetic Constants. The NADPH oxidation assay followed classic Michaelis-Menten kinetics (Figure 2-7). However, substrate inhibition was observed with the hydroxylation assay as the initial velocities decreased with increasing substrate above 5 mM ornithine. The V_{max}, K_{m}, and k_{cat} values for both assays are comparable (Table 2-2) indicating uncoupling of PvdA at high substrate concentrations to allow electrons from NADPH to be transferred to FAD without hydroxylated substrate formation.

Ternary Complex Formation. Initial velocities were measured for PvdA with excess FAD varying both NADPH and ornithine concentrations monitored with the NADPH oxidation assay. Double reciprocal plots of the resulting velocities intersect in the upper left quadrant indicating formation of a tertiary complex (Figure 2-8) (*18*).

Lysine Inhibition. When L-lysine was used as a substrate analogue, NADPH oxidation was detected with no hydroxylated product formed suggesting enzyme uncoupling and potential inhibition (Table 2-1 and Figure 2-6). Therefore, the

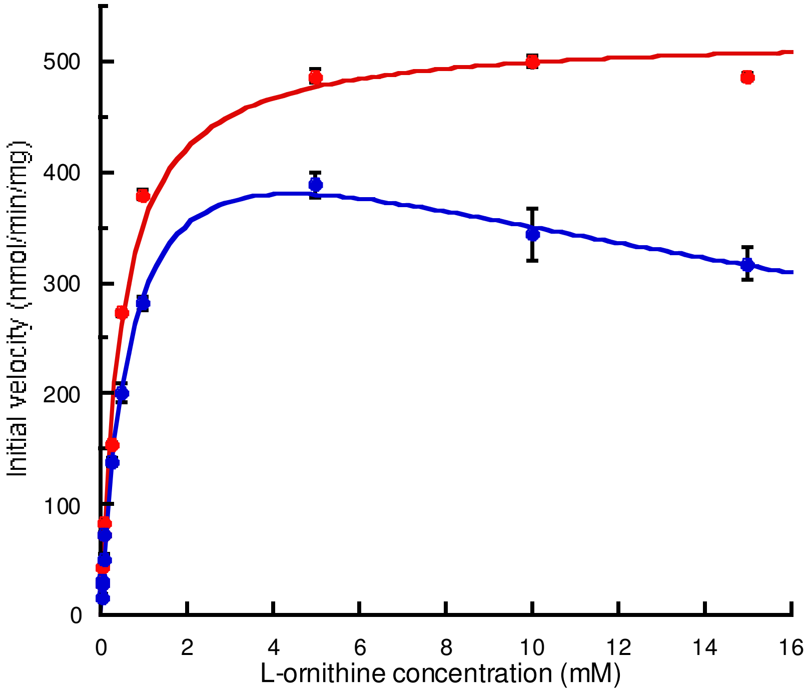

Figure 2-7: Kinetic analysis of PvdA as determined by NADPH oxidation and hydroxyornithine production. Initial velocities were measured as a function of NADPH oxidation versus L-ornithine concentration (red circles) and as the amount of hydroxyornithine produced versus L-ornithine concentration (blue circles). The curve for the NADPH oxidation assay was fit to the standard equation for Michaelis-Menten reactions and the curve for the hydroxylation assay was fit to $V_o = V_{max}$ [Substrate] / [K_m + [Substrate] + ([Substrate]^2/K_I)] for substrate inhibition due to the decrease in activity at substrate concentrations above 5 mM.

Table 2-2: Summary of the PvdA Kinetic Parameters

	NADPH oxidation assay	Hydroxylated product formation assay
V_{max} (nmol/min/mg)	528 ± 8	479 ± 54
K_m (μM)	593 ± 12	600 ± 70
k_{cat} (min^{-1})	26.4 ± 0.4	24 ± 3
k_{cat}/K_m ($M^{-1}s^{-1}$)	742	670
K_I* (mM)	n.a.	31 ± 5

* = inhibition constant determined for substrate inhibition

n.a. = not applicable

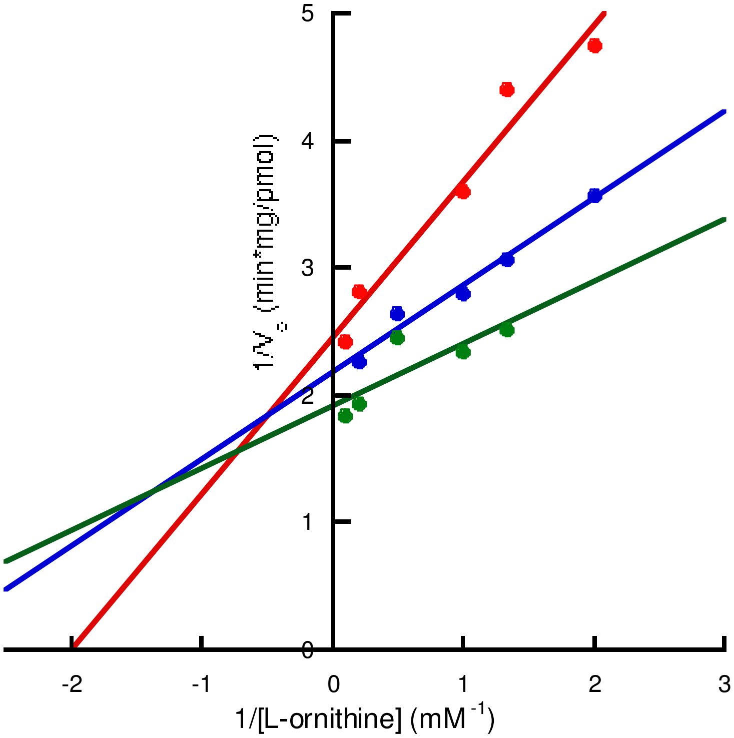

Figure 2-8: Ternary complex formation of FAD loaded PvdA with NADPH and ornithine. NADPH oxidation is plotted as a function of L-ornithine concentration. NADPH concentrations were 0.05 mM (red circles), 0.075 mM (blue circles), and 0.125 mM (green circles).

inhibition of PvdA activity by L-lysine was investigated with the hydroxylation assay. Adding L-lysine to the PvdA activity assay resulted in mixed inhibition with a K_I determined as 5.4 ± 1.4 mM and a K_I’ of 4.3 ± 1.5 mM (Figure 2-9).

Chloride Inhibition. Initial studies to determine PvdA catalytic activity as a function of ionic strength showed decreased activity with increasing ionic strength (Figure 2-10). Later, this decrease in activity was shown to be due to chloride inhibition, not ionic strength. The inhibition by chloride was determined as mixed inhibition with respect to L-ornithine (K_I of 134 ± 31 μM and K_I’ of 213 ± 36 μM), whereas the inhibition was competitive with respect to NADPH (K_I of 67 ± 6 μM) as monitored by the NADPH oxidation assay (Figure 2-11).

Mercurial Inhibition. *p*-Chloromercuribenzoate (PCMB) is a mercury compound that binds cysteines not involved in disulfide bonding. PvdA inhibition by PCMB was tested with the NADPH oxidation assay. Mixed inhibition was detected with a K_I of 4.1 ± 0.6 μM and a K_I’ of 2.9 ± 0.4 μM (Figure 2-12). Addition of 10 μM PCMB to the reaction mixture caused complete inhibition of PvdA activity (data not shown).

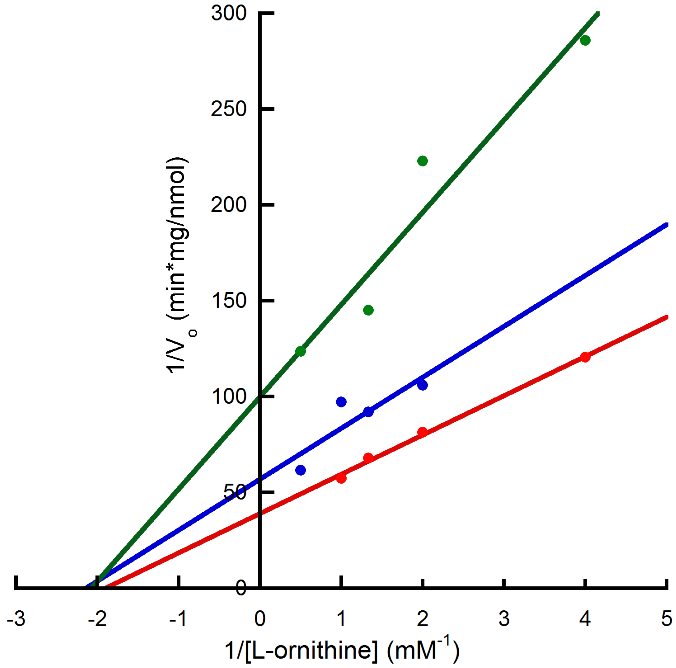

Figure 2-9: Mixed inhibition of PvdA by L-lysine as determined by the hydroxylation assay. L-lysine concentrations used were 0 mM (red circles), 2.5 mM (blue circles), and 10 mM (green circles). The K_I was determined as 5.4 ± 1.4 mM and the K_I' as 4.3 ± 1.5 mM.

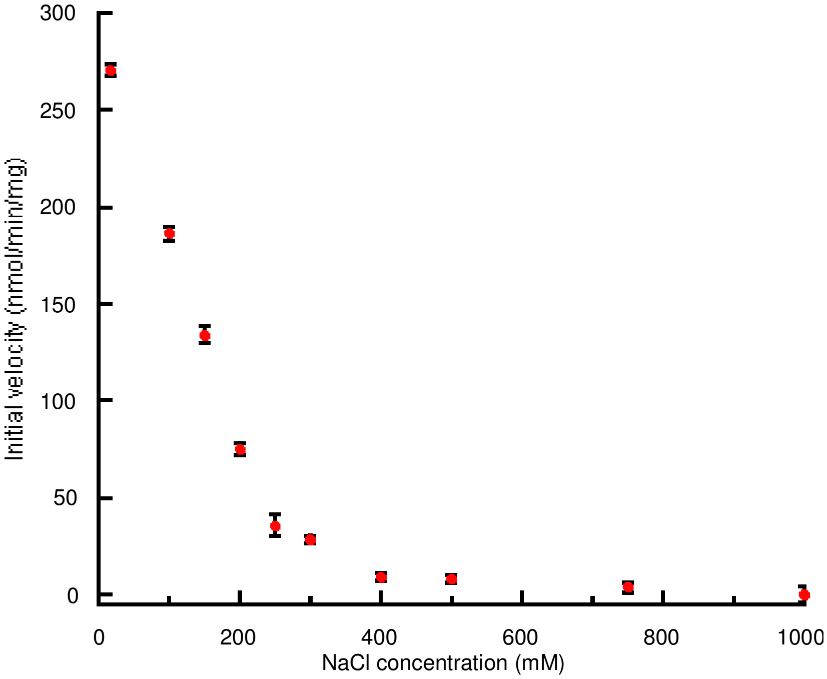

Figure 2-10: Effect of NaCl on PvdA activity. The rate of NADPH oxidation was measured as a decrease in absorbance at 366 nm measured as a function of NaCl concentration. The activity assay buffer contained 100 mM Tris-HCl pH 8.0.

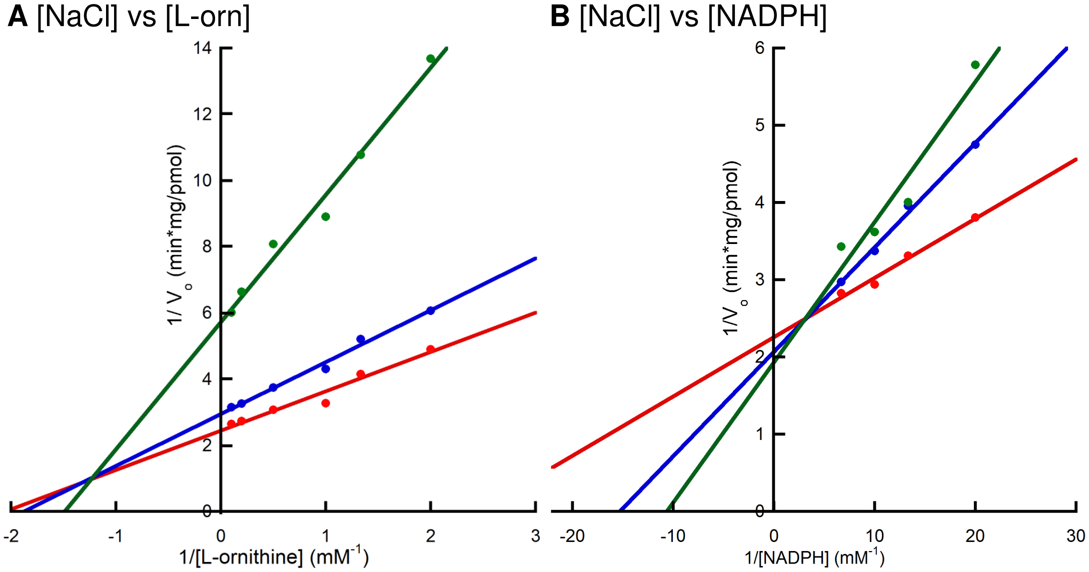

Figure 2-11: Inhibition of PvdA by chloride as determined by the NADPH oxidation assay. Double reciprocal plots of hydroxyornithine production as a function of (*A*) L-ornithine and (*B*) NADPH concentration. Chloride concentrations used were 0 mM (red circles), 50 mM (blue circles), and 250 mM (green circles). Chloride inhibition was mixed in respect of L-ornithine with a K_I of 134 ± 31 μM and a K_I’ of 213 ± 36 μM and competitive in respect to NADPH with a K_I of 67 ± 6 μM.

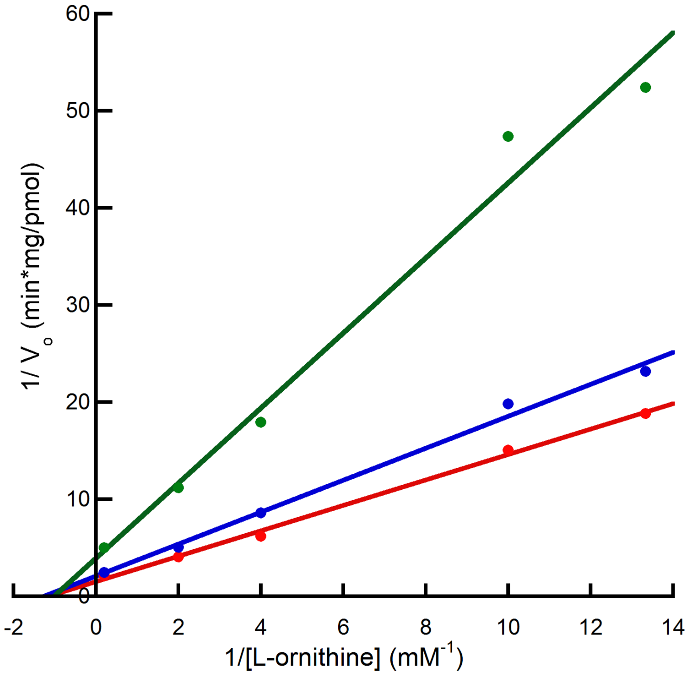

Figure 2-12: Mixed inhibition of PvdA by *p*-chloromercuibenzoate (PCMB) as determined by the NADPH oxidation assay. PCMB concentrations used were 0 µM (red circles), 1 µM (blue circles), and 5 µM (green circles). The K_I was determined as 4.1 ± 0.6 µM and the K_I' as 2.9 ± 0.4 µM.

Discussion

The ornithine hydroxylase from *P. aeruginosa*, PvdA, is functionally related to the lysine hydroxylase, IucD, from *E. coli*. Both of the enzymes hydroxylate the side chain primary amine of amino acids and are involved in siderophore biosynthesis (Figure 2-1). The sequence similarity between the enzymes is 46% and the structure of IucD is not known. There has been some debate in the literature about the cellular localization and solubility of IucD (*19-22*). IucD was initially described as a membrane-bound protein due to two hydrophobic segments believed to be transmembrane helices (*21*). Later, the hydrophobic stretches were described as coenzyme binding sites, FAD binding at the N-terminus of the protein and NADPH in the middle of the protein (*19*). Production of the IucD protein with an N-terminal His_6 tag yielded soluble protein with an active oligomerization state of tetramers (*4, 22, 23*). PvdA is soluble when produced with an N-terminal histidine tag, and is a monomer in solution (Figure 2-2). In a buffer containing chloride, an inhibitor, along with FAD and ornithine, PvdA shifts to predominantly tetramers. This indicates that in contrast to IucD, tetrameric PvdA could be an inactive state of the enzyme. However, neither PvdA nor IucD is copurified with the flavin coenzyme and both proteins bind FAD with a dissociation constant in the micromolar range (*5, 24*).

Flavin-containing monooxygenases (FMOs), which are well characterized enzymes involved in drug detoxication are also functionally related to PvdA. FMOs are substrate promiscuous individually and hydroxylate a variety of nucleophilic and electrophilic substrates including primary, secondary, and tertiary amines, as well as iodine-, sulfur-, and selenium-containing groups (*3*). FMOs in mammalian systems (the hog liver microsomal FMO, mFMO) have been studied biochemically in depth and act as membrane-bound tetramers or octamers (*3*). However, in bacterial and unicellular eukaryotes, FMOs are cytoplasmic dimers (*25, 26*). The structure of the FMO of *Schizosaccharomyces pombe* (yFMO) is composed of two domains: a large FAD-binding domain containing the FMO identifying sequence (residues 1 – 175, 292 – 457) and a smaller, insertion domain involved in stabilizing NADPH (residues 176 – 291) (*27*).

A third enzyme related functionally to PvdA is the well-studied *p*-hydroxybenzoate hydroxylase (PHBH). PHBH is a dimer with high substrate specificity, hydroxylating the activated aromatic ring of *p*-hydroxybenzoate (*2*). The structure of PHBH consists of three domains: an N-terminal FAD binding domain with a Rossman-fold (residues 1 – 174), a central substrate-binding domain of primarily β-structure (residues 175 – 295), and a C-terminal helical dimerization domain (residues 296 – 394) (*28*). Both PHBH and the FMOs are copurified with FAD and the K_d for FAD binding to PHBH is in the nanomolar range (*2, 27, 29*).

PvdA is dependent upon FAD and NADPH for activity (Table 2-1, Figure 2-4, and ref (*5*)). In PHBH and mFMO, flavin reduction occurs as a two-electron transfer from NADPH. The flavin re-oxidizes by hydroxylating the substrate with molecular oxygen (Figure 2-1) (*10, 29*). The oxidized flavin bound to PvdA is similar to other flavin-containing enzymes (*3*), which have a distinctive absorbance spectrum with peaks at 380 and 450 nm. Once the flavin becomes reduced, the 450 nm peak disappears leaving only the 380 nm peak (Figure 2-5). Flavin reduction in PHBH in the presence of substrate is very rapid with a rate constant or 256 s^{-1}. However, without substrate the flavin reduction slows considerably to 0.41 min^{-1} (*8*). The re-oxidation of the reduced flavin without substrate occurs on the millisecond timescale (*30*). In contrast, in mFMO flavin reduction is substrate-independent and the reduced enzyme binds molecular oxygen to form a stable flavin-hydroperoxy intermediate (2 h half-life at pH 7.2) until substrate binds (*3*). In this initial characterization of the flavin reduction and reoxidation, PvdA does not require substrate for flavin reduction, and is similar in this respect to mFMO (Figure 2-5). The reoxidation of the flavin in PvdA is four orders of magnitude slower than PHBH but two orders of magnitude faster than seen in mFMO.

Kinetic studies of PHBH report the turnover number as 1370 min^{-1} at 25 °C (*8, 11, 12*). PvdA shows a slower k_{cat} (26.4 min^{-1} with the NADPH oxidation and 24 min^{-1} by the hydroxylation assay at 25 °C) (Table 2-2) comparable to that seen for IucD (*17*). Kinetic parameters for mFMO are an order of magnitude slower than PvdA but are reported at 4 °C (*16, 17*) and no turnover numbers have been reported for yFMO. Substrate inhibition has been seen in PHBH and IucD (*2, 24*). Similarly, PvdA activity is inhibited at high substrate concentrations using the hydroxylation assay measuring the amount of product formation with a K_I determined as 31 ± 5 mM (Figure 2-7 and Table 2-2). However, when measuring the amount of NADPH oxidation, no substrate inhibition is observed (Figure 2-7). Therefore, at high substrate concentrations, only the hydroxylated product formation in inhibited not NADPH oxidation indicating uncoupling of the reaction.

When measuring steady-state kinetics, PHBH loaded with FAD forms a ternary complex with NADPH and a nonsubstrate effector, 6-hydroxynicotinate (*8*). From this work, it was shown that the PHBH reaction mechanism is a rapid equilibrium random order mechanism and not a compulsory order mechanism. The FAD loaded mFMO also forms a ternary complex with NADPH and substrate, but operates by a compulsory order mechanism (*3, 12*). Similarly, FAD loaded PvdA forms a ternary complex with NADPH and ornithine (Figure 2-8). However, whether the mechanism is random order or compulsory order can not be determined from the data obtained (*18*). Furthermore, the weak interaction between PvdA and FAD (K_d = 26 μM) compared to the stable PHBH:FAD complex (K_d = 45 nM, (*31*)) could cause a change in the steady state mechanism.

The substrate required for PvdA activity is very specific. Changing the chirality of the substrate to D-ornithine resulted in no enzymatic activity by PvdA using either assay (Table 2-1, Figure 2-6, and ref (*5*)). The peptide amine and carboxyl groups are required for activity and may be important in substrate-binding and positioning into the active site, similar to that seen for IucD (Table 2-1 and Figure 2-6). The side-chain amine is also required for catalysis and substitution with a methyl group eliminates activity. Collectively, these data indicate that the peptide groups and the side chain amine are important for substrate positioning and binding. Shortening the side-chain resulted in no significant activity. However, extending the side-chain by one methylene group to L-lysine resulted in NAPDH oxidation at 80% of full activity without hydroxylated product formation, indicating uncoupling of the reaction. The result of this uncoupling is hydrogen peroxide production (*5*). Therefore, we hypothesize that L-lysine binding leads to closure of the active site allowing the transfer of electrons from NADPH to FAD. However, the primary amine of the L-lysine side-chain is positioned too far from the active site for effective hydroxyl transfer from FAD to the substrate resulting in uncoupling of the reaction similar to that seen in nonsubstrate effectors of PHBH and IucD (*8, 24, 32, 33*).

Lysine has been shown to be a mixed inhibitor of PvdA (Figure 2-9) indicating that lysine can compete for binding with ornithine at the active site. Ornithine and lysine bind to the active site (as substrate and competitive inhibitor), as well as to a secondary binding site that leads to substrate inhibition (ornithine) and uncompetitive inhibition (lysine). Most likely this occurs by two molecules of substrate (substrate inhibition) or one molecule of substrate and one molecule of inhibitor similar to that seen for invertase (*34*). In contrast, competitive inhibition has been observed for nonsubstrate effectors of PHBH (*32*) and with L-2,4-diaminobutyric acid, 5-aminopentanoic acid, and L-homoserine for PvdA (*5*).

Initially, the biochemical characterization of PvdA was carried out in Tris-HCl buffer. PvdA was kept stable in solution only by the addition of 500 mM NaCl. In a test of the PvdA activity as a function of ionic strength, PvdA showed decreased activity with increasing sodium chloride concentration (Figure 2-10). This was initially believed to be the result of the ionic strength. IucD has been reported to have increased activity with increased chloride concentrations, presumably by the formation of the active tetramer (*23*). In contrast, inhibition by halides, including chloride, has been described for PHBH (*35*) and three chloride binding sites were observed in the crystal structure (*3, 36*). One of the chloride binding sites has been shown to interfere with flavin intermediate formation and subsequent substrate hydroxylation. Chloride inhibition studies of PvdA showed mixed inhibition with respect to ornithine (Figure 2-11A). This inhibition indicates that the decrease in the activity observed with increased salt concentration was not a result of ionic strength but of chloride concentration. Competitive inhibition was observed in respect to NADPH (Figure 2-11B), suggesting a specific chloride-binding site in or near the coenzyme-binding site and not merely a disruption of ionic interactions. Therefore, PvdA activity was re-assayed in the absence of monovalent anions.

IucD and PHBH show inhibition by bulky mercurial compounds (~60%) with the activity completely restored with the addition of reducing agents (*2, 4, 37, 38*). With the mercurial compound PCMB, mixed inhibition was observed in PvdA with respect to ornithine (Figure 2-12). Mercurial compounds are not site-specific. However, when they bind to a cysteine possibly in or near the active site or coenzyme binding sites, the activity is disrupted in all three enzymes.

Conclusions. PvdA shares many similarities to PHBH: coenzyme and substrate specificities, nonsubstrate effectors, substrate inhibition, and inhibition by halides and bulky mercury compounds (Figure 2-13). In contrast, several

	PHBH	**PvdA**	**IucD**	**FMO**
Oligomerization State	Dimer *(28)*	Monomer	Tetramer *(4,23)*	Tetramer/octomer *(3,25,26)*
Coenzyme Specificity	Specific for FAD and NADPH *(2)*	Specific for FAD and NADPH	Specific for FAD can use NADH *(4,23)*	Specific for FAD can use NADH *(3)*
Substrate Specificity	Very specific, Aromatic compound *(2)*	Very specific, 1° amine	Very specific, 1° amine *(4,24)*	Nucleophilic compounds including 1°, 2°, and 3° amines *(3)*
Substrate Inhibition	Yes *(2)*	Yes	Yes *(4,24)*	No *(11,12)*
Nonsubstrate effectors	Yes *(8,32,33)*	Yes	Yes *(4,24)*	?
Ternary Complex	Yes *(8)*	Yes	?	Yes *(3,12)*
Nonsubstrate effector inhibition	Mixed *(32)*	Mixed	?	?
Halide Inhibition	Mixed for Substrate, Competitive for NADPH *(35)*	Mixed for Substrate, Competitive for NADPH	Activity is enhanced with high halide concentration *(23)*	?
Mercurial Inhibition	Yes *(2)*	Yes	Yes *(4)*	?
Flavin Reoxidation Rate Constant	256 s^{-1} *(30)*	0.019 ± 0.002 s^{-1}	?	2 hour half-life *(3)*

Figure 2-13: PvdA biochemical characterization in comparison to the functional homologues; PHBH from *P. fluorescens* (red), IucD from *E. coli* (blue), and FMO from hog liver microsomes (green). PvdA characteristics are labeled according to the homologue with similarities and characteristics shared with multiple homologues are labeled in purple.

characteristics seen in PvdA are similar to mFMO: hydroxylation of primary amines and flavin reduction in the absence of substrate (Figure 2-13). Several PvdA characteristics are distinct from either PHBH or mFMO, including the monomeric oligomerization state and the rate of flavin reoxidation in the absence of substrate (Figure 2-13). The sequence similarity between PvdA and PHBH (18% identity, 34% similarity) and between PvdA and yFMO (19% identity, 37% similarity) are of the same magnitude as that seen between PHBH and yFMO (18% identity, 38% similarity). However, the structural similarity between PHBH and yFMO lies primarily in the FAD-binding domains (DALI Z-score of 10.5 for ~180 amino acids, RMSD of 4.0 Å, ref (*39*)). Our data suggest that PvdA is likely to have a novel reaction mechanism. Further elucidation of the mechanism has been examined using transient-state kinetics as described in the following chapter.

References

(1) Neilands, J. B. (1981) Microbial iron compounds. *Annu Rev Biochem 50*, 715-31.

(2) Hosokawa, K., and Stanier, R. Y. (1966) Crystallization and properties of *p*-hydroxybenzoate hydroxylase from *Pseudomonas putida*. *J Biol Chem 241*, 2453-60.

(3) Palfey, B. A., and Massey, V. (1998) Flavin-Dependent Enzymes, in *Comprehensive Biological Catalysis* (Sinnott, M., Ed.) pp 83-154, Academic Press, San Diego.

(4) Plattner, H. J., Pfefferle, P., Romaguera, A., Waschutza, S., and Diekmann, H. (1989) Isolation and some properties of lysine N6-hydroxylase from *Escherichia coli* strain EN222. *Biol Met 2*, 1-5.

(5) Ge, L., and Seah, S. Y. (2006) Heterologous expression, purification, and characterization of an l-ornithine N(5)-hydroxylase involved in pyoverdine siderophore biosynthesis in *Pseudomonas aeruginosa*. *J Bacteriol 188*, 7205-10.

(6) Ballou, D. P., Entsch, B., and Cole, L. J. (2005) Dynamics involved in catalysis by single-component and two-component flavin-dependent aromatic hydroxylases. *Biochem Biophys Res Commun 338*, 590-8.

(7) Cashman, J. R. (2000) Human flavin-containing monooxygenase: substrate specificity and role in drug metabolism. *Curr Drug Metab 1*, 181-91.

(8) Howell, L. G., Spector, T., and Massey, V. (1972) Purification and Properties of *p*-Hydroxybenzoate Hydroxylase from *Pseudomonas fluorescens*. *J Biol Chem 247*, 4340-4350.

(9) Spector, T., and Massey, V. (1972) *p*-Hydroxybenzoate Hydroxylase from *Pseudomonas fluorescens*, Evidence for an Oxygenated Flavin Intermediate. *J Biol Chem 247*, 5632-5636.

(10) Husain, M., and Massey, V. (1979) Kinetic studies on the reaction of *p*-hydroxybenzoate hydroxylase. Agreement of steady state and rapid reaction data. *J Biol Chem 254*, 6657-66.

(11) Beaty, N. B., and Ballou, D. P. (1981) The reductive half-reaction of liver microsomal FAD-containing monooxygenase. *J Biol Chem 256*, 4611-8.

(12) Beaty, N. B., and Ballou, D. P. (1981) The oxidative half-reaction of liver microsomal FAD-containing monooxygenase. *J Biol Chem 256*, 4619-25.

(13) Jones, K. C., and Ballou, D. P. (1986) Reactions of the 4a-hydroperoxide of liver microsomal flavin-containing monooxygenase with nucleophilic and electrophilic substrates. *J Biol Chem 261*, 2553-9.

(14) Csaky, T. Z. (1948) On the Estimation of Bound Hydroxylamine in Biological Materials. *Acta Chem Scand 2*, 450-454.

(15) Tomlinson, G., Cruickshank, W. H., and Viswanatha, T. (1971) Sensitivity of substituted hydroxylamines to determination by iodine oxidation. *Anal Biochem 44*, 670-9.

(16) Gillam, A. H., Lewis, A. G., and Andersen, R. J. (1981) Quantitative Determination of Hydroxamic Acids. *Anal Chem 53*, 841-844.

(17) Stehr, M., Smau, L., Singh, M., Seth, O., Macheroux, P., Ghisla, S., and Diekmann, H. (1999) Studies with lysine N6-hydroxylase. Effect of a mutation in the assumed FAD binding site on coenzyme affinities and on lysine hydroxylating activity. *Biol Chem 380*, 47-54.

(18) Cornish-Bowden, A. (1995) *Fundamentals of Enzyme Kinetics*, Portland Press Ltd., London.

(19) Stehr, M., Diekmann, H., Smau, L., Seth, O., Ghisla, S., Singh, M., and Macheroux, P. (1998) A hydrophobic sequence motif common to N-hydroxylating enzymes. *Trends Biochem Sci 23*, 56-7.

(20) Krone, W. J., Luirink, J., Koningstein, G., Oudega, B., and de Graaf, F. K. (1983) Subcloning of the cloacin DF13/aerobactin receptor protein and identification of a *pColV-K30*-determined polypeptide involved in ferric-aerobactin uptake. *J Bacteriol 156*, 945-8.

(21) Herrero, M., de Lorenzo, V., and Neilands, J. B. (1988) Nucleotide sequence of the *iucD* gene of the *pColV-K30* aerobactin operon and topology of its product studied with *phoA* and *lacZ* gene fusions. *J Bacteriol 170*, 56-64.

(22) Seth, O., Smau, L., Welte, W., Ghisla, S., Stehr, M., Diekmann, H., and Macheroux, P. (1998) A reply to Dick et al. *Trends Biochem Sci 23*, 414-415.

(23) Thariath, A., Socha, D., Valvano, M. A., and Viswanatha, T. (1993) Construction and biochemical characterization of recombinant cytoplasmic forms of the IucD protein (lysine:N6-hydroxylase) encoded by the *pColV-K30* aerobactin gene cluster. *J Bacteriol 175*, 589-96.

(24) Macheroux, P., Plattner, H. J., Romaguera, A., and Diekmann, H. (1993) FAD and substrate analogs as probes for lysine N6-hydroxylase from *Escherichia coli* EN 222. *Eur J Biochem 213*, 995-1002.

(25) Schlenk, D. (1998) Occurrence of flavin-containing monooxygenases in non-mammalian eukaryotic organisms. *Comp Biochem Physiol C Pharmacol Toxicol Endocrinol 121*, 185-95.

(26) Choi, H. S., Kim, J. K., Cho, E. H., Kim, Y. C., Kim, J. I., and Kim, S. W. (2003) A novel flavin-containing monooxygenase from *Methylophaga* sp strain SK1 and its indigo synthesis in *Escherichia coli*. *Biochem Biophys Res Commun 306*, 930-6.

(27) Eswaramoorthy, S., Bonanno, J. B., Burley, S. K., and Swaminathan, S. (2006) Mechanism of action of a flavin-containing monooxygenase. *Proc Natl Acad Sci U S A 103*, 9832-7.

(28) Entsch, B., and Van Berkel, W. J. H. (1995) Structure and mechanism of *para*-hydroxybenzoate hydroxylase. *The FASEB J. 9*, 476-483.

(29) Poulsen, L. L., and Ziegler, D. M. (1979) The liver microsomal FAD-containing monooxygenase. Spectral characterization and kinetic studies. *J Biol Chem 254*, 6449-55.

(30) Spector, T., and Massey, V. (1973) *p*-Hydroxybenzoate Hydroxylase from *Pseudomonas fluorescens*, Reactivity with Oxygen. *J Biol Chem 247*, 7123-7127.

(31) Muller, F., and van Berkel, W. J. (1982) A Study on *p*-Hydroxybenzoate Hydroxylase from *Pseudomonas fluorescens*. *Eur J Biochem 128*, 21-27.

(32) Spector, T., and Massey, V. (1972) Studies of the Effector Specificity of *p*-Hydroxybenzoate Hydroxylase from *Pseudomonas fluorescens*. *J Biol Chem 247*, 4679-4687.

(33) Howell, L. G., and Massey, V. (1970) A Non-substrate Effector of *p*-Hydroxybenzoate Hydroxylase. *Biochem Biophys Res Commun 40*, 887-893.

(34) Combes, D., and Monsan, P. (1983) Sucrose Hydrolysis by Invertase. Characterization of Products and Substrate Inhibition. *Carbohydr. Res. 117*, 215-228.

(35) Steennis, P. J., Cordes, M. M., Hilkens, J. H., and Muller, F. (1973) On the interaction of *para*-hydroxybenzoate hydroxylase from *Pseudomonas fluorescens* with halogen ions. *FEBS Lett 36*, 177-80.

(36) Gatti, D. L., Palfey, B. A., Lah, M. S., Entsch, B., Massey, V., Ballou, D. P., and Ludwig, M. L. (1994) The Mobile Flavin of 4-OH Benzoate Hydroxylase. *Science 266*, 110-114.

(37) Dick, S., Marrone, L., Duewel, H., Beecroft, M., McCourt, J., and Viswanatha, T. (1999) Lysine: N6-hydroxylase: stability and interaction with ligands. *J Protein Chem 18*, 893-903.

(38) Marrone, L., and Viswanatha, T. (1997) Effect of selective cysteine --> alanine replacements on the catalytic functions of lysine: N6-hydroxylase. *Biochim Biophys Acta 1343*, 263-77.

(39) Holm, L., and Sander, C. (1993) Protein structure comparison by alignment of distance matrices. *J Mol Biol 233*, 123-38.

Chapter 3

Determination of the PvdA Reaction Mechanism by Stopped-Flow Techniques

In Chapter 2, PvdA was shown to have some characteristics similar to *p*-hydroxybenzoate hydroxylase (PHBH) and flavin monooxygenase (FMO) yet also contain characteristics distinct from these two biochemically well-characterized proteins. Therefore, it was suggested that PvdA would have a novel reaction mechanism. To determine the reaction mechanism for flavo-enzyme catalysis, transient kinetics may be examined using stopped-flow techniques. By monitoring the absorbance changes over time, the flavin redox state may be determined and therefore, a model for how the enzyme proceeds through the catalytic cycle can be developed (Figure 3-1). The flavin redox states determined for PHBH and FMO are similar and proceed from the oxidized flavin (Figure 3-1A) to the reduced flavin (Figure 3-1B) and then back to the oxidized flavin by way of two transient intermediates, hydroperoxyflavin (Figure 3-1C) and hydroxyflavin (Figure 3-1D) (*1*). However, the catalytic mechanisms are different for PHBH and FMO.

PHBH requires substrate to be bound prior to reduction (Figure 3-2A). Once substrate binds, the flavin is quickly reduced (256 s^{-1}) and is converted through the intermediates to reform the oxidized flavin (*1-6*). In the absence of substrate, flavin

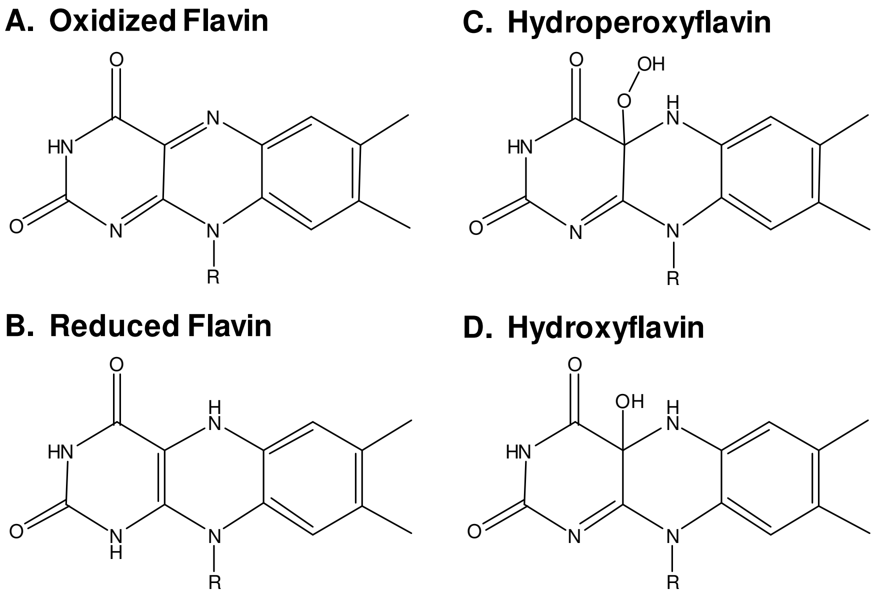

A. Oxidized Flavin

C. Hydroperoxyflavin

B. Reduced Flavin

D. Hydroxyflavin

Figure 3-1: Common flavin oxidation states of hydroxylase enzymes including PHBH and FMO. *A*. Oxidized flavin. *B*. Reduced flavin. *C*. Hydroperoxyflavin. *D*. Hydroxyflavin. Each state has different absorbance and fluorescence properties that are exploited for determining the reaction mechanism. R = ribityl chain attached to adenine dinucleotide.

reduction is much slower (0.41 min^{-1}) and the reduced flavin binds oxygen to form hydroperoxyflavin. The hydroperoxyflavin is converted directly to the oxidized flavin by release of hydrogen peroxide (*7*). In contrast, FMO reduces the flavin in the absence of substrate (Figure 3-2B) (*1, 8-10*). The reduced flavin binds oxygen to form hydroperoxyflavin as a very long-lived intermediate (2 hr half-life) until substrate binds. Once substrate binds to FMO, the reaction quickly proceeds through the hydroxyflavin intermediate to the oxidized flavin. If substrate is not bound, FMO will release hydrogen peroxide and return to the oxidized flavin state (*10*).

In Chapter 2, we determined that in PvdA, the FAD cycles from the oxidized to the reduced forms similar to PHBH and FMO. As expected, the absorbance traces for FAD differ depending on the redox state of the flavin: oxidized flavin has two peaks, one at 390 nm and another at 450 nm, whereas reduced flavin has only one peak at 390 nm. The flavin is reduced by NADPH oxidation. The reduced flavin binds molecular oxygen, reacts with substrate and returns to the oxidized flavin state. Here we continue the biochemical characterization of PvdA to determine the reaction mechanism using stopped-flow techniques. This mechanism is novel in that the reduction of the flavin is independent of substrate binding, passes through two transient intermediate steps upon reoxidation in the presence of substrate, while only forming the hydroxyflavin intermediate in the absence of substrate.

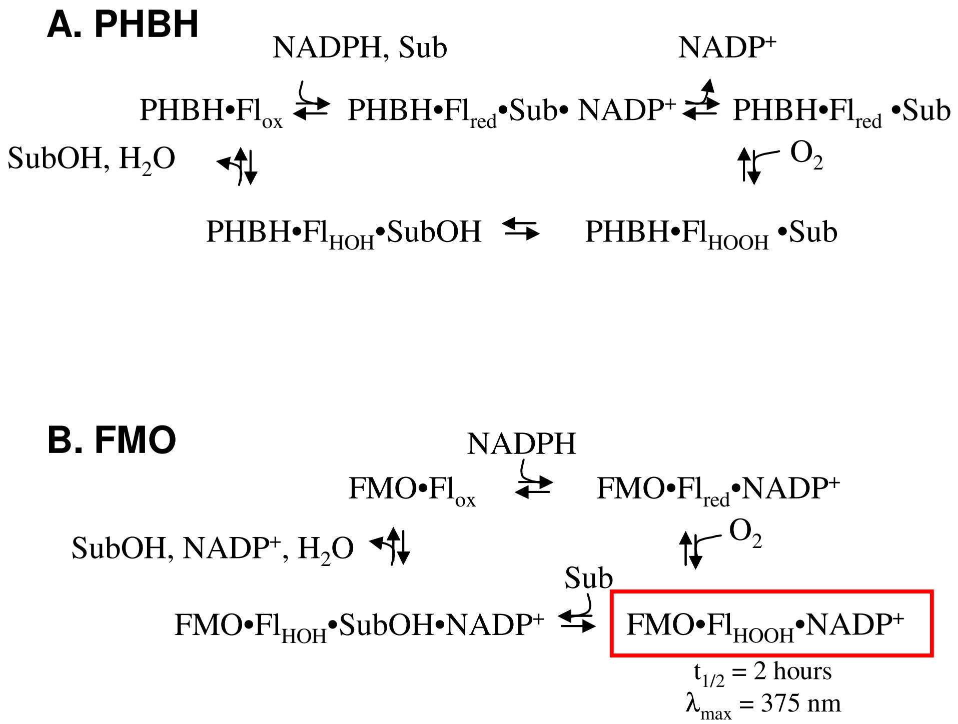
A. PHBH
NADPH, Sub
NADP+
PHBH•Flox
PHBH•Flred•Sub• NADP+
PHBH•Flred •Sub
SubOH, H2O
O2
PHBH•FlHOH•SubOH
PHBH•FlHOOH •Sub
B. FMO
NADPH
FMO•Flox
FMO•Flred•NADP+
SubOH, NADP+, H2O
O2
Sub
FMO•FlHOH•SubOH•NADP+
FMO•FlHOOH•NADP+
t1/2 = 2 hours
λmax = 375 nm

Figure 3-2: The reaction mechanisms for p-hydroxybenzoate hydroxylase (PHBH) and flavin monooxygenase (FMO). *A*. PHBH requires substrate (Sub) for flavin reduction (Fl_{red}) from the oxidized redox state (Fl_{ox}). Upon binding of molecular oxygen, the flavin progresses through two transient intermediate redox states, hydroperoxyflavin (Fl_{HOOH}) and hydroxyflavin (Fl_{HOH}) before returning to the oxidized state by the release of hydroxylated substrate and water. *B*. FMO does not require substrate for flavin reduction but reacts with molecular oxygen to form a stable hydroperoxyflavin intermediate (boxed in red). Reaction of this intermediate with substrate, forms the hydroxyflavin and hydroxylated substrate, which is released, and the flavin returns to the oxidized state.

Materials and Methods

PvdA Purification. PvdA was purified as described in Chapter 2 with a final concentration of 258 - 292 μM in 100 mM potassium phosphate pH 8.0 and 100 mM sodium citrate.

Stopped-Flow Experiments. All stopped-flow data were collected in the lab of Dr. J. M. Bollinger at the Pennsylvania State University. PvdA, coenzymes, substrate and buffers were deoxygenated with argon gas. Stopped-flow experiments were performed at 22 °C with an Applied Photophysics SX.18MV (Surrey, U.K.) stopped-flow apparatus housed in an anaerobic chamber. Absorption traces were obtained with a photomultiplier tube or a photo-diode array detector with a 1 cm pathlength. Fluorescence was detected and integrated at wavelengths above 515 nm upon excitation at 370 or 390 nm with a 0.2 cm pathlength. All experiments were repeated twice.

PvdA Reduction Experiments. For the FAD reduction traces, PvdA, FAD, and NADPH with and without ornithine were mixed into 100 mM potassium phosphate pH 8.0 in various combinations in the absense of oxygen. Final concentrations of components were: 129 - 146 μM PvdA, 30 μM FAD, 180 μM NADPH, and 5 mM ornithine.

PvdA Oxidation Experiments. Flavin oxidation studies consisted of a deoxygenated solution of 129 - 146 μM PvdA, 30 μM FAD, and 180 μM NADPH with and without 5 mM ornithine mixed in the stopped-flow apparatus with an equal volume of 100 mM potassium phosphate pH 8.0 equilibrated with oxygen concentrations ranging from 0 – 450 μM. Absorbance (350 – 700 nm) and fluorescence (excitation at 250 – 510 nm, emission >515 nm) were monitored over time.

NADPH Oxidation Studies. The NADPH oxidation assay was described in Chapter 2. These experiments were conducted in parallel with the hydrogen peroxide assay (next section) to correlate NADPH oxidation with hydrogen peroxide formation. Therefore, the assay buffer was modified to include the components required for hydrogen peroxide detection as follows: 100 mM potassium phosphate, pH 8.0, 0.03 mM FAD, 0.1 mM NADPH, 5 μM PvdA, 0.01 mg horseradish peroxidase, and 0.4 mM *o*-dianisidine in 0.2% Triton X-100. The reaction was initiated by the addition of substrate (ornithine or lysine). NADPH oxidation was monitored as a decrease in absorbance at 366 nm ($\varepsilon = 2850\ M^{-1}\ cm^{-1}$) with a BioMate 3 spectrophotometer (Thermo Spectronics) at 24 °C.

Hydrogen Peroxide Formation Assay. The amount of hydrogen peroxide formed by PvdA was measured according to the protocol described by Macheroux et al. (*11*). Briefly, the assay buffer is the same as for the NADPH oxidation assay above. Upon initiation of the reaction by substrate (ornithine) or substrate analogue (lysine) addition, any hydrogen peroxide formed by the uncoupling of PvdA was oxidized by the horseradish peroxidase, converting *o*-dianisidine to *o*-dianisidine radical. The amount of radical formed was monitored by an increase in absorbance at 440 nm (ε = 11,600 M^{-1} cm^{-1}) at 24 °C and is directly proportional to the amount of hydrogen peroxide produced by PvdA.

Data Analysis. Curve fitting analysis was performed with KaleidaGraph 4 (Synergy Software) using a sum of exponentials equation.

Results

PvdA Flavin Reduction. The change in the FAD oxidation state can be monitored as the disappearance of the peak at 450 nm upon reduction. With the stopped-flow apparatus in the lab of Dr. J. M. Bollinger at Pennsylvania State University, the reduction of flavin in PvdA was monitored over time at 450 nm in an anaerobic chamber. The exclusion of oxygen from the reaction allows only the reductive half-reaction to be monitored as a single turnover event. Initial optimization of the reduction mix determined that maximal reduction required four times more enzyme concentration than FAD concentration. This ratio assured that 80% of the flavin is bound to enzyme due to the weak binding of FAD to PvdA (Figure 3-3A). Therefore, all experiments contained PvdA at 129 – 146 μM and an FAD concentration of 30 μM such that at least 80% of the FAD was bound to the protein.

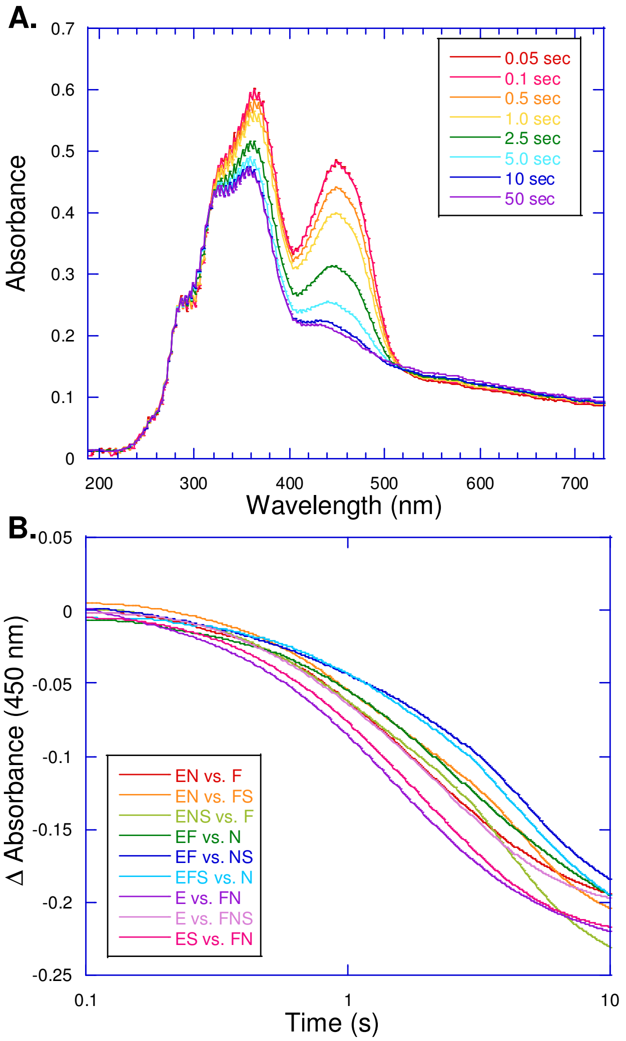

Figure 3-3: Flavin reduction in PvdA. *A*. Absorbance change over time at different wavelengths. PvdA was mixed anaerobically with FAD and NADPH in the absence of ornithine. The largest change is a decrease at 450 nm and was used to monitor flavin reduction. *B*. Different mixing schemes for flavin reduction. The schemes have comparable rates (0.185 – 0.452 s^{-1}) with or without the addition of ornithine indicating substrate is not required for flavin reduction. Mixing schemes include: 146 μM PvdA (E), 30 μM FAD (F), 180 μM NADPH (N), and 5 mM ornithine (S).

PvdA was mixed with FAD, NADPH, and ornithine in different reaction mixes (Table 3-1, Figure 3-3B) to determine if the reduction rate is affected by the order of addition of the components. A solution of PvdA, FAD, and NADPH to be mixed with substrate was completely reduced prior to mixing, thus making the determination of the reduction rate impossible. However, all other reaction mixes reduced the flavin at comparable rates from 0.185 – 0.452 s^{-1} (Table 3-1) indicating that the substrate is not required for flavin reduction and the binding of the coenzymes is not a rate-limiting step in flavin reduction.

FAD Binding Rate. The rate of FAD binding to PvdA was monitored by a fluorescence increase above 515 nm upon excitation at 450 nm (Figure 3-4). The rate was determined as ~11 s^{-1} and was not affected by substrate addition before or during mixing (Table 3-2). The FAD binding rate is faster than the overall reduction rate of 0.19 – 0.45 s^{-1} and is not a rate-limiting step in reduction.

PvdA Flavin Oxidation with Ornithine. PvdA containing reduced flavin in the presence of ornithine and NADPH was mixed with oxygenated buffer to monitor the reoxidation of the flavin by stopped-flow. As the flavin was converted from reduced to oxidized the peak at 450 nm reappeared (Figure 3-5A). When the absorbance at 390 nm is monitored over time, two peaks are detected (Figure 3-5B). The first peak is designated as the formation of the hydroperoxyflavin intermediate and is oxygen

Table 3-1: PvdA flavin reduction rate constants

Order of mixing	Rate constant (s^{-1})
EN vs. F	0.358
EN vs. FS	0.278
ENS vs. F	0.266
EF vs. N	0.243
EF vs. NS	0.200
EFS vs. N	0.185
EFN vs. S	n.d.
E vs. FN	0.452
E vs. FNS	0.391
ES vs. FN	0.431

E = PvdA, F = FAD, N = NADPH, S = ornithine

n.d. = not determinable

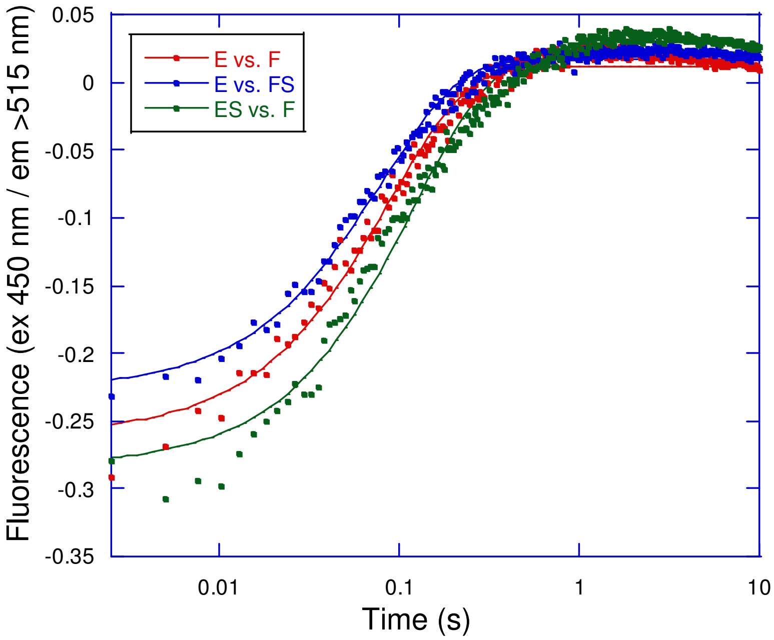

Figure 3-4: The binding of flavin to PvdA monitored as an increase in fluorescence. The rate of flavin binding is independent of the presence of substrate.

Table 3-2: FAD binding rate to PvdA

Order of substrate addition	Binding rate (s^{-1})
E vs. F	11.3
E vs. FS	11.0 ± 2.0
ES vs. F	9.7 ± 2.3

E = PvdA, F = FAD, S = ornithine

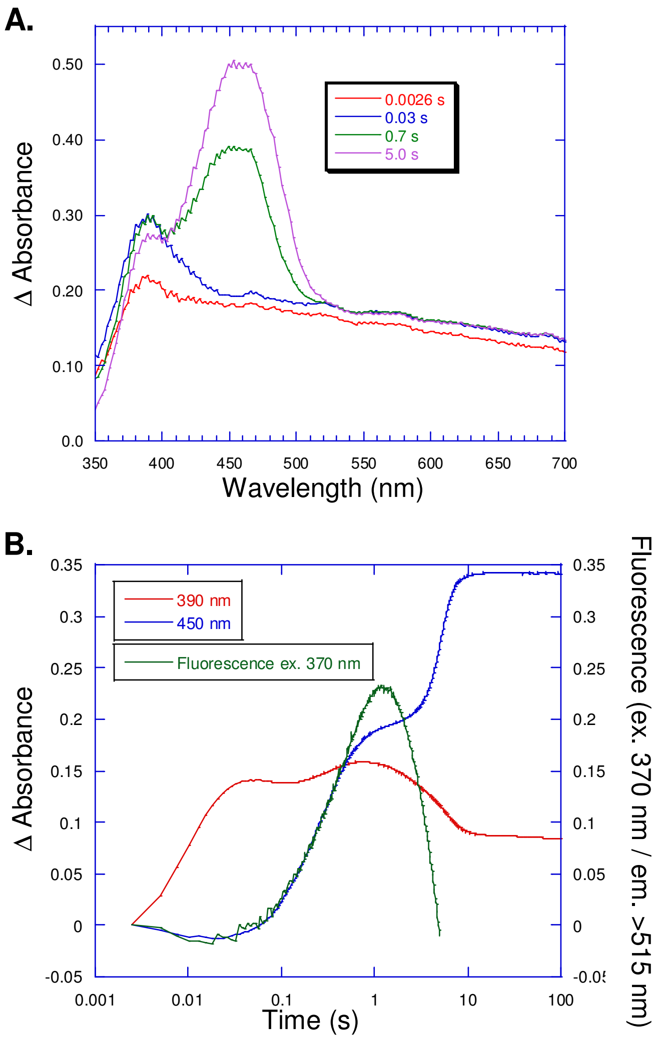

Figure 3-5: Flavin oxidation in PvdA in the presence of substrate. *A*. Absorbance difference spectra of flavin over time at different wavelengths by mixing anaerobic PvdA, FAD, NADPH, and ornithine (to form reduced flavin) with 450 μM O_2. The largest absorbance change is the reappearance of a peak at 450 nm as the flavin becomes reoxidized. A transient absorbance change is detected at 390 nm indicating the formation and decay of transient intermediates. *B*. Absorbance changes were monitored over time at 390 nm (red line) and 450 nm (blue line). Fluorescence changes above 515 nm were compiled and integrated upon excitation at 370 nm (green line). The fluorescence peak forms and decays on the same time scale as the second intermediate and was assigned as hydroxyflavin.

dependent (Figure 3-6A). The formation rate can be plotted versus the oxygen concentration as an inverse plot (Figure 3-6B). From this graph the rate of hydroperoxyflavin formation (the inverse of where the line crosses the y-axis) was determined as a first order rate constant of 142 s^{-1} with a K_d for O_2 of 240 mM (the negative inverse where the line crosses the x-axis). The second absorbance peak detected at 390 nm is oxygen independent with a formation rate constant of 2.8 s^{-1} and is determined as the intermediate hydroxyflavin.

When monitoring the absorbance at 450 nm, a shoulder is detected with a formation rate constant of 3.78 s^{-1}, similar to the second absorbance peak at 390 nm assigned to hydroxyflavin. A final absorbance change was detected with a formation rate constant of 0.16 s^{-1} and is the formation of the oxidized flavin (Figure 3-5B). Taken together these data suggest two intermediates are formed during flavin oxidation. The first intermediate is hydroperoxyflavin formed with a rate constant of 142 s^{-1} which decays as the second intermediate, hydroxyflavin, is formed at ~3 s^{-1}. The hydroxyflavin decays to form the oxidized flavin at 0.16 s^{-1}.

Hydroxyflavin has been shown to emit fluorescence above 525 nm when excited at 390 nm in other flavoproteins (*12*). To confirm that the second intermediate formed in the above experiment was indeed hydroxyflavin, the fluorescence of PvdA flavin oxidation was monitored over time. A scan of fluorescence emission upon excitation by a variety of wavelengths shows two fluorescent species that appear over time (Figure 3-7A). An initial fluorescence peak

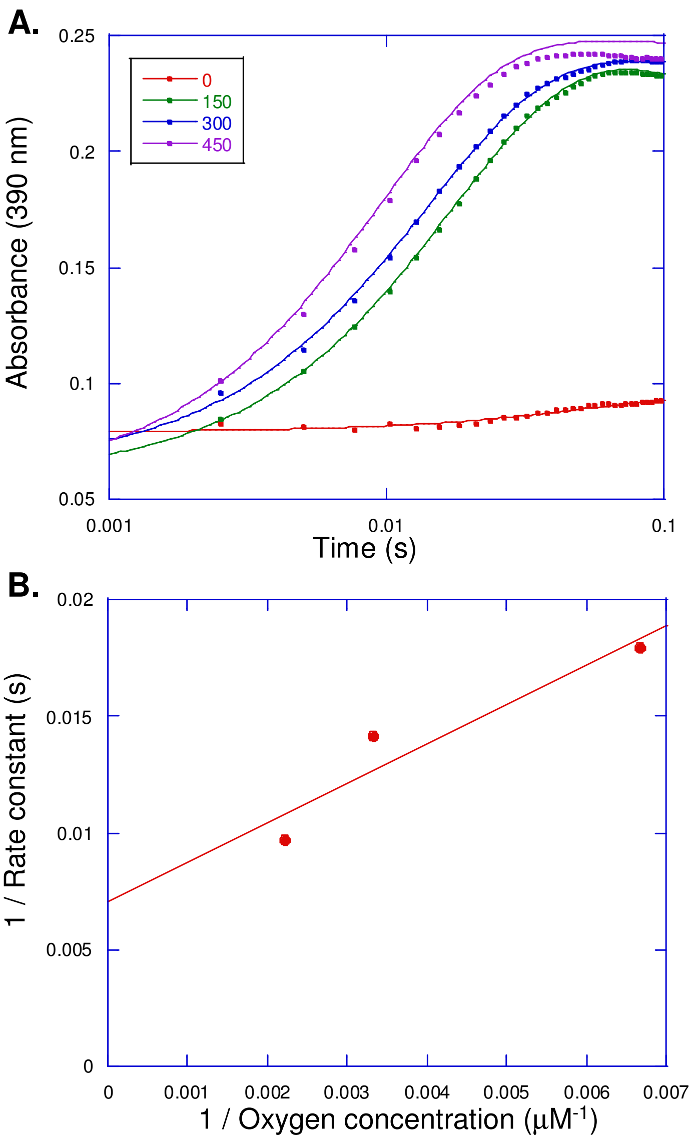

Figure 3-6: Oxygen dependence for the formation of hydroperoxyflavin in PvdA. *A*. Absorbance changes detected at 390 nm correspond to hydroperoxy formation with 0 mM (red circles), 150 mM (green circles), 300 mM (blue circles), and 450 mM (purple circles) O_2. Lines were fit with the sum of exponentials equation. *B*. Rate constants obtained from the fitted lines in (A) were plotted versus the oxygen concentration as an inverse plot. A first order rate constant for the formation of hydroperoxyflavin was determined as 142 s^{-1} and a K_d for O_2 was determined as 240 mM.

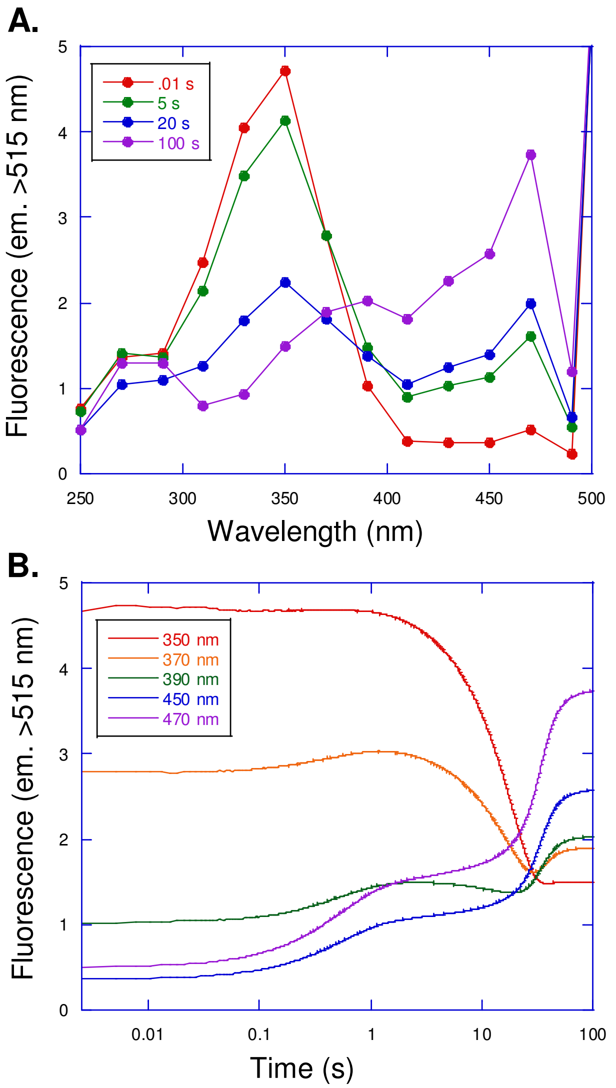

Figure 3-7: PvdA excitation scan monitoring fluorescence above 515 nm. *A*. Fluorescence emission was monitored upon excitation at different wavelengths over time. An initial fluorescence peak at 350 nm disappears over time as a second fluorescence peak appears at 470 nm. Transient peaks can be detected at 370 – 470 nm. *B*. The flavin fluorescence was monitored over time at 350 nm (red line), 370 nm (orange line), 390 nm (green line), 450 nm (blue line), and 470 nm (purple line).

when excited at 350 nm disappears over time as a second fluorescence peak appears with excitation at 470 nm. Transient fluorescence changes can also be detected upon excitation at 370 – 450 nm (Figure 3-7B). When exciting at 450 nm, transient fluorescence is detected at 2 s followed by a final fluorescence increase at 30 s with the two peaks overlapping. When exciting at 390 nm, the fluorescence disappearance of the first species contains less overlap with the fluorescence increase of the second species. However, when exciting at 370 nm, the two species form distinct peaks allowing accurate rate determination possible. Upon addition of excess NADPH (0.9 mM), the second fluorescence species disappears completely due to the re-reduction of the FAD. Therefore, the fluorescence trace upon excitation at 370 nm with excess NADPH was overlaid on the absorbance traces in Figure 3-5B. The formation rate constant of the fluorescence peak is 1.1 s^{-1} when excited at 370 nm and 1.7 s^{-1} when excited at 390 nm. This fluorescence peak correlates with the absorbance intermediate determined as hydroxyflavin to give an average formation rate constant of 2.3 s^{-1}. The second fluorescence peak correlates with the accumulation of the oxidized flavin.

PvdA Oxidation in the Absence of Ornithine. The flavin oxidation in PvdA in the absence of ornithine is very different from when ornithine is present. Transient absorbance changes over time at 390 nm and 450 nm are still detected (Figure 3-8). However, only one long-lived intermediate is detected at 2 s. The formation of the

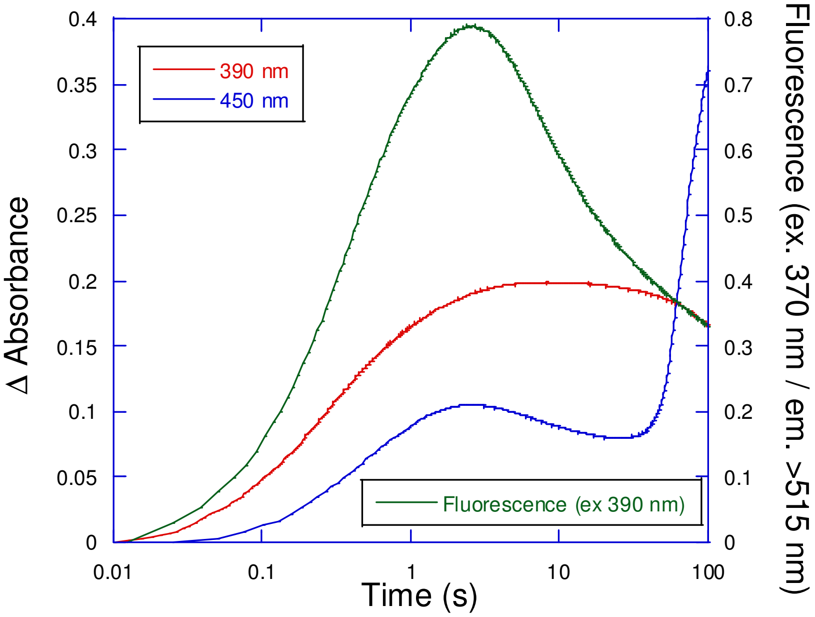

Figure 3-8: Flavin oxidation in PvdA in the absence of substrate. Absorbance changes were monitored over time at 390 nm (red line) and 450 nm (blue line). Fluorescence changes above 515 nm were detected upon excitation at 370 nm (green line). The fluorescence peak forms and decays on the same time scale as the first absorbance peak and was designated as hydroxyflavin.

intermediate is oxygen dependent with a rate constant determined as 1.7 s^{-1} (Figure 3-9). Fluorescence emission over time upon excitation at 390 nm indicated the presence of one intermediate that formed with a rate constant of 1.8 s^{-1} and decayed with a rate of 0.04 s^{-1}. The correlation between the absorbance and fluorescence traces indicates that the long-lived intermediate formed is hydroxyflavin.

Hydrogen Peroxide Formation in PvdA. PvdA has been shown to produce hydrogen peroxide in the presence of L-lysine, a nonsubstrate effector (*13*). However, the production of hydrogen peroxide in the absence of substrate has not been tested. Therefore, the NADPH oxidation and hydrogen peroxide formation of PvdA was tested under several experimental conditions (Figure 3-10, Table 3-3). With 2 mM L-ornithine as the substrate, very little hydrogen peroxide (0.39 μM) was formed compared to the amount of NADPH oxidized (59.93 μM). When 40 mM L-ornithine was used, the NADPH oxidation was comparable to that for 2 mM ornithine, but three times more hydrogen peroxide was formed (1.32 μM after 45 s) indicating enzyme uncoupling due to substrate inhibition. Using L-lysine as the substrate resulted in less NADPH oxidation (similar to the results in Chapter 2) but a large increase in the hydrogen peroxide formation (7.79 μM) detected at 45 s. Lastly, when no substrate was added, there was a steady amount of NADPH oxidation over time (2.65 μM after 45 s) and little hydrogen peroxide formed (0.14 μM). Even with a 40-fold increase in PvdA concentration, there was little production of hydrogen peroxide (data not shown).

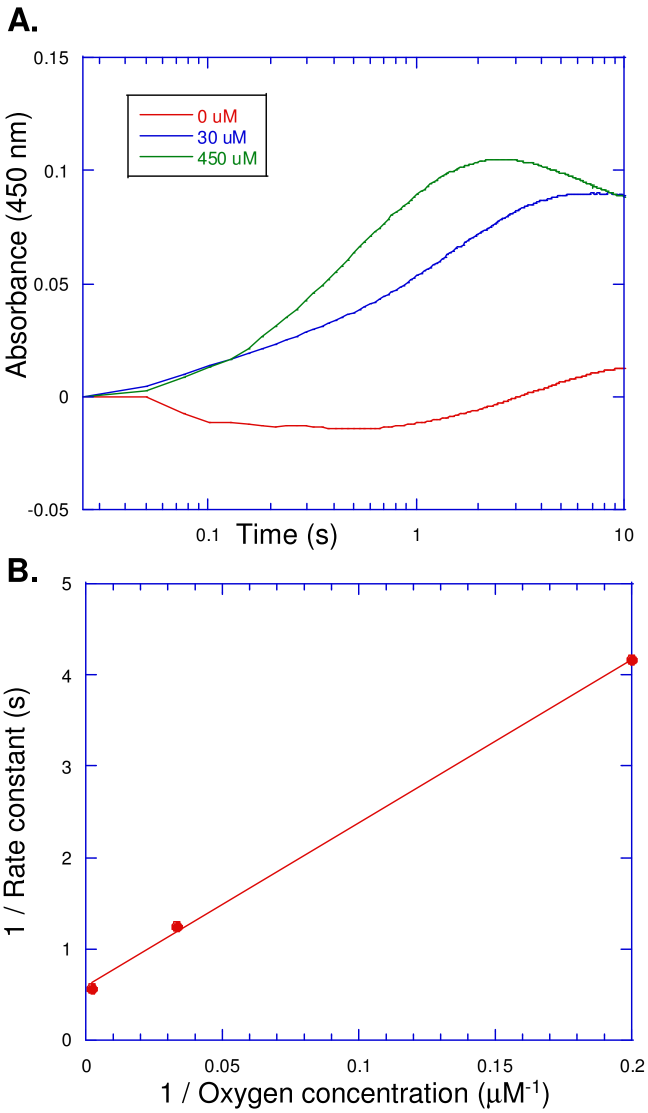

Figure 3-9: Oxygen dependence of the intermediate formation in PvdA in the absence of substrate. *A*. Absorbance changes detected at 450 nm with 5 μM (red line), 30 μM (green line), and 450 μM (blue line) O_2. Lines were fit with the sum of exponentials equation. *B*. Rate constants obtained from the fitted lines in (A) were plotted versus the oxygen concentration as an inverse plot to determine the first order rate constant of 1.7 s^{-1} and the K_d for O_2 of 30.7 μM.

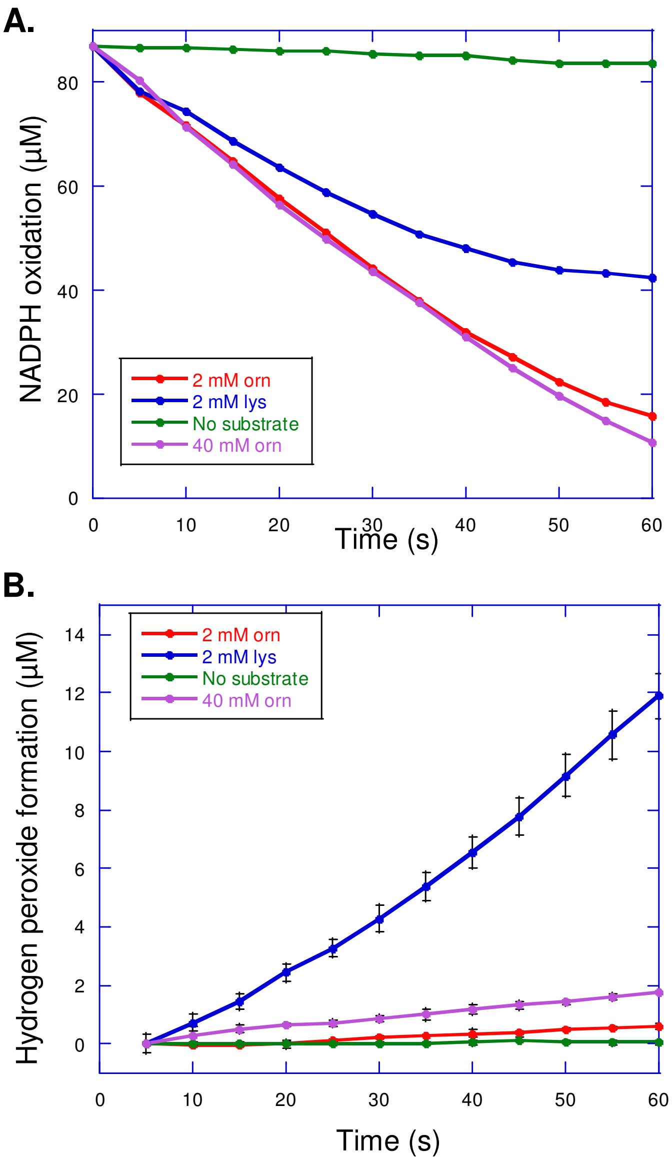

Figure 3-10: PvdA NADPH oxidation and hydrogen peroxide formation in the presence and absence of substrates. *A*. NADPH oxidation was monitored as an absorbance decrease at 366 nm with 2 mM L-ornithine (red line), 2 mM L-lysine (blue line), no substrate (green line), or 40 mM L-ornithine (purple line). *B*. The formation of hydrogen peroxide by PvdA uncoupling as monitored by an increase in absorbance at 440 nm for 2 mM L-ornithine (red line), 2 mM L-lysine (blue line), no substrate (green line), or 40 mM L-ornithine (purple line).

Table 3-3: PvdA hydrogen peroxide formation after 45 seconds

Substrate	NADPH oxidized (μM)	H_2O_2 formed (μM)	Ratio*
2 mM L-ornithine	59.93	0.39	0.01
2 mM L-lysine	41.72	7.79	0.19
No substrate	2.65	0.14	0.05
40 mM L-ornithine	61.92	1.32	0.02

* = the ratio of hydrogen peroxide formation to the amount of NADPH oxidized

Discussion

PvdA has steady-state characteristics distinct from *p*-hydroxybenzoate hydroxylase (PHBH) and flavin monooxygenase (FMO) thus indicating that the reaction mechanism employed by PvdA may differ from its two homologues. Therefore, stopped-flow techniques were employed to determine the different states of the flavin along the catalytic cycle to identify possible reaction mechanisms for PvdA and understand how the mechanisms compare to the homologues PHBH and FMO.

The flavin reduction in PvdA was monitored as a decrease in absorbance at 450 nm in all possible mixing variations (Figure 3-3B). All the different mixing schemes had similar rate constants (Table 3-1). From these data it can be concluded that flavin reduction occurs in the absence of ornithine and that the order of addition of the coenzymes does not affect the reduction rate. Therefore, the PvdA flavin reduction is more similar to the substrate-independent reduction of FAD in FMO. In contrast, PHBH requires substrate for effective FAD reduction.

The oxidation of the reduced flavin in PvdA in the presence of ornithine shows two transient intermediates (Figure 3-5B). The first intermediate, hydroperoxyflavin, forms rapidly (142 s^{-1}), is oxygen-dependent (Figure 3-7), and is characterized by changes in the absorbance at 390 nm but not at 450 nm, and is not fluorescent. The second intermediate formed during PvdA flavin oxidation, hydroxyflavin, is characterized by absorbance changes at 390 nm and 450 nm and is highly fluorescent. This second intermediate forms with an average rate constant of 2.3 s^{-1} and decays as the oxidized flavin is formed with a rate constant of 0.16 s^{-1}. The formation of the oxidized flavin is detected as an absorbance change only at 450 nm not at 390 nm. A similar oxidation pathway has been determined for PHBH and FMO (*1, 3, 4, 7-10*).

In the absence of substrate, only one intermediate is detected in PvdA with a rate constant for formation of 1.7 s^{-1} (Figure 3-8). The intermediate shows an increase in absorbance at 390 nm and 450 nm was well as fluorescence emitting >515 nm when excited at 390 nm. Therefore, the intermediate detected is hydroxyflavin. In PHBH and FMO, only hydroperoxyflavin is detected in the absence of substrate, which is eliminated from the enzyme as hydrogen peroxide to yield the oxidized flavin (*3, 7, 10*). Therefore, the mechanism of PvdA is distinct from those of the two homologues in the absence of substrate.

To determine if hydrogen peroxide is being formed in the absence of substrate in PvdA, the hydrogen peroxide formation over time was monitored with different substrates and in the absence of substrate (Figure 3-10, Table 3-3). When ornithine is added as the substrate, NADPH oxidation occurs at a constant rate with the two saturating concentrations of ornithine tested. However, the hydrogen peroxide produced increases with increasing ornithine concentration from 1% to 2% of the NADPH oxidation. This increase in hydrogen peroxide formation is indicative of uncoupling of the enzyme most likely due to substrate inhibition, which was observed by steady-state kinetics as presented in Chapter 2. When L-lysine was used as a nonsubstrate effector, a decrease in the amount of overall NADPH oxidation was observed as compared to ornithine as the substrate. Under these conditions, a large increase in the production of hydrogen peroxide is detected with 19% of the NADPH oxidation being channeled into hydrogen peroxide formation. This result is consistent with the substrate specificity studies in Chapter 2 and (*13*). In contrast, when no substrate is added to PvdA, little NADPH is oxidized with very little hydrogen peroxide formed even at very high enzyme concentrations. The ratio of hydrogen peroxide to NADPH oxidation is only 5% suggesting that the electrons donated by NADPH oxidation are not being channeled into hydrogen peroxide formation. This agrees with the stopped-flow studies that the hydroperoxyflavin is not being generated and thus cannot decompose to form hydrogen peroxide in the absence of substrate. However, enzyme inactivation was detected after ~45 s in this assay solution potentially by the Triton X-100 used to stabilize the chromophore. The formation of hydrogen peroxide at longer time points will be retested in future experiments with Amplex Red (Molecular Probes), a chromophore that does not require Triton X-100 for stability, thus simplifying the assay solution.

The PvdA reaction mechanism has been determined using transient state kinetics (Figure 3-11). PvdA begins the catalytic cycle by binding FAD with a binding rate constant of 11 s^{-1} and NADPH. The FAD becomes reduced in the absence of substrate (0.452 s^{-1}) indicating that the PvdA catalytic mechanism is distinct from that of PHBH. Once PvdA has bound ornithine and molecular oxygen,

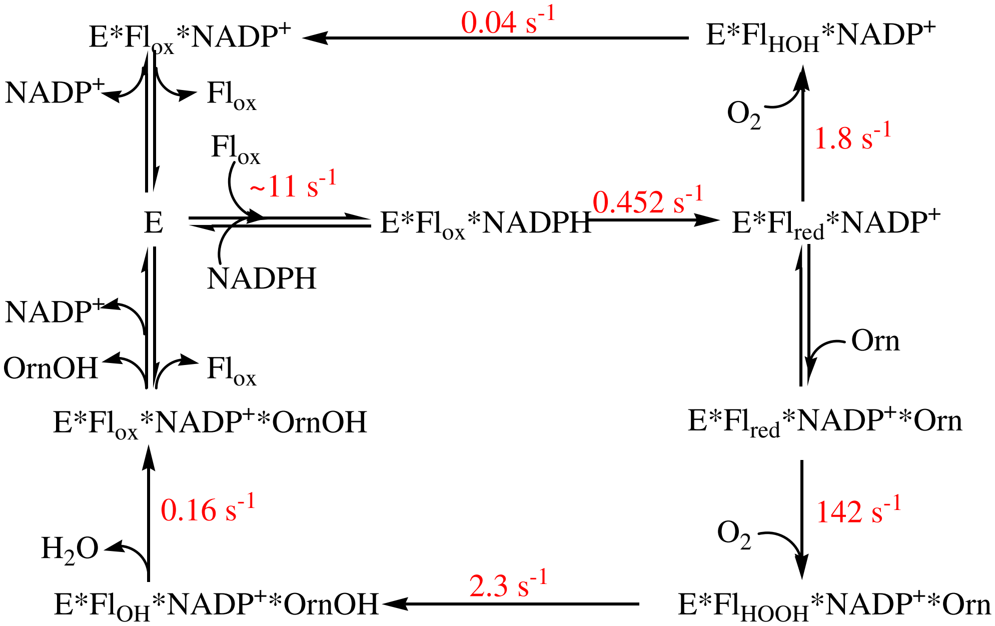
E*Fl$_{ox}$*NADP$^+$
0.04 s^{-1}
E*Fl$_{HOH}$*NADP$^+$
NADP$^+$
Fl$_{ox}$
O$_2$
1.8 s^{-1}
Fl$_{ox}$
~11 s^{-1}
E
E*Fl$_{ox}$*NADPH
0.452 s^{-1}
E*Fl$_{red}$*NADP$^+$
NADPH
NADP$^+$
Orn
OrnOH
Fl$_{ox}$
E*Fl$_{ox}$*NADP$^+$*OrnOH
E*Fl$_{red}$*NADP$^+$*Orn
0.16 s^{-1}
142 s^{-1}
O$_2$
H$_2$O
2.3 s^{-1}
E*Fl$_{OH}$*NADP$^+$*OrnOH
E*Fl$_{HOOH}$*NADP$^+$*Orn

Figure 3-11: PvdA reaction mechanism. PvdA (E) binds FAD (Fl$_{ox}$) and NADPH, and the FAD becomes reduced (Fl$_{red}$). Ornithine (Orn) and molecular oxygen (O$_2$) bind to PvdA and the FAD is reoxidized passing through two transient intermediate steps, hydroperoxyflavin (Fl$_{HOOH}$) and hydroxyflavin (Fl$_{OH}$). In the absence of ornithine, the FAD forms hydroxyflavin and becomes oxidized. The rate constants for the formation of each step are labeled in red.

the reduced flavin is converted to hydroperoxyflavin, the first of two transient intermediates, with a rate constant of 142 s^{-1} followed by hydroxylation of the substrate into hydroxyornithine and conversion of the hydroperoxyflavin into hydroxyflavin, the second transient intermediate. The flavin returns to the oxidized form by release of the hydroxylated product and water (0.16 s^{-1}). In contrast, in the absence of substrate, the reduced flavin is converted to hydroxyflavin (1.8 s^{-1}) and is slowly reoxidized (0.04 s^{-1}). The substrate-independent reoxidation of PvdA is distinct from both PHBH and FMO. While further work is needed to refine the reaction mechanism, in particular to determine the order of substrate and coenzyme addition and product release, this first transient mechanism suggests that PvdA has a novel reaction mechanism.

References

(1) Palfey, B. A., and Massey, V. (1998) Flavin-Dependent Enzymes, in *Comprehensive Biological Catalysis* (Sinnott, M., Ed.) pp 83-154, Academic Press, San Diego.

(2) Nakamura, S., Ogura, Y., Yano, K., Higashi, N., and Arima, K. (1970) Kinetic Studies of the Reaction Mechanism of *p*-Hydroxybenzoate Hydroxylase. *Biochem 9*, 3235-3242.

(3) Howell, L. G., and Massey, V. (1970) A Non-substrate Effector of *p*-Hydroxybenzoate Hydroxylase. *Biochem Biophys Res Commun 40*, 887-893.

(4) Husain, M., and Massey, V. (1979) Kinetic studies on the reaction of *p*-hydroxybenzoate hydroxylase. Agreement of steady state and rapid reaction data. *J Biol Chem 254*, 6657-66.

(5) Howell, L. G., Spector, T., and Massey, V. (1972) Purification and Properties of *p*-Hydroxybenzoate Hydroxylase from *Pseudomonas fluorescens*. *J Biol Chem 247*, 4340-4350.

(6) Spector, T., and Massey, V. (1972) *p*-Hydroxybenzoate Hydroxylase from *Pseudomonas fluorescens*, Evidence for an Oxygenated Flavin Intermediate. *J Biol Chem 247*, 5632-5636.

(7) Spector, T., and Massey, V. (1972) Studies of the Effector Specificity of *p*-Hydroxybenzoate Hydroxylase from *Pseudomonas fluorescens*. *J Biol Chem 247*, 4679-4687.

(8) Beaty, N. B., and Ballou, D. P. (1981) The reductive half-reaction of liver microsomal FAD-containing monooxygenase. *J Biol Chem 256*, 4611-8.

(9) Beaty, N. B., and Ballou, D. P. (1981) The oxidative half-reaction of liver microsomal FAD-containing monooxygenase. *J Biol Chem 256*, 4619-25.

(10) Jones, K. C., and Ballou, D. P. (1986) Reactions of the 4a-hydroperoxide of liver microsomal flavin-containing monooxygenase with nucleophilic and electrophilic substrates. *J Biol Chem 261*, 2553-9.

(11) Macheroux, P., Plattner, H. J., Romaguera, A., and Diekmann, H. (1993) FAD and substrate analogs as probes for lysine N6-hydroxylase from *Escherichia coli* EN 222. *Eur J Biochem 213*, 995-1002.

(12) Yeh, E., Cole, L. J., Barr, E. W., Bollinger, J. M., Jr., Ballou, D. P., and Walsh, C. T. (2006) Flavin redox chemistry precedes substrate chlorination during the reaction of the flavin-dependent halogenase RebH. *Biochemistry 45*, 7904-12.

(13) Ge, L., and Seah, S. Y. (2006) Heterologous expression, purification, and characterization of an l-ornithine N(5)-hydroxylase involved in pyoverdine siderophore biosynthesis in *Pseudomonas aeruginosa*. *J Bacteriol 188*, 7205-10.

Chapter 4

Siderophore Biosynthetic Protein Purification, Crystallization, and X-ray Diffraction Collection

A good first step in rationally designing inhibitors of an enzyme is to determine the three-dimensional structure of the protein to be inhibited. There are two main ways of protein structure determination, nuclear magnetic resonance (NMR) and x-ray crystallography. For NMR studies, the protein typically needs to be less than ~30 kDa for good resolution of the chemical shift peaks. Above 30 kDa, the protein contains many amino acids in similar environments so the chemical shift peaks overlap. The finished NMR structure is representative of the protein's various conformations in solution. In contrast, determining a structure by x-ray crystallography can be performed on a protein of any size. However, the determined structure is usually one protein conformation. Therefore, x-ray crystallography gives snapshot views of the protein along the catalytic cycle.

To determine a protein structure using x-ray crystallography, the protein must assemble in an ordered manner (in a crystal) so x-rays diffracting from the ordered protein can be strong enough to be measured. Therefore, large three-dimensional crystals of the protein are required of at least 0.1 mm per side. Protein purity promotes crystal formation, making protein purification a very important step. Packing of the protein into a crystalline state requires protein in the same oligomerization state as monomer, dimers, etc. Therefore, being monodispersed (or having only one oligomerization state) in solution is preferred. Monitoring the oligomerization state in solution can occur using a variety of methods. Two simple methods are gel filtration chromatography and dynamic light scattering (DLS). Gel filtration chromatography separates particles based primarily on size; therefore, the molecular weight of proteins and protein complexes can be determined by comparison to proteins of known molecular mass. DLS monitors the time-dependent fluctuations of scattered light arising from Brownian motion, the random thermal motion of the particles. By analyzing the time-dependence of the motion, the hydrodynamic radius of the molecules in solution, or the effective radius of the hydrated molecule, can be determined.

Once the protein is pure and monodispersed, crystallization can begin. The protein needs to be at a sufficient concentration (initial trials begin at about 10 mg/ml) to promote crystallization. Initial crystallization experiments use sparse matrix screening, a protocol that uses a variety of different buffer components to find a condition that promotes crystalline formation (*1, 2*). A drop is prepared with a 1:1 ratio of protein solution and precipitant solution. The drop is placed or hung over a sealed well containing more precipitant solution to create a closed environment (Figure 4-1). The drop slowly dehydrates as water is transferred from the less concentrated drop to the more concentrated well solution by vapor diffusion, causing the protein solution to become supersaturated. A particular precipitant solution may

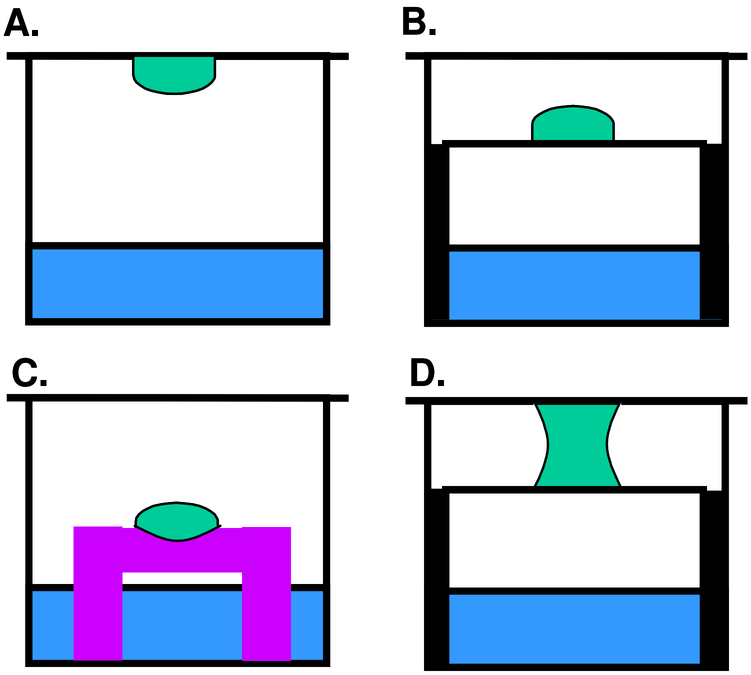

Figure 4-1: Crystallization vapor diffusion drop geometries in sealed wells using a 1:1 ratio of protein to precipitant solution (green) suspended above a well of precipitant solution. *A.* Hanging drop with the crystallization drop inverted and suspended above the precipitant solution. *B.* Sitting drop with the drop resting on a cover slip above the precipitant solution. *C.* Bridging drop with the drop resting in a concave indention in a bridge (purple) above the precipitant solution. *D.* Sandwich drop with the drop suspended between two cover slips above the precipitant solution.

promote crystal growth, may promote protein precipitation, or may leave the protein unchanged and soluble. Initial crystallization trials often employ hanging drop vapor diffusion in which the drop is inverted above the crystallization solution (Figure 4-1A). Several other methods of vapor diffusion can be employed. Sitting (Figure 4-1B) and bridging (Figure 4-1C) techniques rest the drops on cover slips or bridges, while sandwich drops (Figure 4-1D) suspend the drop between two cover slips. These different geometries modify the surface tension of the drop and may change the morphology of forming crystals. Hanging drops are first attempted because of the relative ease of setting up the drops.

Formation of a regular crystal lattice is extremely important. If the lattice is not a regular repeating unit, the data collected from x-ray diffraction is not interpretable. Good quality diffraction is collected with sufficiently large, three-dimensional crystals. If crystals grow in only one direction, needles form. When growth is in two dimensions, crystals form as plates. Neither needle nor plate crystals are useful in diffraction analysis. Crystals must also be single for diffraction data collection. However, sometimes crystals nucleate in groups forming clusters. Each crystal in a cluster diffracts independently, preventing regular diffraction required for structure determination. Therefore, optimization of the crystal conditions to produce large, single crystals is necessary.

For crystal optimization, the concentrations of the precipitant solution components are varied (*3*). If the formed crystals are small or are grouped, seeding techniques can be used to obtain single crystals (*2, 4*). Macroseeding places a single small, nicely formed crystal into a fresh drop containing protein and crystallization solution to further the growth from a single crystal. For groups of crystals, the crystals can be collected, crushed, and used as a seed stock for microseeding (adding crushed crystals into a fresh drop) or streak seeding (streaking crushed crystals through a fresh drop using a cat whisker).

If crystals develop too fast, the lattice can be irregularly formed, making diffraction collection impossible. Several methods can be used to slow down the rate of crystal development. One method involves adding a layer of oil (silicone or paraffin) between the drop and the crystallization solution, which slows down the rate of vapor diffusion and thus the rate of protein concentration (Figure 4-2A). Equilipro buttons (Hampton Research) only allow diffusion through small holes, producing results similar to an oil layer (Figure 4-2B). A final method involves using dialysis buttons (Hampton Research), in which the protein solution is placed in a button inside a dialysis membrane (Figure 4-2C) (*2*). The crystallization solution slowly diffuses into the protein solution and can slow down crystal growth.

If the crystals cannot be optimized with any of the above techniques, less well-known techniques can be attempted. Varying the ratio of protein to crystallization solution in the drops can change the dynamics of the vapor diffusion and may optimize crystal formation. If the crystals nucleate and grow against the glass cover slip, switching to a plastic cover slip or using plates containing plastic lids (such as plates from Nextal) may optimize crystal formation. Growing crystals inside

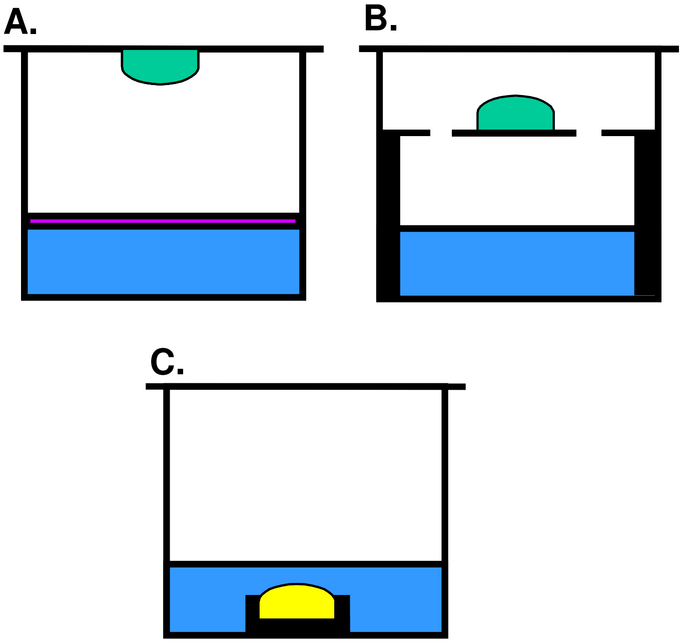

Figure 4-2: Optional crystal optimization techniques. *A*. Addition of a layer of oil (purple) between the crystallization solution (blue) and the crystallization drop (green) to slow the rate of vapor diffusion. *B.* Equilipro buttons with small holes between the crystallization solution and the crystallization drop. *C.* Dialysis buttons to allow the slow diffusion of the crystallization solution across a membrane to the protein solution (yellow).

silica or agarose gels may stimulate single crystal formation (*2*). Finally, techniques such as feeding, adding fresh protein to a drop already containing crystals, or weeding, removing some of the crystals from a drop once crystals have formed can be used to optimize crystal formation (*2, 4*).

Once single, large, three-dimensional crystals are formed, x-ray diffraction analysis is undertaken. X-rays are used for structure determination because the wavelength of light must be on the order of the desired resolution (*5, 6*). For protein structure determination, the resolution needed is 1.5 – 2.5 Å. The crystal is oscillated in the x-ray beam and a full data set consists of a series of oscillated images generated by rotating the crystal 90 – 360°, depending on the symmetry of the crystal. Crystals with high symmetry require fewer degrees of data collection than lower symmetry crystals. From the collected x-ray data, two pieces of data can be obtained, the position (*h*, *k, l*) and intensity of the spots. To determine the three-dimensional structure of a protein, one additional piece of data must be obtained, the phases for each spot. The phases for each spots are the cumulative effect of all the diffracted waves from each atom in the crystal. The phases cannot be directly measured from the x-ray diffraction data and must be mathematically approximated. Three techniques used for phase approximation are molecular replacement (MR), multiple isomorphous replacement (MIR), and multi-wavelength anomalous dispersion (MAD).

Molecular replacement uses a homologous protein that is hypothesized to be a very similar structure to the crystallized protein (*5, 6*). With this assumption, the phases of the two proteins should be very similar. The model protein is placed into the unit cell of the crystallized protein by performing rotation and translation functions in Patterson space and initial phases are calculated. These initial phases are used along with the measured reflection positions and intensities to generate a map of the protein's electron density. This technique works very well with proteins of high sequence similarity and with similar function. However, if the model protein does not have a similar structure to the crystallized protein, molecular replacement will not work. Furthermore, if there is no determined structure for the homologous proteins, there is no initial model to use in the calculations.

A second technique, multiple isomorphous replacement, does not require a model protein to obtain phase information (*5, 6*). Instead, this method requires soaking or co-crystallization of the protein with heavy metals. One consideration is that the crystal lattice remains intact or isomorphous. Perturbing the crystal lattice will change the unit cell lengths (thus make the crystals non-isomorphous) and cannot be used for MIR. A second consideration is that the heavy metal must bind specifically (in a similar spot) for all or most of the protein molecules in the crystal or the diffraction contribution of the heavy metal cannot be measured. A wide variety of heavy metals can be used for MIR and each metal has different amino acid binding preferences depending on the chemical nature of the metal. Diffraction data of crystals containing heavy atom derivatives are collected in a similar manner to native crystals (crystals not containing heavy metals). The native data is subtracted from the heavy metal data leaving intensities corresponding only to the heavy metal. This leaves only a few atoms that must be positioned in each unit cell. Once the heavy atoms are placed and the phases obtained, these phases can be used to approximate the phases for the protein atoms. However, with one heavy metal, two possible phases result for each atom. Therefore, to remove the phase ambiguity, two or more heavy metals must be used that bind at different sites in the unit cell.

A third method for obtaining phases is multi-wavelength anomalous dispersion (*5, 6*). A heavy metal, which absorbs light at known wavelengths, is incorporated into the crystal lattice. The heavy metal absorbs x-rays, creating an anomalous signal by disrupting the relationship of the reflection positions (*h*, *k*, *l*) to (-*h*, -*k*, -*l*). With molecules that do not absorb x-rays, the (*h*, *k*, *l*) and (-*h*, -*k*, -*l*) positions have identical intensities and are called Friedel pairs. When a heavy metal with an anomalous signal absorbs x-rays, the intensities are no longer the same between the Friedel pairs and the difference can be measured. X-ray data is collected at three wavelengths near the edge of the heavy metal absorption; the inflection point, the peak of absorbance, and a remote position where absorbance from the heavy metal is not detected. The collection of several wavelengths requires the use of tunable synchrotron radiation for data collection. The data cannot be collected on a copper anode-rotating disc (a home source), which only provides x-rays at a wavelength of 1.54 Å. By comparing the Friedel pairs from the data collected at the three different wavelengths, the phases for the heavy metals can be determined. These phases can help approximate the phases for the remainder of the molecules in the unit cell. Most MAD data is collected on proteins with selenomethionine incorporated into the sequence. This places a heavy metal with anomalous scattering (selenium) at a known position within the protein sequence. Once the position of the heavy atom is known, the phases can be approximated for the remainder of the atoms in the unit cell and an electron-density map can be generated.

A fourth, hybrid phasing technique can be used if a single heavy metal derivative has an anomalous signal, termed single isomorphous replacement with anomalous scattering (SIRAS). The position of the heavy metal can be determined in a similar manner to MIR. However, by using the anomalous scattering of the heavy metal, the phases can be determined with only one heavy metal. One heavy metal, iodine, can be used for SIRAS using a rotating copper anode because the anomalous absorption peak is near 1.54 Å (*7*). Once the phases have been approximated and an electron density map has been generated, the protein's sequence can be built into the density. The completed structure can be generated after several rounds of refinement to place the atoms into the correct position into the electron density.

My project includes the purification and crystallization of four proteins involved in siderophore biosynthesis, PvdA, PvdF, and PchG from *Pseudomonas aeruginosa*, and Irp3 from *Yersinia enterocolitica*. The derivatization of ornithine into formyl-hydroxyornithine is one of the initial steps in pyoverdin production by *P. aeruginosa*. Ornithine modification is a two-step process involving two enzymes, PvdA and PvdF (*8-10*). Knockout mutations of *pvdA* or *pvdF* result in pyoverdin-deficient bacteria (*8-10*), indicating that the modification of ornithine is required for siderophore biosynthesis. PvdA is an FAD-dependent monooxygenase that converts ornithine into hydroxyornithine. The biochemical characterization and reaction mechanism have been elucidated and are detailed in Chapters 2 and 3. PvdF is a formyl-transferase that produces formyl-hydroxyornithine from hydroxyornithine. PvdF studies have been done with *P. aeruginosa* cells containing overproduction plasmids and deletion mutants of *pvdF* (*10*). The biochemical characterization of PvdF has not been accomplished and the cofactors for PvdF catalysis are not known.

PchG and Irp3 are NADPH-dependent reductase homologues involved in the biosynthesis of pyochelin in *P. aeruginosa* and yersiniabactin in *Y. enterocolitica*, respectively (*11-13*). Knockout mutations of *pchG* and *irp3* are deficient in pyochelin and yersiniabactin production, respectively, indicating the proteins are required for completed siderophores. These reductases are the only downstream, stand-alone proteins involved in the NRPS assembly line, while all other modifications to the siderophores (for example, epimerization and methylation) occur by domains incorporated into the NRPS proteins (*14*). PchG and Irp3 homologues are all involved in siderophore biosynthesis. No siderophore reductase structures are known.

Here we report the initial steps to determining the three-dimensional structures of four accessory proteins involved in siderophore production: PvdA, PvdF, PchG, and Irp3. These steps include cloning the genes, overproduction and purification of the proteins, buffer optimization, crystallization, data collection, and initial phasing. Obtaining the structures of these proteins is the first step towards rational design of inhibitors to siderophore biosynthesis.

Materials and Methods

Standard Cloning Procedure. The pyoverdin and pyochelin biosynthetic genes of interest delineated in the following sections were amplified from PAO1 *P. aeruginosa* genomic DNA using polymerase chain reaction (PCR) with Herculase polymerase (Stratagene). The *irp3* gene was amplified from *Y. enterocolitica* strain 33114 genomic DNA by PCR with Eppendorf® MasterMix (Eppendorf) and 1.5 mM magnesium acetate. The primers for each clone are described in Table 1. The amplified fragments were digested with restriction enzymes (Table 4-1), and ligated with T4 DNA ligase (New England Biolabs) into: pET28b (Novagen) for recombinant proteins designed to include an N-terminal His_6 tag, pET29b (Novagen) for recombinant proteins with a C-terminal His_6 tag, pET26b (Novagen) for periplasmic recombinant proteins, or pTYB1 (New England Biolabs) for Intein fusion recombinant proteins. The resulting plasmids were transformed into BL21(DE3) *E. coli* strain (Stratagene) for overproduction of the proteins of interest. B834(DE3) *E. coli* cells (Stratagene) were used for production of selenomethionine (Se-Met) protein for use in multi-wavelength anomalous dispersion (MAD) phasing experiments.

Site-Directed Mutagenesis. Specific mutations were incorporated into the gene of interest with the QuikChange® site-directed mutagenesis kit (Stratagene). As per the manufacturer's instructions, the plasmid containing the gene was PCR amplified

Table 4-1: Cloning primers

Protein	Primer	Primer sequence	Restriction Enzyme	Plasmid	Cloning procedure[$]
PvdA	forward	5’-GAA TTC CAT ATG ACT CAG GCA ACT GCA ACC-3’	*Nde*I	pET28b	Standard *
	reverse	5’-CCC AAG CTT TCA GCT GGC CAG GGC GTG-3’	*Hind*III		Standard *
PvdF-throm-His$_6$	forward	5’-AAT TAT ATA CAT ATG ACG AAA AGG AAA CTG GCC TA-3’	*Nde*I	pET29b	Standard
	reverse	5’- AAT ATA ATA CAG ATC TGG GAG CTT CTC GGC GAG CAG C -3’	*Bgl*II		Standard
PvdF	forward	5’-CTG CTC GCC GAG AAG CTC TGA TGA CTG GGT ACC CTG GTG-3’	n.a.	pET29b	Mutagenesis
	reverse	5’-CAC CAG GGT ACC CAG TCA TCA GAG CTT CTC GGC GAG CAG-3’	n.a.		Mutagenesis
PchG-His$_6$	forward	5’-ATG CCA GAG GAG GCG AGC ATA TGA GCG ACG TTC GTT CCG-3’	*Nde*I	pET29b	Standard [#]
	reverse	5’-AGC AGG CGC CAC AGC ACC GCT CGA GCG AGG CTT GCT CC-3’	*Xho*I		Standard [#]
PchG	forward	5’-G GAA CAG GTG CTG GAG CAA GCC TCG TAA TAA CAC CAC CAC CAC CAC C-3’	n.a.	pET29b	Mutagenesis
	reverse	5’-G GTG GTG GTG GTG GTG TTA TTA CGA GGC TTG CTC CAG CAC CTG TTC C-3’	n.a.		Mutagenesis
PchG-throm-His$_6$	forward	5’-AAT TAT ATA CAT ATG AGC GAC GTC CGT TCC GTG-3’	*Nde*I	pET29b	Standard
	reverse	5’-ATA ATA CAG ATC TGG CGA GGC TTG CTC CAG CAC CTG-3’	*Bgl*II		Standard
ss-PchG	forward	5’-A TTG GAT CCG ATG AGC GAC GTC CGT TCC GTG-3'	*BamH*I	pET26b	Standard
	reverse	5’-GA TTC AAG CTT TCA CGA GGC TTG CTC CAG CTC-3'	*Hind*III		Standard
PchG-Intein	forward	Same as PchG1 forward primer	*Nde*I	pTYB1	Standard
	reverse	5’-ATA ATA GGA AGA GCC CGA GGC TTG CTC CAG CAC CTG-3'	*Sap*I		Standard
	reverse	5’-TAA ATA CTC GAG CGA GGC TTG CTC CAG CAC CTG-3'	*Xho*I		Standard
Irp3	forward	5’-ATT CTT CAT ATG CCG TCC GCC TCC CCA AAA CA-3'	*Nde*I	pET29b	Standard
	reverse	5'-GGA TCC CTC GAG CGC CTC CTT ATC ATC ATC GTT G-3'	*Xho*I		Standard

n.a. = not applicable

* = Primer sequence and cloning described in chapter 2.

[#] = Primer sequence and cloning described in (*11*).

[$] Standard = amplification for incorporation of the gene of interest into the over-production plasmid. Mutagenesis = procedure used to introduce a stop codon for elimination of the C-terminal tag from a previous clone.

using mutagenic primers flanking the mutation site to incorporate the required nucleotide changes, and the non-mutated template plasmid was digested with *Dpn*I, leaving only the amplified vector containing the desired mutation. The plasmid was transformed into BL21(DE3) *E. coli* cells for the overproduction of the protein of interest.

Cloning of the genes of interest. The cloning of the *pvdA* gene was performed as described in Chapter 2 to yield the 443 amino acid PvdA protein with an N-terminal His_6 tag.

To produce the PvdF-throm-His_6 protein, the *pvdF* gene was amplified from *P. aeruginosa* genomic DNA by PCR with 8% (v/v) DMSO as the adjuvant using the standard cloning procedure. The amplified fragment of 825 base pairs was digested (*Nde*I / *Bgl*II) and ligated into the pET29b vector. The resulting plasmid (*pvdF-throm-His*$_6$) was transformed into BL21(DE3) *E. coli* cells for over-production of the PvdF-throm-His_6 protein with a thrombin cleavage site and a C-terminal His_6 tag, adding 36 amino acids to the end of the native 275 amino acid PvdF protein. The *pvdF-throm-His*$_6$ plasmid was modified by site-directed mutagenesis to incorporate two stop codons at the end of the native *pvdF* gene. The resulting plasmid (*pvdF*) encodes the native PvdF protein with no purification tag.

The *pchG-His*$_6$ clone was kindly provided by Christopher Walsh at Harvard Medical School (*11*). The plasmid encodes for the PchG-His_6 protein with a C-terminal His_6 tag adding 7 amino acids to the end of the native 349 amino acid PchG protein. The *pchG-His*$_6$ clone was modified with the QuikChange® kit to add two stop codons to the end of the native *pchG* gene by site-directed mutagenesis. The resulting plasmid (*pchG*) encodes the native PchG protein containing no purification tag. To produce the PchG protein with a cleavable histidine tag, the *pchG* gene was amplified from *P. aeruginosa* genomic DNA by PCR with 8% (v/v) DMSO as an adjuvant using the standard cloning procedure. The amplified DNA of 1047 base pairs was digested (*Nde*I / *Bgl*II) and ligated into the pET29b vector. The resulting plasmid (*pchG-throm-His*$_6$) was transformed into BL21(DE3) *E. coli* cells for over-production of the PchG-throm-His$_6$ protein with a thrombin cleavage site and a C-terminal His$_6$ tag adding a total of 36 amino acids to the end of the native PchG protein. To produce a periplasmic PchG protein, the *pchG* gene was PCR amplified from *P. aeruginosa* genomic DNA with 10% (v/v) DMSO and 3% (v/v) glycerol as adjuvants. The amplified *pchG* gene was digested (*Bam*HI / *Hind*III) and ligated into the pET26b vector. The resulting plasmid (*ss-PchG*) was transformed into BL21(DE3) *E. coli* cells for over-production of the ss-PchG protein containing an N-terminal periplasmic signal sequence for periplasmic purification. Finally, to produce a PchG fusion protein, the *pchG* gene was amplified from *P. aeruginosa* genomic DNA similar to that of ss-PchG cloning. The resulting amplified DNA was digested with *Nde*I and *Sap*I for ligation into the pTYB1 vector. The reverse primer was redesigned to exchange the 5' *Sap*I site for a *Xho*I site for more efficient digestion.

To produce Irp3 protein, the *irp3* gene was amplified from *Y. enterocolitica* genomic DNA. The amplified DNA of 1095 base pairs was digested with restriction enzymes (*Nde*I / *Xho*I) and ligated into pET29b with the addition of a phosphatase step. The resulting plasmid (*irp3*) was transformed into BL21(DE3) *E. coli* cells for over-production of the 365 amino acid Irp3 protein with a 7 amino acid C-terminal His_6 tag.

Over-production of Cloned Proteins. BL21(DE3) *E. coli* containing the expression plasmid for each protein was grown in LB broth or Terrific broth (Fisher) containing 10% (v/v) glycerol and 50 μg/ml kanamycin while shaking at 225 rpm. The expression protocol for each protein varied by the OD_{600} at induction, the amount of isopropyl-β-D-thiogalactopyranoside (IPTG) added for induction, the temperature before and after induction, and length of growth time before harvesting (Table 4-2). Although the ss-PchG protein over-production was not optimized, several induction conditions were tested as shown in Table 4-3. For selenomethionine over-production of Irp3, the minimal medium contained 1 x M9 salts supplemented with 0.8% (v/v) glycerol, 2 mM $MgSO_4$, 0.1 mM $CaCl_2$, 10 μg/ml thiamine, and a mixture of amino acids (60 mg L-selenomethionine, 50 mg each of leucine, isoleucine and valine and 100 mg each of lysine, threonine and phenylalanine per liter of culture). The media was pre-warmed before inoculation with an overnight culture of BL21(DE3) *E. coli* cells. All cells were harvested by centrifugation (6,000 x g, 10 min, 4 ^{o}C) and resuspended in the buffer required for the initial purification step.

Table 4-2: Protein over-production procedures

Clone	Broth	Pre-induction temperature	OD_{600} at induction	IPTG concentration	Post-induction temperature	Incubation after induction
PvdA	LB	37 °C	0.8	0.2 mM	37 °C	3 – 4 hours
PvdF-throm-His$_6$	LB	37 °C	0.4	0.2 mM	30 °C	3 – 4 hours
PvdF	LB	37 °C	1.0	0.2 mM	30 °C	3 – 4 hours
PchG-His$_6$*	LB	30 °C	0.4	0 mM	25 °C	24 hours
PchG	LB	30 °C	0.4	0 mM	25 °C	24 hours
PchG-throm-His$_6$	LB	30 °C	0.4	0 mM	25 °C	24 hours
Irp3	LB	22 °C	n.a.	0 mM	n.a.	24 hours
Irp3 Se-Met	Minimal media	37 °C	0.16	n.a.	30 °C	20 hours

* = Over-production protocol described in (*11*).

Table 4-3: ss-PchG-His$_6$ over-production procedures

Broth	Pre-induction temperature	OD$_{600}$ at induction	IPTG concentration	Post-induction temperature	Incubation after induction	Result
LB*	37 °C	0.4	0, 0.2, 1.0 mM	24 °C	3 hours	No protein produced
LB*	37 °C	0.4	0, 0.2, 1.0 mM	30 °C	3 hours	No protein produced
LB*	37 °C	0.4	0, 0.2, 1.0 mM	37 °C	3 hours	No protein produced
LB*	37 °C	0.4	0, 0.2, 1.0 mM	18 °C	20 hours	No protein produced
LB*	37 °C	0.4	0, 0.2, 1.0 mM	24 °C	20 hours	No protein produced
LB*	37 °C	0.4	0, 0.2, 1.0 mM	18 °C	24 hours	No protein produced
LB*	37 °C	0.4	0, 0.2, 1.0 mM	24 °C	24 hours	No protein produced
LB*	37 °C	1.0	0, 0.2, 1.0 mM	37 °C	6 hours	No protein produced
LB*	37 °C	1.0	0, 0.2, 1.0 mM	37 °C	12 hours	Some protein produced
LB*	37 °C	1.0	0, 0.2, 1.0 mM	37 °C	17 hours	Some protein produced
TB#	37 °C	0.4	0, 0.2, 1.0 mM	18 °C	20 hours	No protein produced
TB#	37 °C	0.4	0, 0.2, 1.0 mM	24 °C	20 hours	No protein produced
TB#	37 °C	0.4	0, 0.2, 1.0 mM	18 °C	24 hours	No protein produced
TB#	37 °C	0.4	0, 0.2, 1.0 mM	24 °C	24 hours	No protein produced
TB#	37 °C	1.0	0, 0.2, 1.0 mM	37 °C	6 hours	No protein produced
TB#	37 °C	1.0	0, 0.2, 1.0 mM	37 °C	12 hours	Most protein produced
TB#	37 °C	1.0	0, 0.2, 1.0 mM	37 °C	17 hours	Some protein produced

* LB = Luria-Bertani

TB = Terrific broth

General Purification Procedures. Cells resuspended in purification buffer were disrupted by passage through a French pressure cell (35,000 psi) and the cellular debris was removed by centrifugation (12,000 x g, 30 min, 4 °C). The proteins were purified from the lysate using multiple serial chromatographic steps (Table 4-4 A-C). For proteins containing His_6 tags, the first step was affinity chromatography with a nickel chelating Sepharose fast flow column (Amersham Biosciences). The purification buffer was pH 8.0 (Tris-HCl, HEPES, or potassium phosphate) containing 500 mM NaCl. The proteins were eluted with an imidizole gradient. Further purification utilized ion exchange chromatography (Source 30Q or Source 30S column) and/or gel filtration (Superdex 75 or Superdex 200 column) (all resins and columns were purchased from Amersham Biosciences). The basic buffer for anion exchange was 50 mM glycine, pH 9.0 and the proteins were eluted with a sodium chloride gradient from 0 – 500 mM. The buffer for cation exchange was 50 mM MES, pH 6.0 with a salt gradient similar to anion exchange. The buffer for gel filtration varied according to the protein and was the final buffer used for optimal protein stability and solubility. For proteins lacking a His_6 tag, purification began with anion exchange with Tris-HCl, pH 8.5 or glycine, pH 9.5 as the buffer and the proteins were eluted with a sodium chloride gradient. Further purification was obtained using a variety of chromatography steps as listed in Table 4-4.

Table 4-4A: PvdA, PvdF, PchG-His$_6$, and PchG-throm-His$_6$ protein purification procedures

Protein	First Purification Step Buffer	Second Purification Step Buffer	Third Purification Step Buffer	Protein produced (mg/L culture)
PvdA	Affinity – nickel 20 mM potassium phosphate, pH 8, 500 mM NaCl, 50 mM sodium citrate, and 5 - 500 mM imidazole	Gel filtration - Superdex 200 100 mM potassium phosphate, pH 8.0 and 100 mM sodium citrate	n.r.	20 - 45
PvdF-throm-His$_6$	Affinity - nickel 25 mM HEPES, pH 8.0, 500 mM NaCl, and 5 - 300 mM imidazole	Gel filtration - Superdex 75 50 mM HEPES, pH 8, 150 mM NaCl, 1 mM EDTA, and 10 % glycerol	n.r.	186
PvdF-throm	Affinity - nickel (Following thrombin cleavage) 25 mM HEPES, pH 8.0, 500 mM NaCl, and 5 - 300 mM imidazole	Benzamidine 25 mM HEPES, pH 8.0 and 500 mM NaCl	Gel filtration - Superdex 75 50 mM HEPES, pH 8, 150 mM NaCl, 1 mM EDTA, and 10 % glycerol	78
PvdF	Anion exchange - 30Q 25 mM Tris-HCl, pH 8.5 and 0 – 500 mM NaCl	Gel filtration - Superdex 75 50 mM Tris-HCl, pH 7, 150 mM NaCl, and 1 mM EDTA	n.r.	237
PchG-His$_6$	Affinity - nickel 25 mM Tris-HCl, pH 8.0, 500 mM NaCl, and 5 - 300 mM imidazole	Dialysis 75 mM HEPES, pH 7.5, 5% glycerol, and 10 mM MgCl$_2$	n.r.	46
PchG-throm-His$_6$	Affinity - nickel 25 mM Tris-HCl, pH 8.0, 500 mM NaCl, and 5 – 300 mM imidazole	Dialysis 50 mM Tris-HCl, pH 8 and 100 mM NaCl	n.r.	22
PchG-throm-His$_6$	Affinity - nickel 25 mM Tris-HCl, pH 8.0, 500 mM NaCl, and 5 – 300 mM imidazole	Dialysis 50 mM HEPES, pH 8 and 300 mM NaCl	n.r.	n.d.
PchG-throm-His$_6$	Affinity - nickel 25 mM Tris-HCl, pH 8.0, 500 mM NaCl, and 5 – 300 mM imidazole	Hydrophobic - phenyl 25 mM Tris-HCl, pH 8.0, 500 mM NaCl, and 150 - 0 mM imidazole	Hydrophobic - phenyl 25 mM Tris-HCl pH 8.0, 500 - 0 mM NaCl	n.d.

n.r. = not required
n.d. = not detected

Table 4-4B: PchG protein purification procedures

First Purification Step Buffer	Second Purification Step Buffer	Third Purification Step Buffer	Protein produced (mg/L culture)
Anion exchange - 30Q 100 mM glycine, pH 9.5, 5% glycerol, and 0 – 1 M NaCl	n.r.	n.r.	n.d.
Cation exchange - 30 S 50 mM MES, pH 6, 5% glycerol, and 0 – 1 M NaCl	n.r.	n.r.	n.d.
AS precipitation 0, 20, 40, 60, 80, and 100% ammonium sulfate	n.r.	n.r.	n.d.
AS precipitation 80% ammonium sulfate	Anion exchange - 30Q 100 mM glycine, pH 9.5, 5% glycerol, and 0 – 1 M NaCl	Cation exchange - 30 S 50 mM MES, pH 6, 5% glycerol, and 0 – 1 M NaCl	n.d.
Anion exchange - 30Q 100 mM glycine, pH 9.5, 5% glycerol, and 0 – 1 M NaCl	Hydrophobic - phenyl 50 mM HEPES, pH 7.5, 5% glycerol, and 1 – 0 M AS	n.r.	n.d.
Anion exchange - 30Q 100 mM glycine, pH 9.5, 5% glycerol, and 0 – 1 M NaCl	Hydrophobic - butyl 50 mM HEPES, pH 7.5, 5% glycerol, and 1 – 0 M AS	n.r.	n.d.
Anion exchange - 30Q 100 mM glycine, pH 9.5, 5% glycerol, and 0 – 1 M NaCl	Hydrophobic - octyl 50 mM HEPES, pH 7.5, 5% glycerol, and 1 – 0 M AS	n.r.	n.d.
Anion exchange - 30Q 100 mM glycine, pH 9.5, 5% glycerol, and 0 – 1 M NaCl	Red Sepharose 50 mM HEPES, pH 7.5, 5% glycerol, and 0 – 3 M NaCl	n.r.	n.d.
Anion exchange - 30Q 100 mM glycine, pH 9.5, 5% glycerol, and 0 – 1 M NaCl	Hydrophobic - butyl 50 mM Tris-HCl, pH 8.5, 5% glycerol, and 500 – 0 mM AS	n.r.	n.d.
Anion exchange - 30Q 100 mM glycine, pH 9.5, 5% glycerol, and 0 – 1 M NaCl	Hydrophobic - butyl 50 mM Tris-HCl, pH 8.5, 5% glycerol, and 1 – 0 M AS	n.a.	n.d.
Anion exchange - 30Q 100 mM glycine, pH 9.5, 5% glycerol, and 0 – 1 M NaCl	Blue Sepharose 50 mM HEPES, pH 7, and 0 – 2 M NaCl	n.r.	n.d.
Anion exchange - 30Q 100 mM glycine, pH 9.5, 5% glycerol, and 0 – 1 M NaCl	Hydrophobic – phenyl 50 mM HEPES, pH 7.5, 5% glycerol, and 1 – 0 M AS	n.r.	n.d.
Anion exchange - 30Q 100 mM glycine, pH 9.5, 5% glycerol, and 0 – 1 M NaCl	Hydrophobic - phenyl 50 mM Tris-HCl, pH 8.5, 5% glycerol, and 1 – 0 M AS	n.r.	n.d.
Anion exchange - 30Q 100 mM glycine, pH 9.5, 5% glycerol, and 0 – 1 M NaCl	Hydrophobic - phenyl 50 mM glycine, pH 9.5, 5% glycerol, and 1 – 0 M AS	n.r.	n.d.
Anion exchange - 30Q 100 mM glycine, pH 9.5, 5% glycerol, and 0 – 1 M NaCl	Hydrophobic – phenyl 50 mM MES, pH 6.5, 5% glycerol, and 1 – 0 M AS	n.r.	n.d.
Anion exchange - 30Q 100 mM glycine, pH 9.5, 5% glycerol, and 0 – 1 M NaCl	Hydroxyapetite 50 mM HEPES, pH 7, step gradient with 0, 0.2, 0.4, 0.6, 0.8, and 1 M NaCl	n.r.	n.d.
Anion exchange - 30Q 100 mM glycine, pH 9.5, 5% glycerol, and 0 – 1 M NaCl	Hydroxyapetite 50 mM HEPES, pH 7, step gradient with HEPES, pH 8, glycine, pH 9, and glycine, pH 10	n.r.	n.d.

n.r. = not required
n.d. = not detected
AS = ammonium sulfate

Table 4-4C: PchG-throm and Irp3 protein purification procedures

Protein	First Purification Step Buffer	Second Purification Step Buffer	Third Purification Step Buffer	Protein produced (mg/L culture)
PchG-throm	Affinity - nickel (Followed thrombin cleavage) 25 mM Tris-HCl, pH 8.0, 500 mM NaCl, and 5 – 300 mM imidazole	Benzamidine 25 mM Tris-HCl, pH 8, 500 mM NaCl, and 1 mM $MgCl_2$	Gel filtration - Superdex 75 25 mM Tris-HCl, pH 8, 500 mM NaCl, 150 mM imidazole, and 1 mM $MgCl_2$	n.d.
PchG-throm	affinity - nickel, thrombin cleave on column 25 mM Tris-HCl, pH 8.0, 500 mM NaCl, 1 mM BOG, 5 – 300 mM imidazole with 10 mM $MgCl_2$ and 2 μM NADPH added to eluted fractions	Benzamidine 25 mM Tris-HCl, pH 8, 500 mM NaCl, and 1 mM $MgCl_2$	Gel filtration - Superdex 75 25 mM Tris-HCl, pH 8, 500 mM NaCl, and 1 mM $MgCl_2$	n.d.
PchG-throm	affinity - nickel, thrombin cleave on column 25 mM Tris-HCl, pH 8.0, 500 mM NaCl, 1 mM BOG, and 5 – 300 mM imidazole with 10 mM $MgCl_2$ and 2 μM NADPH added to eluted fractions	Benzamidine 25 mM Tris-HCl, pH 8, 1 M NaCl, 1 mM $MgCl_2$, and 1 mM BOG	Gel filtration - Superdex 200 25 mM Tris-HCl, pH 8, 150 mM NaCl, 1 mM $MgCl_2$, and 1 mM BOG	n.d.
PchG-throm	affinity - nickel, thrombin cleave on column 25 mM Tris-HCl, pH 8.0, 500 mM NaCl, 1 mM BOG, 5 – 300 mM imidazole	Anion exchange - 30Q 50 mM Tris-HCl, pH 9, 15% glycerol, 1 mM $MgCl_2$, 1 mM BOG, and 0 – 1 M NaCl	n.r.	n.d.
PchG-throm	affinity - nickel, thrombin cleave on column 25 mM Tris-HCl, pH 8.0, 500 mM NaCl, 1 mM BOG, and 5 – 300 mM imidazole	Cation exchange - 30 S 50 mM Tris-HCl, pH 7, 15% glycerol, 1 mM $MgCl_2$, 1 mM BOG, and 0 – 500 mM NaCl	n.r.	n.d.
PchG-throm	affinity - nickel, thrombin cleave on column 25 mM Tris-HCl pH 8.0, 500 mM NaCl, 1 mM BOG, and 5 – 300 mM imidazole	Ammonium Sulfate precipitation 0, 20, 40, 60, 80, and 100% ammonium sulfate	n.r.	n.d.
PchG-throm	affinity - nickel, thrombin cleave on column 25 mM Tris-HCl, pH 8.0, 500 mM NaCl, 1 mM BOG, and 5 – 300 mM imidazole	Benzamidine 25 mM Tris-HCl, pH 8, 500 mM NaCl, and 1 mM $MgCl_2$	Anion exchange - 30Q 50 mM Tris-HCl, pH 9, 15% glycerol, 1 mM $MgCl_2$, 1 mM BOG, and 0 – 500 mM NaCl	n.d.
Irp3	Affinity - nickel 25 mM Tris-HCl, pH 8.0, 500 mM NaCl, and 5 – 300 mM imidazole	Gel filtration - Superdex 200 25 mM Tris-HCl, pH 8.0, 200 mM NaCl, and 2 mM DTT	n.r.	24
Irp3-semet	Affinity - nickel 25 mM Tris-HCl, pH 8.0, 500 mM NaCl, 1 mM βME, and 5 - 500 mM imidazole	Gel filtration - Superdex 200 25 mM Tris-HCl, pH 8, 200 mM NaCl, and 1 mM βME	n.r.	3.6

n.r. = not required
n.d. = not detected

PvdA purification has been described in detail in chapter 2 and basic procedures are described in Table 4-4A.

The PvdF-throm-His$_6$ cell pellet was resuspended in 25 mM HEPES, pH 8.0, 500 mM NaCl, and 5 mM imidazole. Purification involved nickel affinity chromatography followed by gel filtration with the Superdex 75 column (Table 4-4A). The histidine tag of PvdF-throm-His$_6$ was cleaved with 1U thrombin/mg protein (25 ^{o}C, 30 min) before further purification to produce PvdF-throm, leaving a 7 amino acid tail on the C-terminus of the protein. PvdF-throm was separated from uncleaved PvdF-throm-His$_6$ with a nickel affinity column and from the thrombin on a Benzamidine column (Amersham Biosciences) (Table 4-4A). Further purification of PvdF-throm was accomplished by gel filtration using a Superdex 75 column. The pelleted BL21(DE3) *E. coli* cells containing over-produced PvdF were resuspended in 25 mM Tris-HCl, pH 8.5. After disruption and centrifugation, PvdF was purified on an anion exchange column followed by a gel filtration on a Superdex 75 column (Table 4-4A).

The PchG-His$_6$ protein was purified in one-step manner on the nickel affinity column (Table 4-4A). The collected fractions were dialyzed into 75 mM HEPES, pH 7.5, 5% glycerol, and 10 mM $MgCl_2$. Purification of the PchG protein from the cellular lysate included a wide variety of column combinations (Table 4-4B) including anion exchange, cation exchange, hydrophobic chromatography, red sepharose (binds NADPH-binding proteins), blue sepharose (binds NADH-binding proteins), and hydroxyapetite as well as ammonium sulfate precipitation. The PchG-throm-His$_6$ was purified from the cell lysate on a nickel affinity column. The collected fractions containing PchG-throm-His$_6$ were exchanged into crystallization buffer with a phenyl sepharose hydrophobic interaction column to slowly remove the imidazole and sodium chloride from the buffer or by dialysis (Table 4-4A). PchG-throm-His$_6$ cell lysate was loaded onto the nickel affinity column and washed thoroughly to remove any unbound proteins. Thrombin (10 U/mg protein) was injected onto the column followed by incubation for 24 hours at 4 ^{o}C. The cleaved PchG-throm protein was eluted from the column along with the thrombin and further purification included a variety of columns including Benzamidine, anion exchange, and cation exchange as well as with ammonium sulfate precipitation (Table 4-4C).

The Irp3 protein was purified from the cellular lysate in a two-step process of nickel affinity and gel filtration chromatography (Table 4-4C). Irp3-semet protein was purified in a similar matter with beta-mercaptoethanol (βME) added in every step of the purification process to prevent oxidation of the selenomethionine.

Buffer Optimization for Proteins. The buffer conditions for all of the purified proteins were optimized to increase stability, solubility, and monodispersity. The buffer components tested varied by pH, salt, and glycerol concentration, and a variety of additives including EDTA, DTT, BOG, cofactors, and substrates (Table 4-5 A-G). The effect of the buffer on the protein solubility was measured by gel filtration chromatography, dynamic light scattering (DLS) with a PD2000DLS^{Plus} Dynamic

Table 4-5A: PvdA initial buffer screen for solubility

Tris-HCl, pH 8.0 (mM)	NaCl (mM)	Glycerol (%)	Imidazole (mM)	DTT (mM)	BOG (mM)	EDTA (mM)	FAD (amt excess)	NADPH (amt excess)	Ornithine (amt excess)	Detection Method	Results
25	500									DLS	-
25	500	10								DLS	-
25	500		300							DLS	-
25	500		300				2			DLS	--
25	500		300					2		DLS	-
25	500		300						2	DLS	--
25	500		300				2		2	DLS	--
25	500		300				2	2		DLS	-
25	500		300					2	2	DLS	--
25	500			2						DLS	-
25	500			2			2			DLS	--
25	500			2				2		DLS	--
25	500			2					2	DLS	-
25	500			2			2		2	DLS	--
25	500			2			2	2		DLS	--
25	500			2				2	2	DLS	---
25	500				2					DLS	-
25	500					1				DLS	-
25	500					1	2			DLS	--
25	500					1		2		DLS	--
25	500					1			2	DLS	-
25	500					1	2		2	DLS	--
25	500					1	2	2		DLS	--
25	500					1		2	2	DLS	---
25	500						2			DLS	--
25	500							2		DLS	--
25	500								2	DLS	-
25	500						2		2	DLS	--
25	500						2	2		DLS	--
25	500							2	2	DLS	--

+ = Some monodispersity, ++ = Better monodispersity, +++ = Best monodispersity

- = Little monodispersity, -- = Less monodispersity, --- = Worst monodispersity

Table 4-5B: PvdA final buffer screen for solubility

ADA, pH 7 (mM)	Potassium phosphate, pH 8 (mM)	Sodium citrate (mM)	Glycerol (%)	DTT (mM)	EDTA (mM)	FAD (amt excess)	NADPH (amt excess)	Ornithine (amt excess)	Detection Method	Results
100									DLS	+
50		50							DLS	+
50		50		2					DLS	+
50		50			1				DLS	+
50		50				2	2		DLS	+
50		50		2		2	2		DLS	+
50		50			1	2	2		DLS	+
	100								DLS	--
	100		20						DLS	--
	100	100							DLS	+++
	100	100				2			DLS	+++
	100	100				2		2	DLS	+++
	100	100	5						DLS	++
	100	100	5			2			DLS	+++
	100	100	5			2		2	DLS	++
	100	100	10						DLS	++
	100	100	10			2			DLS	++
	100	100	10			2		2	DLS	++
	100	100	20						DLS	+
	100	100	20			2			DLS	+
	100	100	20			2		2	DLS	+

+ = Some monodispersity, ++ = Better monodispersity, +++ = Best monodispersity

- = Little monodispersity, -- = Less monodispersity, --- = Worst monodispersity

Table 4-5C: PvdF-throm-His$_6$ Protein buffer screen for solubility

MES, pH 6.5 (mM)	HEPES, pH 7.5 (mM)	HEPES, pH 8.0 (mM)	Tris-HCl, pH 8.0 (mM)	Tris-HCl, pH 8.5 (mM)	Glycine, pH 9.5 (mM)	NaCl (mM)	Glycerol (%)	DTT (mM)	BOG (mM)	EDTA (mM)	SAM (amt excess)	Folinic Acid (amt excess)	Ornithine (amt excess)	Detection Method	Results
50														DLS	---
	50													DLS	---
		50				150				1				DLS	+++
		50				150				1	2x			DLS	++
		50				150				1		2x		DLS	++
		50				150				1			2x	DLS	++
		50				150				1	2x		2x	DLS	++
		50				150				1		2x	2x	DLS	++
		50				150	10			1				DLS	--
			20			100								DLS	+
				50										DLS	---
				50		100								DLS	+
				50		100	5							DLS	--
				50		100	10							DLS	--
				50		100		2						DLS	---
				50		100			2					DLS	-
				50		100				1				DLS	+
				50		150								DLS	+
				50		150				1	2x			DLS	-
				50		150				1		2x		DLS	---
					50									DLS	---
					50	100								DLS	---
					50	200								DLS	---
					50	300								DLS	---

+ = Some monodispersity, ++ = Better monodispersity, +++ = Best monodispersity

- = Little monodispersity, -- = Less monodispersity, --- = Worst monodispersity

Table 4-5D: PvdF-throm and PvdF buffer screen for solubility

Protein	MES, pH 6.5 (mM)	ADA, pH 7 (mM)	Bis-tris, pH 7 (mM)	Bis-Tris propane, pH 7 (mM)	HEPES, pH 7 (mM)	Imidazole, pH 7 (mM)	Sodium malonate, pH 7 (mM)	Tris-HCl, pH 7 (mM)	HEPES, pH 7.5 (mM)	HEPES, pH 8.0 (mM)	Imidazole, pH 8 (mM)	Tris-HCl, pH 8.0 (mM)	Tris-HCl, pH 8.5 (mM)	Glycine, pH 9.5 (mM)	NaCl (mM)	Glycerol (%)	DTT (mM)	BOG (mM)	EDTA (mM)	SAM (amt excess)	Folinic Acid (amt excess)	Ornithine (amt excess)	Detection Method	Results
PvdF-throm	50																						DLS	+
PvdF-throm		50																	1				DLS	++
PvdF-throm			50																1				DLS	++
PvdF-throm				50															1				DLS	++
PvdF-throm					50														1				DLS	+
PvdF-throm						50													1				DLS	++
PvdF-throm							50												1				DLS	++
PvdF-throm								50											1				DLS	++
PvdF-throm									50														DLS	--
PvdF-throm										50									1				DLS	+++
PvdF-throm										50					100				1				DLS	+++
PvdF-throm										50					100				1	2x			DLS	+++
PvdF-throm										50					100				1		2x		DLS	+++
PvdF-throm										50					150	10			1				DLS	+
PvdF-throm										50					150				1	2x			DLS	+++
PvdF-throm										50					150				1		2x		DLS	+++
PvdF-throm										50					150				1			2x	DLS	+++
PvdF-throm										50					150				1	2x		2x	DLS	+++
PvdF-throm										50					150				1		2x	2x	DLS	+++
PvdF-throm											50								1				DLS	++
PvdF-throm												50							1				DLS	--
PvdF-throm												50			100								DLS	++
PvdF-throm													50										DLS	+
PvdF-throm													50		100								DLS	--
PvdF-throm													50		100	5							DLS	---
PvdF-throm													50		100	10							DLS	---
PvdF-throm													50		100		2						DLS	-
PvdF-throm													50		100			2					DLS	-
PvdF-throm													50		100				1				DLS	+
PvdF-throm													50		100				1	2x			DLS	++
PvdF-throm													50		100				1		2x		DLS	+
PvdF-throm													50		200								DLS	---
PvdF-throm													50		300								DLS	---
PvdF-throm														50									DLS	-
PvdF								50							150				1				DLS	+++

+ = Some monodispersity, ++ = Better monodispersity, +++ = Best monodispersity

- = Little monodispersity, -- = Less monodispersity, --- = Worst monodispersity

Table 4-5E: PchG-His$_6$ buffer screen for solubility

MES, pH 6.5 (mM)	HEPES, pH 7.5 (mM)	Tris-HCl, pH 8.0 (mM)	Tris-HCl, pH 8.5 (mM)	Glycine, pH 9.5 (mM)	NaCl (mM)	KCl (mM)	Glycerol (%)	DTT (mM)	BOG (mM)	EDTA (mM)	MgCl$_2$ (mM)	NADPH (amt excess)	Nicatinamide (amt excess)	Ethylene Glycol (%)	NiCl$_2$ (µM)	Detection Method	Results
50					150											gel filtration	---
50					200											DLS	---
	50				150											gel filtration	---
	50				200											DLS	--
	50				150		5	10			10					gel filtration	--
	50				150		5	10			10				2.5	gel filtration	--
	50				150		5	10			10				25	gel filtration	--
	50				150		5	10			10				0.25	gel filtration	--
	50				150		5	10			10				0.025	gel filtration	--
	75						5				10					gel filtration, DLS	---
		25			200											gel filtration	---
		25			150		10	2								gel filtration	---
			50													DLS	-
			50				5									DLS	--
			50				10									DLS	--
			50					2								DLS	---
			50						2							DLS	---
			50							1						DLS	--
			50							1		2x				DLS	--
			50									2x				DLS	---
			50								2x					DLS	---
			50								10x					DLS	--
			50								10x	2x				DLS	--
			50								5					DLS	--
			50								5	2x				DLS	--
			50		100											DLS	--
			50		150											gel filtration	--
			50		150		10									gel filtration	---
			50		150			2								gel filtration	--
			50		200											DLS	--
			50		200						5					DLS	---
			50		200						5	2x				DLS	---
			50		200						5		2x			DLS	---
			50		300											gel filtration, DLS	---
			50			200					5					DLS	---
			50			200					5	2x				DLS	---
			50			200					5		2x			DLS	--
				50	150											gel filtration	--
				50	200											DLS	---

+ = Some monodispersity, ++ = Better monodispersity, +++ = Best monodispersity

- = Little monodispersity, -- = Less monodispersity, --- = Worst monodispersity

Table 4-5F: PchG-throm-His$_6$ and PchG-throm buffer screen for solubility

Protein	MES, pH 6.5 (mM)	ADA, pH 7 (mM)	HEPES, pH 7.5 (mM)	HEPES, pH 8.0 (mM)	Imidazole, pH 7.5 (mM)	Tris-HCl, pH 8.0 (mM)	Tris-HCl, pH 8.5 (mM)	Tris-HCl, pH 9.0 (mM)	Glycine, pH 9.5 (mM)	NaCl (mM)	Imidazole (mM)	Glycerol (%)	DTT (mM)	BOG (mM)	EDTA (mM)	MgCl$_2$ (mM)	NADPH (mM or amount excess)	Lucifierin (amt excess)	Detection Method	Results
PchG-throm-His$_6$	50																		DLS	---
PchG-throm-His$_6$			50																DLS	---
PchG-throm-His$_6$						25				500	150								gel filtration	--
PchG-throm-His$_6$						25				500	150					1	50		gel filtration	--
PchG-throm-His$_6$						25				500	150					10	50		DLS	--
PchG-throm-His$_6$						25				500	150					1	5		DLS	--
PchG-throm-His$_6$						50				100									DLS	-
PchG-throm-His$_6$							50												DLS	--
PchG-throm-His$_6$							50			100									DLS	--
PchG-throm-His$_6$							50			200									DLS	--
PchG-throm-His$_6$							50			300									DLS	--
PchG-throm-His$_6$							50			300		5							DLS	--
PchG-throm-His$_6$							50			300		10							DLS	--
PchG-throm-His$_6$							50			300						2x			DLS	---
PchG-throm-His$_6$							50			300							2x		DLS	-
PchG-throm-His$_6$							50			300								2x	DLS	--
PchG-throm-His$_6$							50			300						2x	2x		DLS	---
PchG-throm-His$_6$							50			300							2x	2x	DLS	--
PchG-throm-His$_6$							50			300						2x		2x	DLS	---
PchG-throm-His$_6$							50			300						2x	2x	2x	DLS	---
PchG-throm-His$_6$							50			500		20							gel filtration	--
PchG-throm-His$_6$									50										DLS	--
PchG-throm-His$_6$									50	500	150								gel filtration	---
PchG-throm		50																	DLS	--
PchG-throm		50										5							DLS	--
PchG-throm		50								150									DLS	--
PchG-throm		50								150			2						DLS	--
PchG-throm		50								150				1					DLS	--
PchG-throm		50								150					1				DLS	--
PchG-throm		50								150			2	1					DLS	--
PchG-throm		50								150				1	1				DLS	--
PchG-throm		50								150						1	2x		DLS	--
PchG-throm		50								300									DLS	--
PchG-throm		100																	DLS	--
PchG-throm				100															DLS	--
PchG-throm					100														DLS	--
PchG-throm						25				150				1		1			gel filtration, DLS	--
PchG-throm						25				500				1		1	2x		DLS	--
PchG-throm						25				500	20					10	2x		DLS	--
PchG-throm						25				500	150					1	2x		DLS	-
PchG-throm						25				500						1			gel filtration	--
PchG-throm						100													DLS	--
PchG-throm								25				15		1		1			DLS	-
PchG-throm								50		200		15		1		1			DLS	-

+ = Some monodispersity, ++ = Better monodispersity, +++ = Best monodispersity

- = Little monodispersity, -- = Less monodispersity, --- = Worst monodispersity

Table 4-5G: Irp3 buffer screen for solubility

MES, pH 6.5 (mM)	ADA, pH 7 (mM)	HEPES, pH 7.5 (mM)	Tris-HCl, pH 8.0 (mM)	Tris-HCl, pH 8.5 (mM)	Glycine, pH 9 (mM)	NaCl (mM)	Imidazole (mM)	Glycerol (%)	DTT (mM)	BOG (mM)	EDTA (mM)	Detection Method	Results
25												DLS	--
	25											DLS	-
		25										DLS	-
			25									DLS	+
			25					5				DLS	+
			25					10				DLS	+
			25			100						DLS	+
			25			100		10	2			DLS	--
			25			200						DLS	++
			25			200			2			DLS	++
			25			200				2		DLS	+++
			25			200					1	DLS	++
			25			300						DLS	+
			25			500	300					DLS	+
				25								DLS	-
					25							DLS	--

+ = Some monodispersity, ++ = Better monodispersity, +++ = Best monodispersity
- = Little monodispersity, -- = Less monodispersity, --- = Worst monodispersity

Light Scattering detector (Precision Detectors), or with a solubility protocol using polyethylene glycol (PEG) 8,000 to precipitate the protein (*15*). The precipitated protein was incubated for 20 min with the various buffer components, centrifuged to remove all the aggregated protein (20,000 x g, 4 min, 4 ^{o}C), and the relative absorbance of the supernatant was determined at 595 nm using the Bradford assay.

Limited Proteolysis of PchG-His$_6$. PchG-His$_6$ was incubated with proteases to determine if areas of the protein were highly susceptible to proteolysis. A variety of proteases were tested including; 0.1 μg of trypsin, subtilisin, chymotrypsin, papain, proteinase K, and thrombin. PchG-His$_6$ was incubated with each protease at 4, 25, and 37 ^{o}C and samples were collected at 5, 10, 30, and 60 min. Each sample was subjected to SDS-PAGE to determine the extent of cleavage. Trypsin and thrombin were tested at higher concentrations (0.1, 1, and 10 μg) and for longer times (1, 2, 4, 6, and 24 hrs) at 24 ^{o}C to optimize cleavage.

Standard Crystallization Procedure. Crystal trials were initiated using the hanging drop vapor diffusion method and sparse matrix screening to determine conditions that allowed for crystal formation with a variety of commercially available screening kits from Hampton Research and Emerald BioSystems (Table 4-6 A-D).

Table 4-6A: PvdA crystallization screens

Protein Buffer	Concentration	Additive	Temperature (°C)	Crystal Screen 1	Crystal Screen 2	Index Screen	Salt R_x Screen	PEG/Ion Screen	Wizard Screen 1	Wizard Screen 2
25 mM Tris-HCl, pH 8, 500 mM NaCl, and 300 mM imidazole	9.7 mg/ml	none	25	X	X	X	X	X	X	X
25 mM Tris-HCl, pH 8, 500 mM NaCl, and 300 mM imidazole	15 mg/ml	none	25	X						
25 mM Tris-HCl, pH 8, 500 mM NaCl, and 300 mM imidazole - water in the well	8.6 mg/ml	FAD, orn*	25	X	X	X				
25 mM Tris-HCl, pH 8, 500 mM NaCl, and 300 mM imidazole	8.6 mg/ml	FAD, orn	25	X	X	X	X	X	X	X
25 mM Tris-HCl, pH 8, 500 mM NaCl, and 300 mM imidazole	8.6 mg/ml	FAD, NADPH, norleucine	25	X	X	X	X	X	X	X
100 mM potassium phosphate, pH 8 and 100 mM sodium citrate	11 mg/ml	none	25	X	X	X	X	X		
100 mM potassium phosphate, pH 8 and 100 mM sodium citrate	11 mg/ml	FAD, ornithine	25	X	X	X	X	X		
100 mM potassium phosphate, pH 8 and 100 mM sodium citrate	5.5 mg/ml	none	25	X	X	X				
100 mM potassium phosphate, pH 8 and 100 mM sodium citrate	5.5 mg/ml	FAD, ornithine	25	X	X	X				
50 mM potassium phosphate, pH 8 and 50 mM sodium citrate	5.5 mg/ml	none	25	X	X	X				
50 mM potassium phosphate, pH 8 and 50 mM sodium citrate	5.5 mg/ml	FAD, ornithine	25	X	X	X				
50 mM potassium phosphate, pH 8 and 50 mM sodium citrate	5.5 mg/ml	none	11	X	X	X				
50 mM potassium phosphate, pH 8 and 50 mM sodium citrate	5.5 mg/ml	FAD, ornithine	11	X	X	X				
50 mM ADA, pH 7 and 50 mM sodium citrate	5.5 mg/ml	none	11	X	X	X				
50 mM ADA, pH 7 and 50 mM sodium citrate	5.5 mg/ml	FAD, ornithine	11	X	X	X				
50 mM ADA, pH 7 and 50 mM sodium citrate	5.5 mg/ml	none	25	X	X	X				
50 mM ADA, pH 7 and 50 mM sodium citrate	5.5 mg/ml	FAD, ornithine	25	X	X	X				
100 mM potassium phosphate, pH 8	5.1 mg/ml	FAD, NADPH	25	X	X	X				
100 mM potassium phosphate, pH 8 and 0.2 µM PCMB	5.1 mg/ml	FAD, NADPH	25	X	X	X				

X = Experimental screens conducted on protein in each buffer condition.

* orn = L-ornithine

Crystal Screen 1and 2, Index Screen, Salt Rx Screen, and PEG/Ion Screen were purchased from Hampton Research. Wizard Screen 1 and 2 were purchased from Emerald BioSystems.

Table 4-6B: PvdF-throm-His$_6$ crystallization screens

Protein Buffer	Concentration	Additive	Temperature (°C)	Crystal Screen 1	Crystal Screen 2	Index Screen	Salt R_x Screen	PEG/Ion Screen	Wizard Screen 1	Wizard Screen 2
50 mM Tris-HCl, pH 8 and 100 mM NaCl	16 mg/ml	none	25	X	X	X	X			
50 mM HEPES, pH 8, 150 mM NaCl, and 1 mM EDTA	16 mg/ml	none	25	X	X	X			X	X
50 mM HEPES, pH 8, 150 mM NaCl, and 1 mM EDTA	16 mg/ml	SAM*	25	X	X	X			X	X
50 mM HEPES, pH 8, 150 mM NaCl, and 1 mM EDTA	16 mg/ml	Folinic acid	25	X	X	X			X	X
50 mM HEPES, pH 8, 150 mM NaCl, and 1 mM EDTA	19 mg/ml	none	25	X	X	X	X		X	X
50 mM HEPES, pH 8, 150 mM NaCl, and 1 mM EDTA	19 mg/ml	SAM	25	X	X	X	X		X	X
50 mM HEPES, pH 8, 150 mM NaCl, and 1 mM EDTA	19 mg/ml	Folinic acid	25	X	X	X	X		X	X
50 mM HEPES, pH 8, 150 mM NaCl, and 1 mM EDTA	19 mg/ml	orn*	25	X	X					
50 mM HEPES, pH 8, 150 mM NaCl, and 1 mM EDTA	19 mg/ml	orn, SAM	25	X	X					
50 mM HEPES, pH 8, 150 mM NaCl, and 1 mM EDTA	19 mg/ml	orn, Folinic acid	25	X	X					
50 mM HEPES, pH 7 and 1 mM EDTA	31 mg/ml	none	4, 11, 25	X	X	X	X	X	X	X
50 mM Tris-HCl, pH 8 and 1 mM EDTA	34 mg/ml	none	4, 11, 25	X	X	X	X	X	X	X
50 mM Bis-Tris, pH 7 and 1 mM EDTA	34 mg/ml	none	4, 11, 25	X	X	X	X	X	X	X

X = Experimental screens conducted on protein in each buffer condition.

* SAM = s-adenosyl methionine, orn = L-ornithine

Crystal Screen 1and 2, Index Screen, Salt Rx Screen, and PEG/Ion Screen were purchased from Hampton Research. Wizard Screen 1 and 2 were purchased from Emerald BioSystems.

Table 4-6C: PvdF-throm crystallization screens

Protein Buffer	Concentration	Additive	Temperature (°C)	Crystal Screen 1	Crystal Screen 2	Index Screen	Salt R_x Screen	PEG/Ion Screen	Wizard Screen 1	Wizard Screen 2
50 mM Tris-HCl, pH 8 and 100 mM NaCl	13 mg/ml	none	25	X	X	X	X			
50 mM HEPES, pH 8, 150 mM NaCl, and 1 mM EDTA	10 mg/ml	none	25	X	X	X			X	
50 mM HEPES, pH 8, 150 mM NaCl, and 1 mM EDTA	10 mg/ml	SAM*	25	X	X	X			X	
50 mM HEPES, pH 8, 150 mM NaCl, and 1 mM EDTA	10 mg/ml	Folinic acid	25	X	X	X			X	
50 mM HEPES, pH 8, 150 mM NaCl, 1 mM EDTA, and 10% glycerol	20 mg/ml	none	25	X	X	X	X		X	X
50 mM HEPES, pH 8, 150 mM NaCl, 1 mM EDTA, and 10% glycerol	20 mg/ml	SAM	25	X	X	X	X		X	X
50 mM HEPES, pH 8, 150 mM NaCl, 1 mM EDTA, and 10% glycerol	20 mg/ml	Folinic acid	25	X	X	X	X		X	X
50 mM HEPES, pH 8, 150 mM NaCl, 1 mM EDTA, and 10% glycerol	14 mg/ml	orn*	25	X	X	X			X	X
50 mM HEPES, pH 8, 150 mM NaCl, 1 mM EDTA, and 10% glycerol	14 mg/ml	orn, SAM	25	X	X	X			X	X
50 mM HEPES, pH 8, 150 mM NaCl, 1 mM EDTA, and 10% glycerol	14 mg/ml	orn, Folinic acid	25	X	X	X			X	X
50 mM HEPES, pH 7 and 1 mM EDTA	33 mg/ml	none	4	X	X	X	X	X	X	X
50 mM Tris-HCl, pH 8 and 1 mM EDTA	24 mg/ml	none	4	X	X	X	X	X	X	X
50 mM Bis-Tris, pH 7 and 1 mM EDTA	35 mg/ml	none	4	X	X	X	X	X	X	X

X = Experimental screens conducted on protein in each buffer condition.

* SAM = s-adenosyl methionine, orn = L-ornithine

Crystal Screen 1and 2, Index Screen, Salt Rx Screen, and PEG/Ion Screen were purchased from Hampton Research. Wizard Screen 1 and 2 were purchased from Emerald BioSystems.

Table 4-6D: PvdF, PchG, and Irp3 crystallization screens

Protein	Protein Buffer	Concentration	Additive	Temperature (°C)	Crystal Screen 1	Crystal Screen 2	Index Screen	Salt R_x Screen	PEG/Ion Screen	Wizard Screen 1	Wizard Screen 2
PvdF	50 mM Tris-HCl, pH 7, 150 mM NaCl, and 1 mM EDTA	18 mg/ml	none	25	X	X	X	X			
PvdF	50 mM Tris-HCl, pH 7, 150 mM NaCl, and 1 mM EDTA	18 mg/ml	none	11	X	X	X	X	X	X	X
PvdF	50 mM HEPES, pH 7, 150 mM NaCl, and 1 mM EDTA	18 mg/ml	Folinic acid	25	X	X	X	X	X	X	X
PchG-His$_6$	75 mM HEPES, pH 7.5, 5% glycerol, and 10 mM $MgCl_2$	6.7 mg/ml	none	25	X	X	X	X			
PchG-His$_6$	25 mM Tris-HCl, pH 8 and 200 mM NaCl	5 mg/ml	none	25	X	X	X	X			
PchG-His$_6$	25 mM Tris-HCl, pH 8 and 200 mM NaCl	5 mg/ml	NADPH	25	X	X	X	X			
PchG-His$_6$	50 mM Tris-HCl, pH 8.5 and 0.5 mM $MgCl_2$	6 mg/ml	NADPH	25	X	X	X				
PchG-His$_6$	50 mM Tris-HCl, pH 8.5 and 0.5 mM $MgCl_2$	4.3 mg/ml	NADPH	25	X	X		X			
PchG-His$_6$	50 mM Tris-HCl, pH 8.5 and 0.5 mM $MgCl_2$	4.3 mg/ml	NADPH, luciferin	25	X	X		X			
PchG-His$_6$	50 mM Tris-HCl, pH 8.5, 200 mM KCl, and 5 mM $MgCl_2$	6 mg/ml	NADPH	25	X	X					
PchG-His$_6$	50 mM Tris-HCl, pH 8.5, 200 mM KCl, and 5 mM $MgCl_2$	6 mg/ml	NADPH, luciferin	25	X	X					
PchG-throm-His$_6$	50 mM Tris-HCl, pH 8 and 100 mM NaCl	28 mg/ml	none	25	X	X					
PchG-throm	25 mM Tris-HCl, pH 8, 150 mM NaCl, 1 mM $MgCl_2$, and 1 mM BOG*	8.5 mg/ml	none	25	X		X				
PchG-throm	50 mM Tris-HCl, pH 9, 200 mM NaCl, 15% glycerol, 1 mM $MgCl_2$, and 1 mM BOG	12 mg/ml	none	25	X	X	X	X		X	X
PchG-throm	50 mM Tris-HCl, pH 9, 200 mM NaCl, 15% glycerol, 1 mM $MgCl_2$, and 1 mM BOG	30 mg/ml	none	25	X	X	X				
Irp3	25 mM Tris-HCl, pH 8, 200 mM NaCl, and 2 mM DTT	19 mg/ml	none	25	X	X	X				

X = Experimental screens conducted on protein in each buffer condition

* BOG = octyl-β-D-glucopyranoside

Crystal Screen 1and 2, Index Screen, Salt Rx Screen, and PEG/Ion Screen were purchased from Hampton Research. Wizard Screen 1 and 2 were purchased from Emerald BioSystems.

Standard Crystal Optimization. Conditions that led to crystal formation were optimized to produce diffraction quality crystals (Table 4-7). Initial optimization involved varying the concentration of the buffer components, the temperature, and adding components that may enhance crystallization (Table 4-8). For further optimization, the geometry of the crystallization drop was altered from the standard hanging drop method to sitting, bridging, or sandwich drops. Seeding techniques were also employed to optimize the crystal growth (macroseeding, microseeding, and streak seeding). The use of dialysis buttons (Hampton Research), adding a layer of oil (silicone, parrafin) on top of the well solution, or using Equilipro buttons (Hampton Research) were also attempted to slow the diffusion rate between the drop and the well solution. The protein to crystallization solution ratio in the drops was altered from the standard 1:1 to 2:1. Changing the standard siliconized glass coverslips to plastic coverslips or using plates that have plastic lids (Nextal) to alter the crystal nucleation or growth on the glass, and using feeding, weeding, and growing crystals in gels were also attempted.

Data Collection of Irp3 Crystals. Diffraction quality crystals of Irp3 were flash cooled in the cryostream with 20% ethylene glycol in the crystallization solution as the cryoprotectant. Native data were collected at the Protein Structure Laboratory at the University of Kansas (www.psl.ku.edu) with an RaxisIV image plate detector mounted on a Rigaku RUH3R rotating anode. The exposure time per frame was 10

Table 4-7: Crystal Optimization

Protein	Component concentration variation	Temperature variation	Additive addition*	Double additive addition	Sitting drops	Bridging drops	Sandwich drops	Macroseeding	Microseeding	Streak seeding	Dialysis buttons	Silicon oil	Paraffin oil	Equilipro buttons	Ratio variation	Plastic cover slips	Nextal plates with plastic lids	Feeding	Weeding	Silica gel	Agarose gel
PvdA	X																				
PvdF-throm-His$_6$	X	X	X		X	X	X		X	X	X	X	X		X	X	X	X	X		
PvdF-throm	X		X																		
PvdF	X		X	X				X		X				X						X	X
Irp3	X																				

* = the additives used are described in Table 4-8

Table 4-8: Crystallization Additives

Additive Name	Class of Compound
0.01 M Ammonium chloride	Salt
0.01 M Cadmium chloride	Salt
0.01 M Calcium chloride	Salt
0.05 M Cesium chloride	Salt
0.01 M Cobalt chloride	Salt
0.01 M Ferric chloride	Salt
0.01 M Lanthanum chloride	Salt
0.1 M Lithium chloride	Salt
0.01 M Magnesium chloride	Salt
0.01 M Nickel chloride	Salt
0.1 M Potassium chloride	Salt
0.2 M Sodium chloride	Salt
0.01 M Strontium chloride	Salt
0.1 M Ammonium sulfate	Salt
3% (v/v) Ethylene glycol	Organic, non-volatile
3% (v/v) Glycerol	Organic, non-volatile
2.5% (w/v) 1,6 Hexanediol	Organic, non-volatile
3% (v/v) MPD	Organic, non-volatile
5% (w/v) PEG 400	Organic, non-volatile
1.5% (v/v) Jeffamine M-600	Organic, non-volatile
3% (v/v) Dioxane	Organic, volatile
3% (v/v) Ethanol	Organic, volatile
3% (v/v) Iso-propanol	Organic, volatile
3% (v/v) Methanol	Organic, volatile
0.5% (v/v) Ethyl acetate	Organic, volatile
4% (v/v) Acetone	Organic, volatile
0.7% (v/v) n-Butanol	Organic, volatile
0.1 M Guanadine HCl	Chaotrope
0.01 M Urea	Chaotrope
3% (v/v) DMSO	Chaotrope
0.01 M L-cysteine	Reducing Agent
0.01 M DTT	Reducing Agent
0.01 M EDTA	Chelator
0.1 M Glycine	Linker
0.03 M Gly-Gly	Linker
0.01 M Taurine	Linker
0.01 M Betaine	Linker
3% (w/v) L-(-)-Fucose	Carbohydrate
3% (w/v) D-(+)-Glucose	Carbohydrate
3% (w/v) Sorbitol	Carbohydrate
3% (w/v) L-(-)-Sorbose	Carbohydrate
3% (w/v) D-Sucrose	Carbohydrate
3% (w/v) D-(+)-Xylose	Carbohydrate

min with 0.5° oscillations for 180° at a 150 mm detector distance. Irp3 crystals diffracted to 2.25 Å and were assigned to the space group P222 (a = 83.45, b = 92.54, c=180.24) (Table 4-9). Diffraction data were processed with DENZO and SCALEPACK (*16*).

Phasing of Irp3. Phasing for Irp3 was attempted by molecular replacement with AutoMolRep in CCP4 (*17*) and Phaser (*18*) programs. The models for molecular replacement were human neutrophil gelatinase-associated lipocalin (NGAL) (Protein Data Bank accession code 1L6M, 16.1% identity) and a Gfo/Idh/Moca family oxidoreductase from *Vibrio cholerae* (Protein Data Bank accession code 1XEA, 19.8% identity). Multiwavelength anomalous dispersion (MAD) with Irp3 Se-Met crystals was attempted. The crystals were flash cooled in liquid nitrogen and sent to Louisiana State University to the Center for Advanced Microstructures and Devices (CAMD). X-ray diffraction data were collected on the Gulf Coast Protein Crystallography Consortium (GCPCC) beamline. Crystals were soaked with a variety of heavy metals for MIR (Table 4-10). Irp3 was also co-crystallized with PCMB, dichloroethylenediamino platinate, and gold potassium cyanide for MIR phasing. Short soaks (30 s – 1 min) of crystals into cryoprotectant containing potassium iodide were also used to obtain heavy metal adducts for MIR (*19*). All MIR diffraction data were collected on the home source.

Table 4-9: Irp3 Data Collection Statistics

Space Group	P222
Unit Cell (Å)	a = 83.45, b = 92.54, c = 180.24
Resolution Range (Å)	100-2.25
Unique Observations	67,331
Total Observations	391,913
Completeness (%)	98.6 (95.3)
R_{sym}	0.081 (0.384)
% > 3σ (I)	74.0 (45.3)

Values in parentheses are for the highest resolution shell: 2.25-2.33 Å.

Table 4-10: Heavy metals used for Irp3 MIR studies

Reagent Name	Heavy Metal
Potassium Tetrachloroplatinate (II)	Platinum
Ammonium Tetrachloroplatinate (II)	Platinum
Potassium Tetranitroplatinate (II)	Platinum
Potassium Tetracyanoplatinate (II)	Platinum
Dichloroethylenediamine Platinum (II)	Platinum
Platinum Potassium Iodide	Platinum
Gold (I) Potassium Cyanide	Gold
Potassium Tetrachloroaurate (III)	Gold
Sodium Tetrachloroaurate (III)	Gold
Gold Potassium Bromide	Gold
Mersalyl Acid	Mercury
Ethyl Mercuric Phosphate	Mercury
Mercury (II) Chloride	Mercury
Ethylmercurithiosalycylic Acid, sodium salt	Mercury
Mercury (II) Potassium Iodide	Mercury
para-Chloromercuribenzoic Acid, sodium salt	Mercury
Thallium (III) Chloride hydrate	Thallium
Thalium (I) Chloride	Thallium
Thalium (III) Acetate hyrdate	Thallium
lead (II) acetate trihydrate	Lead
lead (II) Nitrate	Lead
lead (II) Chloride	Lead
Silver Nitrate	Silver
Cadmium Chloride hydrate	Cadmium
Cadmium lodide	Cadmium
Potassium Hexachlororidate (IV)	Iridium
Iridium (III) Chloride hydrate	Iridium
Sodium Hexachlororidate (III) hydrate	Iridium
Ammonium Hexachloroiridate (III) hydrate	Iridium
Potassium Hexanitroiridium (III)	Iridium
Potassium Osmate (VI) dihydrate	Osmium
Ammonium Hexabromoosmate (IV)	Osmium
Potassium Hexchloroosmate (IV)	Osmium
Sodium Tungstate dihydrate	Tungsten
Ammonium Tetrathiotungstate (VI)	Tungsten
Samarium (III) Chloride hexahydrate	Samarium
Samarium (III) Acetate hydrate	Samarium
Samarium (III) Nitrate hexahydrate	Samarium
Lanthanum (III) Nitrate hexahydrate	Lanthanum
Europium (III) Nitrate hexahydrate	Europium
Europium (III) Chloride hexahydrate	Europium
Gadolinium (III) Chloride hydrate	Gadolinium
Lutetium (III) Chloride hexhydrate	Lutetium
Lutetium (III) Acetate hexhydrate	Lutetium
Ytterbium (III) Chloride hydrate	Ytterbium
Dysprosium (III) Chloride hexahydrate	Dysprosium
Praseodymium (III) Chloride heptahydrate	Praseodymium
Neodymium Chloride hydrate	Neodymium
Holmium (III) Chloride hexahydrate	Holmium
Potassium Hexachlororhenate (IV)	Holmium
Potassium Perrhenate	Holmium

Results and Discussion

PvdA

The cloning, production, and purification of PvdA are described in detail in chapter 2 and summarized in Tables 4-1, 4-2, and 4-4A. PvdA was produced as a monomeric, 51.6 kDa protein.

The original buffer components for PvdA included Tris-HCl, pH 8.0, a high concentration of sodium chloride (500 mM), and imidazole (300 mM) as the protein was eluted from the nickel affinity column. PvdA in this buffer quickly aggregated in solution making the protein unstable and would precipitate upon freezing for storage. Initial buffer optimization, monitored by dynamic light scattering, was used to test the solubility of PvdA in buffers containing a wide variety of additives including glycerol, DTT (to reduce disulfide bonds), EDTA (to chelate any trace metals), and β-octylglucoside (BOG) (a detergent used to solubilize hydrophobic patches on the protein) (Table 4-5A). The further addition of coenzymes (FAD and NADPH) and substrate (ornithine) was tested for their ability to promote the stability of PvdA in solution by decreasing aggregation. However, the protein remained unstable and buffer exchange by dialysis or de-salting columns such as a PD-10 column (Amersham Biosciences) resulted in protein precipitation. Therefore, a wide screen of buffer conditions was undertaken using the buffer screen protocol described by Izaac et al. (*15*). Briefly, PEG 8,000 was used to precipitate the protein. A buffer screen was added to the precipitated protein and the amount of protein in solution was monitored with the Bradford Assay (Figure 4-3). PvdA was most soluble in ADA, pH 7.0, and sodium citrate (Figure 4-3A). Further screening resulted in a large increase in PvdA stability in potassium phosphate, pH 8.0 (Figure 4-3B). Therefore, all purification steps were conducted using potassium phosphate, pH 8.0 and sodium citrate. A second gel filtration step was added to the PvdA purification to remove the sodium chloride and imidazole after nickel affinity chromatography and to remove any remaining contaminating proteins. Further buffer optimization in potassium phosphate, pH 8.0 or ADA, pH 7 was monitored by dynamic light scattering to determine if further stability could be achieved with the addition of glycerol, cofactors, or substrate (Table 4-5B). The protein was monomeric in either potassium phosphate or ADA when sodium citrate was present. PvdA lost stability and began to precipitate without sodium citrate. To remain in solution, PvdA requires a minimum of 50 mM potassium phosphate, pH 8.0 and 50 mM sodium citrate. Freezing PvdA in this buffer does not affect the solubility or activity of the protein.

Initial crystallization trials for PvdA using protein in Tris-HCl, pH 8.0 with 500 mM sodium chloride and 300 mM imidazole yielded only salt crystals (Table 4-6A). However, crystallization experiments with PvdA in 50 mM potassium phosphate, pH 8.0 and 50 mM sodium citrate with a two-fold excess of FAD and NADPH, yielded small crystallites grown in 0.01 M cobalt chloride and 20% (w/v) polyvinylpyrrolindone K15. Further optimization of this condition has not yet yielded diffraction quality crystals (Table 4-7).

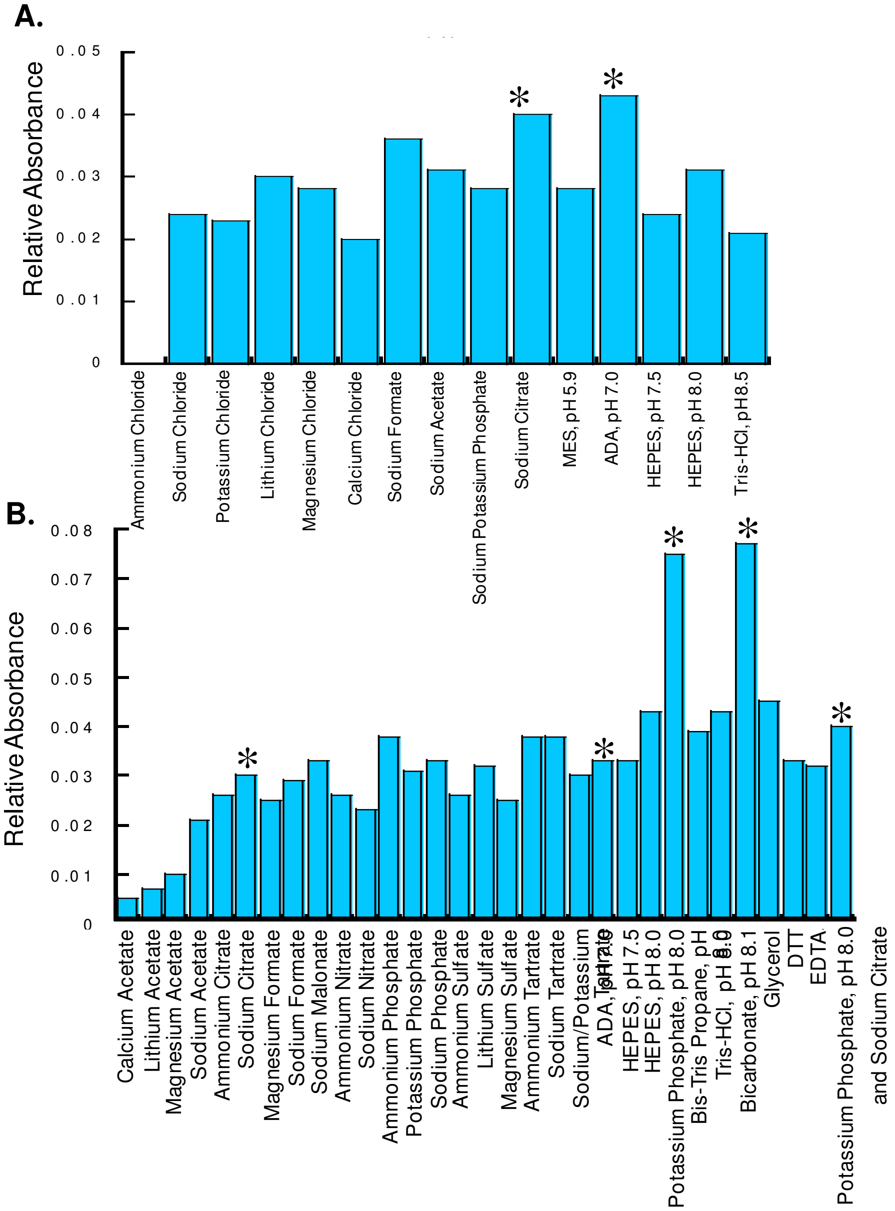

Figure 4-3: PvdA Buffer Optimization Screen. Protein precipitated by PEG 8000 was resolubilized by the addition of a variety of salts (100 mM), buffers (100 mM), and additives (10% glycerol, 2 mM DTT and EDTA). Buffer additions that have a positive effect on the protein solubility have a larger relative absorbance. *A*. An initial buffer screen indicated ADA, pH 7.0 and sodium citrate to have a positive effect on protein solubility denoted by *. *B*. Further buffer screening implicated potassium phosphate, pH 8.0 and bicarbonate, pH 8.1 as having the greatest effect of PvdA solubility denoted by *.

PvdF

The PvdF protein was produced with two plasmids to obtain three variations of the protein. The *pvdF-throm-His*$_6$ plasmid produces PvdF-throm-His$_6$ protein, which contains a cleavable C-terminal histidine tag that can be processed to produce PvdF-throm, a variation of the PvdF protein. A second plasmid, *pvdF*, produces the native PvdF protein with no purification tag.

PvdF-throm-His$_6$

The *pvdF* gene was cloned into the pET29b vector for over-production of a 34.8 kDa PvdF protein containing a thrombin-cleavable His$_6$ tag named PvdF-throm-His$_6$ (Table 4-1). Over-production of this gene in BL21(DE3) *E. coli* cells was induced by 0.2 mM IPTG (Table 4-2). After further growth of 3 – 4 hours, the cells were harvested by centrifugation and the pellet was resuspended in nickel affinity column buffer. A two-step purification using nickel affinity and gel filtration chromatography yielded pure PvdF-throm-His$_6$ at 186 mg/L culture (Table 4-4A).

The best buffering conditions for the purified PvdF-throm-His$_6$ were screened by DLS (Table 4-5C). The buffer conditions that provided the most monodisperse protein were 50 mM HEPES, pH 8, 150 mM NaCl, and 1 mM EDTA with and without the addition of substrates. Therefore, all purification steps were conducted using HEPES, pH 8 and 1 mM EDTA.

Initial crystallization trials of PvdF-throm-His$_6$ yielded several conditions that formed needle-shaped crystals: 1.3 M sodium malonate, pH 7, 0.1 M HEPES, pH 7, and 0.7% (v/v) Jeffamine ED-2001; 5% (v/v) Tacsimate, 0.1 M HEPES, pH 7, and 10% (w/v) PEG MME 5000; and 1.2 M sodium potassium tartrate (Table 4-6B and Figure 4-4A,B). Further optimization (Table 4-7) of the crystal conditions did not change the geometry of the needles into three-dimensional crystals. Therefore, the His_6 tag was cleaved with thrombin to determine if the morphology of the crystals could be improved with protein missing the long C-terminal tail.

PvdF-throm

PvdF-throm-His_6 was cleaved with thrombin to produce PvdF-throm. The cleaved PvdF-throm was separated from the uncleaved PvdF-throm-His_6 by nickel affinity chromatography (Table 4-4A). Further purification of the PvdF-throm from the thrombin was performed using a Benzamidine column that specifically binds thrombin. The purified PvdF-throm protein was 31.9 kDa.

PvdF-throm solubility was optimized by varying the buffer components and monitoring by DLS (Table 4-5D). PvdF-His_6 was least heterodispersed in 50 mM HEPES, pH 8, 150 mM NaCl, 1 mM EDTA, and 10% (v/v) glycerol. Therefore, a final gel filtration step was added to the purification procedure to exchange PvdF-His_6 into the optimized buffer.

Initial crystallization trials of PvdF-His_6 yielded needle-shaped crystals under the same conditions as PvdF-throm-His_6 (Table 4-6C). A variety of additives were included in the crystallization trials to determine if any would change the morphology

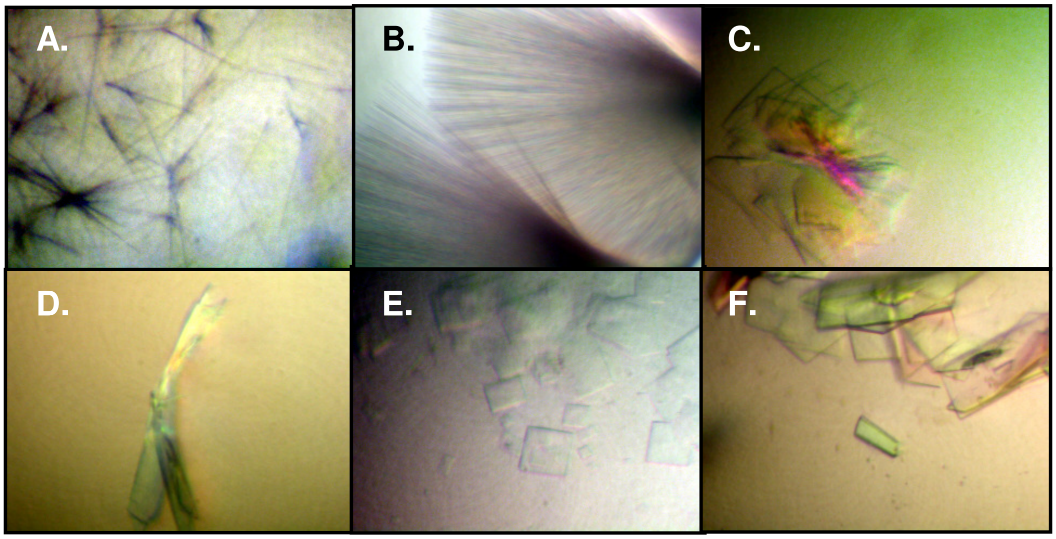

Figure 4-4: PvdF crystal images. PvdF-throm-His_6 needle crystals grown with (*A*) sodium malonate with Jeffamine ED-2001 and (*B*) sodium potassium tartrate as the precipitant. PvdF plate crystals grown with (*C*) Tacsimate, (*D,E*) sodium malonate, and (*F*) sodium citrate as the precipitant.

of the crystals (Table 4-7 and 4-8). However, as with PvdF-throm-His_6, the crystals would not grow in a second or third dimension. Therefore, the protein was redesigned to remove the C-terminal tail and the thrombin cleavage site to produce the native PvdF protein.

PvdF

The native PvdF protein containing no purification tag was produced by introducing two stop codons into the *pvdF-throm-His*$_6$ vector in the position of the native stop codon using site-directed mutagenesis (Table 4-1). The 31.0 kDa protein was overproduced in a similar manner to PvdF-throm-His_6 except the cells were induced at mid log phase (A_{600} = 1.0) instead of early log phase A_{600} = 0.4) (Table 4-2). The cells were harvested by centrifugation and resuspended in anion exchange loading buffer. PvdF was purified in two steps using anion exchange and gel filtration chromatography yielding 237 mg protein/L cells (Table 4-4A). The final buffer for PvdF was the same as for PvdF-throm-His_6 and PvdF-throm and the protein was monodispersed in solution as determined by DLS (Table 4-5D).

Initial crystallization trials yielded needle crystals under similar conditions to PvdF-throm-His_6 and PvdF-throm (Table 4-6D). By screening a variety of additives, several of the conditions altered the morphology of the crystals from needles to plates (Table 4-11 and Figure 4-4 C-F). However, with a double additive screen, the plate crystals did not further change morphology to obtain three-dimensional character

Table 4-11: Crystal conditions which formed PvdF needles and plates

Condition	Crystal morphology
1.7 M lithium sulfate and 0.1 M Tris-HCl, pH 8.5	needles
1.4 M sodium potassium phosphate	needles
1.3 M sodium potassium tartrate and 0.1 M Tris-HCl, pH 9.5	needles
1.1 M sodium potassium tartrate, 0.1 M Tris-HCl, pH 9, and 0.2 M lithium sulfate	needles
53% (v/v) Tacsimate and 0.1 M HEPES, pH 7.5	plates
1.7 M sodium malonate and 0.1 M ADA, pH 6.7	needles
1.5 M sodium malonate and 0.1 M Tris-HCl, pH 8.3	plates
0.8 M sodium citrate, 0.2 M NaCl, and 0.1 M Tris-HCl, pH 8	plates

(Table 4-7). The largest and most well formed plate crystals were obtained in wells with: 53% (v/v) Tacsimate, 0.1 M HEPES, pH 7, ethyl acetate, and EDTA; 1.5 M sodium malonate, 0.1 M Tris-HCl, pH 8.3, ethyl acetate, and EDTA; and 0.8 M sodium citrate, 0.2 M NaCl, 0.1 M Tris-HCl, pH 8, EDTA, and urea. With these three conditions, the drop geometry was changed to sitting, bridging, or sandwich drops but this still did not alter the morphology. Macroseeding and streak seeding were also tried, as well as Equilipro buttons (Hampton Research) to slow the rate of vapor diffusion. Setting up crystallization drops in silica or agarose gels was attempted to provide a different environment for crystal formation. None of the conditions tried changed the morphology and achieved the three dimensional crystals needed for diffraction collection.

Addition of the substrate, hydroxyornithine, to the crystallization drop may change the protein conformation and allow growth of diffraction quality crystals. However, the synthesis of hydroxyornithine is very difficult. The Chemical Methodologies & Library Development (CMLD) Center at the University of Kansas has been working to produce hydroxyornithine. A method for obtaining hydroxylysine has been described (*20*). However, hydroxylation of ornithine using the same synthesis method was not achieved due to unwanted cyclization of the side chain. A variety of alternative synthesis methods have been attempted with no success. Generation of hydroxyornithine by PvdA is not efficient enough to get high quantities of hydroxyornithine for use in PvdF crystallization trials. Further PvdF crystallization experiments will be conducted once hydroxyornithine can be obtained.

PchG

The PchG protein was produced from five plasmids. The *pchG-His*$_6$ plasmid produced PchG containing a histidine tag. The *pchG* plasmid produced the native PchG with no purification tag. A third plasmid, *pchG-throm-His*$_6$, produced PchG with a cleavable histidine tag, which was cleaved to produce PchG-throm. The fourth plasmid, *ss-pchG*, produced a periplasmic PchG protein. The final PchG plasmid, *pchG-Intein*, was cloned to produce a fusion protein for purification.

PchG-His$_6$

The clone for PchG-His$_6$ was generously provided by the Walsh lab at Harvard Medical School (Table 4-1). The plasmid, *pchG-His*$_6$ encodes for a 38.7 kDa PchG-His$_6$ protein with a C-terminal His$_6$ tag. Protein over-production occurs without promoter induction according to the protocol from Reimann et al (*11*) (Table 4-2). PchG-His$_6$ was purified by nickel affinity chromatography with a yield of 46 mg/L *E. coli* (Table 4-4A).

A variety of buffering conditions ranging from pH 6.5 – 9.5 and a range of additives were monitored by DLS and gel filtration to determine the conditions that decreased PchG-His$_6$ aggregation in solution (Table 4-5E). None of the conditions resulted in monodispersed protein and the protein precipitated out of solution when concentrated above 1-2 mg/ml in all of the solutions tested. PchG-His$_6$ eluted from the nickel column and remained soluble at 6.7 mg/ml. Crystallization trials of protein in the nickel elution buffer were undertaken.

A variety of crystallization screens were performed in different protein buffers with the addition of NADPH and luciferin, a substrate analog (Table 4-6D). No protein crystals were obtained, suggesting either that the protein has flexible regions interfering with the crystal packing, the protein concentration was not high enough, or the protein was not in a single oligomeric state, thus interfering with crystallization.

Many proteins will not crystallize if small regions of the protein are flexible (*2*). To determine if the reason that no PchG-His$_6$ crystals formed was because of flexible regions, limited proteolysis experiments were conducted. If small regions of the protein could be removed by proteolysis, then PchG would be re-cloned to remove the regions and crystallization experiments would be conducted. Six proteases were tested to determine if PchG-His$_6$ could be consistently cleaved into smaller pieces without complete degradation (data not shown). Thrombin, trypsin, and papain did not show any cleavage at low concentrations of protease detected by SDS-PAGE. With larger concentrations of protease, trypsin completely degraded PchG-His$_6$, while no cleavage was seen with thrombin. Chymotrypsin cleavage was not specific and many degradation products were detected in a range of sizes. Subtilisin and proteinase K cleaved PchG-His$_6$ into one detectable band of around 25 kDa indicating 15 kDa of the protein was cleaved off. The cleaved fragment is large and therefore not suitable for the removal of small flexible regions.

To determine if the protein solubility, stability, and crystallization problems were due to the His_6 tag, the protein was redesigned to remove the tag and leave only the native PchG protein.

PchG

The *pchG* plasmid was produced by introduction of two stop codons into the *pchG-His*$_6$ plasmid at the end of the native *pchG* gene (Table 4-1). Over-production of PchG in BL21(DE3) *E. coli* cells was identical to that for PchG-His_6 (Table 4-2). The PchG protein was 37.7 kDa.

PchG purification included a wide variety of chromatographic steps as well as ammonium sulfate precipitation. Purification steps included; ammonium sulfate precipitation, anion exchange, cation exchange, hydrophobic (phenyl, butyl, and octyl), Red Sepharose to bind NADPH-binding proteins, Blue Sepharose to bind NADH-binding proteins, and hydroxyapetite (Table 4-4B). However, purified PchG was never obtained. With some purification strategies, the protein did not adhere to the column resin and eluted in the flowthrough, or eluted throughout the gradient seen in ammonium sulfate precipitation and cation exchange. With anion exchange and hydrophobic resins, PchG eluted with many other proteins, such that these columns did not increase purity. PchG adhered too strongly and never eluted from the Red and Blue Sepharose and the hydroxyapetite columns. Therefore, PchG was recloned to form a protein with a cleavable His_6 tag similar to the PvdF-throm-His_6 protein. This new clone would take advantage of the histidine tag for purification but the tag could be cleaved for increases solubility.

PchG-throm-His$_6$

The *pchG* gene was amplified from *P. aeruginosa* genomic DNA and ligated into the pET29b vector such that the PchG protein contained a thrombin-cleavable His$_6$ tag named PchG-throm-His$_6$ (Table 4-1). PchG-throm-His$_6$ was overproduced in *E. coli* cells in an identical manner to PchG-His$_6$ and PchG proteins (Table 4-2). The 41.4 kDa PchG-throm-His$_6$ protein was purified with one step on a nickel affinity column to yield 22 mg/L of culture and could be concentrated above 10 mg/ml (Table 4-4A).

Buffer components for PchG-throm-His$_6$ were varied to obtain monodispersed protein as monitored by DLS and gel filtration (Table 4-5F). No condition provided monodispersed protein, even with the addition of NADPH, a coenzyme. However, crystallization experiments were conducted on PchG-throm-His$_6$ in 50 mM Tris-HCl, pH 8 and 100 mM NaCl.

Initial crystallization experiments of PchG-throm-His$_6$ were unsuccessful and no crystals formed in any of the crystallization conditions (Table 4-6D). Therefore, the histidine tag was cleaved off of the PchG-throm-His$_6$ protein to produce PchG-throm to try to optimize protein solubility.

PchG-throm

Thrombin cleavage in solution resulted in aggregated protein. Thrombin was added to PchG-throm-His$_6$ bound to the nickel affinity column and allowed to incubate for 24 hours. The cleaved PchG-throm (38.5 kDa) and the thrombin were eluted from the column (Table 4-4C). Further purification of PchG-throm from thrombin was complicated since both proteins are ~38 kDa (Table 4-4A). However, PchG-throm further purified by a benzamidine column to selectively bind thrombin was subjected to buffer optimization.

PchG-throm solubility and monodispersity were monitored by DLS and gel filtration using a wide variety of buffer conditions (Table 4-5F). None of the buffer systems produced monodispersed protein similar as was the case with PchG-throm-His$_6$.

Crystallization experiments were conducted on protein in the buffer that produced the least heterogeneity or polydispersity (50 mM Tris-HCl, pH 9, 200 mM NaCl, 15% glycerol, 1 mM $MgCl_2$, and 1 mM BOG) (Table 4-6D). However, no crystals were produced. Therefore, PchG was recloned to add an N-terminal signal sequence for periplasmic delivery for easier purification of the non-histidine tagged protein.

ss-PchG

The *pchG* gene was cloned from *P. aeruginosa* genomic DNA and ligated into the pET26b vector for periplasmic expression of the 42.4 kDa ss-PchG (Table 4-1).

However, over-production of the ss-PchG protein in LB or Terrific broth with a range of temperatures and induction concentrations had limited success (Table 4-3). The condition that yielded the best over-production was growth in Terrific broth at 37 ^{o}C for 12 hours after 1 mM IPTG induction. However, a large-scale preparation with purification by anion exchange did not yield any ss-PchG. Therefore, PchG was re-cloned again to create a fusion protein with inducible self-cleaving activity.

PchG-Intein

The Impact (Intein Mediated Purification with an Affinity Chitin-binding Tag) System (New England Biolabs) fuses the protein of interest to a protein containing self-cleaving activity. The fusion protein is purified on a chitin affinity column followed by subsequent auto-cleavage and purification of the two halves of the fusion protein. Because PchG has shown low solubility and problems with purity when in the native form without an affinity tag, the Impact system was a good option. The *pchG* gene was amplified from *P. aeruginosa* genomic DNA and ligation into the pTYB1 plasmid was attempted (Table 4-1). However, one of the restriction enzymes used for digestion (SapI) was not effective at cleaving the DNA. Therefore, the PCR primer was redesigned with a XhoI site. This new restriction site did improve cleavage of the DNA but no *pchG-Intein* plasmid was created. After the many attempts to produce sufficient quantity of PchG with the necessary quality required for structural biology experiments, we decided to work on a functional homologue from a different species. Therefore, the production of the homologue Irp3, an NADPH-dependent reductase, in *Y. enterocolitica*, was next undertaken.

Irp3

The *irp3* gene was amplified from *Y. enterocolitica* genomic DNA and ligated into the pET29b vector to yield Irp3 with a C-terminal His_6 tag (Table 4-1). Over-production of Irp3 was similar to PchG and yielded a 41.8 kDa protein (Table 4-2). Irp3 was purified in two steps with nickel affinity and gel filtration chromatography yielding 24 mg of Irp3 per liter of culture (Table 4-4C). Irp3 eluted from the gel filtration column primarily as a ~70 kDa protein suggesting Irp3 exists as a dimer. The protein was concentrated to 19 mg/ml.

Variation of the buffering components yielded monodispersed Irp3 in 25 mM Tris-HCl, pH 8, 200 mM NaCl, and 2 mM DTT (Table 4-5G). Therefore, crystallization experiments were conducted in this buffer.

Initial crystallization trials yielded nicely formed, single crystals in several conditions (Table 4-6D). Optimization of crystal growth was achieved by varying the crystallization conditions (Table 4-7). The conditions that provided diffraction quality crystals were: PEG 8K, 10K, or 20K and MES, pH 6.5; 14 – 37% (w/v) PEG 3350, pH 7.3 – 8.5, and 0.11 – 0.25 M of a variety of organic salts (magnesium formate, ammonium citrate, sodium tartrate, ammonium phosphate, and lithium sulfate) (Table 4-12 and Figure 4-5 A-H).

Table 4-12: Irp3 Optimal Crystallization Conditions

Precipitate	Salt	Buffer (0.1 M)
9 – 12% (w/v) PEG 8,000	None	MES, pH 6.5
7 – 10% (w/v) PEG 10,000	None	MES, pH 6.5
7 – 10% (w/v) PEG 20,000	None	MES, pH 6.5
14 – 15 % (w/v) PEG 3350	0.11 – 0.12 M magnesium formate	Tris-HCl, pH 8
30 – 33 % (w/v) PEG 3350	0.25 M ammonium citrate	HEPES, pH 7.3
32 – 35 % (w/v) PEG 3350	0.125 M sodium tartrate	Tris-HCl, pH 8.5
34 – 37 % (w/v) PEG 3350	0.125 M ammonium phosphate	HEPES, pH 7
28 – 31 % (w/v) PEG 3350	0.2 M lithium sulfate	HEPES, pH 7.5

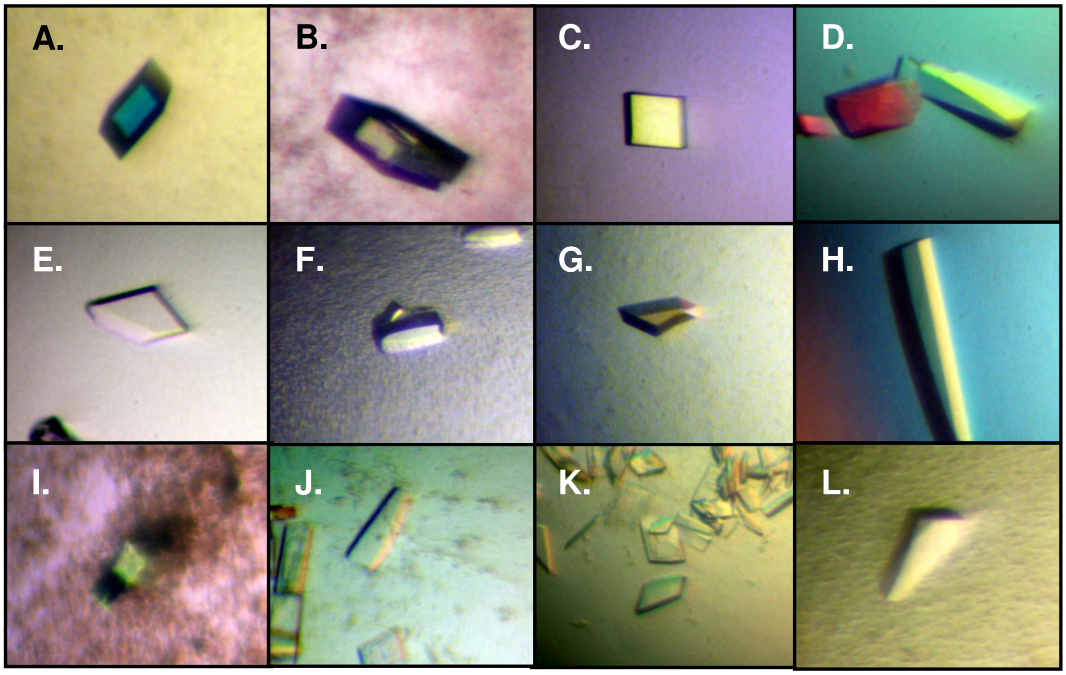

Figure 4-5: Irp3 protein crystals grown with (*A*) PEG 8000, (*B*) PEG 10,000, and (*C*) PEG 20,000 as the precipitant. Irp3 protein crystals grown with PEG 3350 and (*D*) magnesium formate, (*E*) ammonium citrate, (*F*) sodium tartrate, (*G*) ammonium phosphate, and (*H*) lithium sulfate as the precipitant. Irp3 Se-Met crystals grown in PEG 3350 with (*I*) magnesium formate, (*J, K*) ammonium citrate, and (*L*) sodium tartrate as the salt. Native diffraction data were collected on crystals grown in conditions identical to (*H*) while Irp3 Se-Met diffraction data was collected on crystals grown in conditions identical to

Crystals grown in high molecular weight PEG (PEG 8,000, PEG 10,000, or PEG 20,000) did not diffract well with the highest resolution at ~6 Å. However, Irp3 crystals grown in PEG 3350 with a variety of organic salts diffracted to ~2 – 2.5 Å. Therefore, x-ray diffraction data were collected on an Irp3 crystal grown with the salt lithium sulfate, which diffracted to 2.25 Å (Figure 4-6). The space group was P222 with unit lengths of a = 83.45 Å, b = 92.54 Å, and c = 180.24 Å (Table 4-9). This diffraction data set was used as the native data set for phasing.

Irp3 phasing was initially attempted using molecular replacement with three potential model proteins obtained from a Blast search; biliverdin reductase (Protein Data Bank accession number 1LC0, 20.5% identity), human neutrophil gelatinase-associated lipocalin (NGAL) (Protein Data Bank accession number 1L6M, 16.1 % identity), and an oxidoreductase from *Vibrio cholerae* (Protein Data Bank accession number 1XEA, 19.8 % identity). Biliverdin reductase is a heme protein (Irp3 is not a heme protein) and therefore, was eliminated as a model protein. MR was performed using AutoMolRep and Phaser programs with NGAL and the oxidoreductase as model proteins. No clear rotation or translation peaks were detected indicating that the two proteins are not good model proteins for Irp3. The two model proteins are not structural homologues of each other and are likely not structural homologues to Irp3.

Irp3 phasing using multi-wavelength anomalous dispersion (MAD) was attempted next. To use MAD for protein phasing, the crystal needs to incorporate a

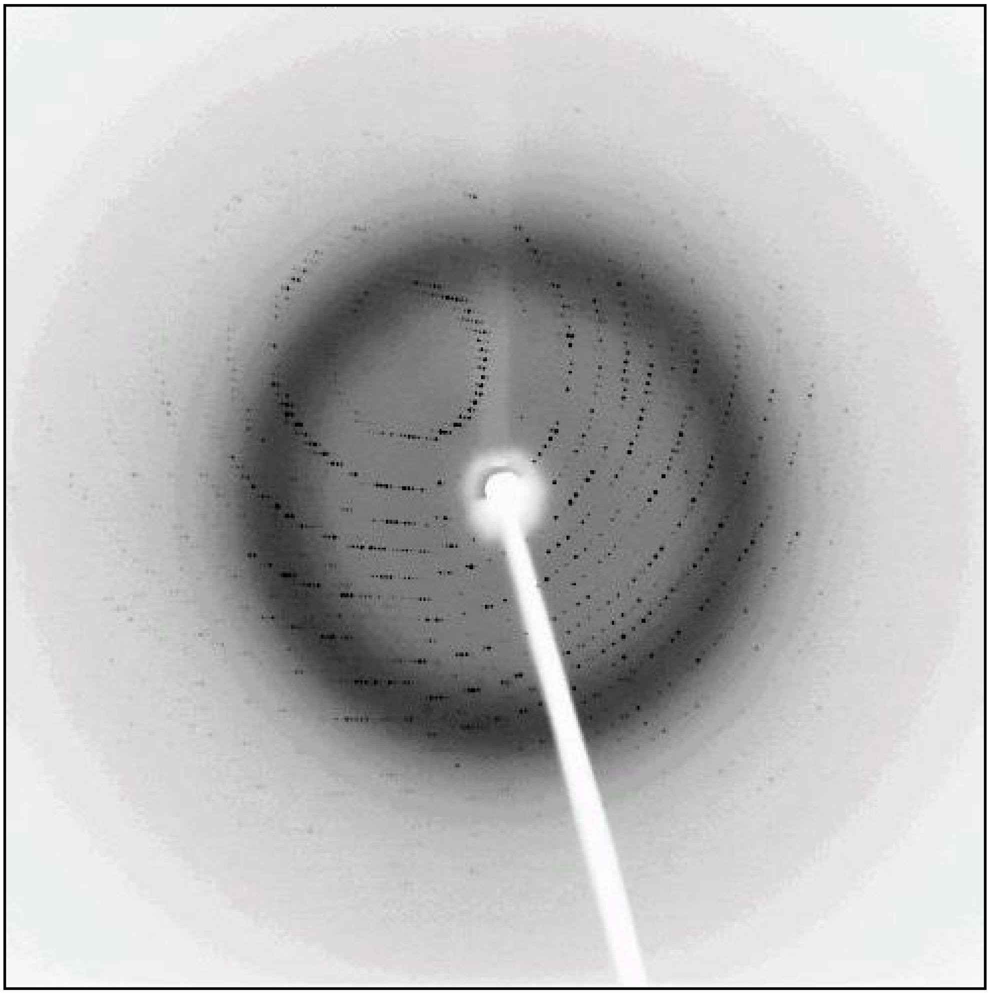

Figure 4-6: Irp3 crystal diffraction image. Irp3 crystals were grown with PEG 3350 and lithium sulfate as the precipitant and the image was collected at the Protein Structure Laboratory at the University of Kansas (www.psl.ku.edu) using an RaxisIV image plate detector mounted on a Rigaku RUH3R rotating anode. The native data was limited to > 2.25 Å during processing.

heavy metal with an anomalous signal. The most common way of performing MAD phasing is with protein that has incorporated a selenomethionine in the place of methionine. To do this, Irp3 protein was overproduced in minimal media containing selenomethionine and no methionine to produce Irp3 Se-Met (Table 4-2). Irp3 Se-Met was purified in a manner similar to that for native Irp3 with the addition of βME to all of the purification buffers (Table 4-4C). Irp3 Se-Met protein was sent to the Mass Spectrometry Lab for mass spectrometry analysis. The results showed a 180 – 348 Da difference between the native Irp3 and Irp3 Se-Met depending on the batch of Se-Met Irp3 overproduced. This difference indicates 4 – 7 selenium atoms were incorporated into the protein. Irp3 contains 5-6 methionine residues depending on whether the initial methionine is included in the protein. Irp3 Se-Met protein crystallized under similar conditions as the native Irp3 (Figure 4-5 I-L) and the crystals were sent to the Center for Advanced Microstructures and Devices (CAMD) synchrotron at Louisiana State University for data collection. Irp3 Se-Met crystals belong to the space group P222. However, the a unit cell length was 41.246 Å instead of the 83.45 Å seen in the native Irp3. Phases from the Irp3 Se-Met diffraction data could not be extracted because no anomalous signal was detected in the data. Therefore, phasing of Irp3 must be done with MIR.

Irp3 crystals were soaked with heavy metals for MIR phasing studies. A wide variety of heavy metals were tested to determine if the crystal lattice of the Irp3 crystals changed making the crystals non-isomorphous and thus not suitable for MIR. All of the heavy metals listed in Table 4-10 did not crack or perturb the Irp3 crystals as viewed through the microscope. Diffraction data collected from soaked Irp3 crystals could not be processed and scaled. We hypothesize this is due to cryoprotectant soaking for preparing the crystals for data collection (Table 4-13). Co-crystallization of Irp3 protein with heavy metals before crystallization and diffraction collection resulted in similar problems. The cryoprotectant has now been optimized and heavy metal diffraction data will be collected.

Conclusions

Great strides have been made towards the structure determination of four siderophore biosynthetic enzymes (Table 4-14). PvdA has been purified and initial crystals have been formed. However, more work is needed to optimize the crystal conditions to produce diffraction quality crystals. PvdF protein without a histidine tag has been purified and forms plate crystals that are very close to diffraction quality. The synthesis of hydroxyornithine, the substrate for PvdF, may change the morphology of the crystals to three-dimensional crystals suitable for diffraction. Co-crystallization of PvdF with hydroxyornithine is the next step in crystallization experiments and will be undertaken after hydroxyornithine can be produced in sufficient quantities.

Kinetic analyses of PvdF will also be undertaken. However, the PvdF activity assay is a very complicated, coupled assay with PvdA. Detection of PvdF activity

Table 4-13: Irp3 heavy metal diffraction collection for MIR phasing

Heavy Metal Reagent	Metal	Method of incorporation	Resolution (Å)	R_{sym}* (5 - 100 Å)	Problem
Platinum Potassium Iodide	Platinum	soak	3	0.146	R_{sym} was too high
PCMB, sodium salt	Mercury	co-crystallization	3.2	0.178	R_{sym} was too high
Potassium Hexchloroosmate (IV)	Osmium	soak	2.9	0.6	R_{sym} was too high
Potassium Hexanitroiridium (III)	Iridium	soak	3.5	n.a.	problems with cryostream
Dysprosium (III) Chloride hexahydrate	Dysprosium	soak	3 - 4	n.a.	problems with cryostream
potassium iodide	Iodide	soaked in cryoprotectant	3 - 4	0.6	R_{sym} was too high
PCMB, sodium salt	Mercury	co-crystallization	3	0.15 - 0.2	R_{sym} was still high, problems with the cryostream
potassium iodide	Iodide	soaked in cryo	3	0.17 - 0.4	R_{sym} was high, problems with the cryostream

* = useable data has $R_{sym} < 0.10$.
PCMB = *p*-Chloromercuribenzoic Acid
n.a. = not applicable

Table 4-14: Current progress made on siderophore biosynthetic proteins

Protein	Clone name	Cloned	Overproduced	Purified	Buffer Optimized	Crystallized	Diffraction quality crystals	Data collection	Phasing	Structure	Kinetics
PvdA											
	His$_6$-PvdA	X	X	X	X	/					X
PvdF											
	PvdF-throm-His$_6$	X	X	X	X	X					
	PvdF-throm	X	X	X	X	X					
	PvdF	X	X	X	X	X	/				/
PchG											
	PchG-His$_6$	X	X	X							
	PchG	X	X								
	PchG-throm-His$_6$	X	X	X							
	PchG-throm	X	X	X							
	ss-PchG	X									
	PchG-Intein										
Irp3											
	Irp3-His$_6$	X	X	X	X	X	X	X	/		

X = completed

/ = in progress

involves the conversion of the formyl-hydroxyornthine, produced by PvdF, to hydroxyornithine with an acid hydrolysis step that requires autoclaving. The assay protocol is not conducive to in-depth kinetic analysis. Production of large quantities of the PvdF substrate, hydroxyornithine, would simplify the assay by not requiring PvdA. The assay could be further simplified by monitoring the decrease in the amount of substrate, thus making acid hydrolysis unnecessary. However, the synthesis of hydroxyornithine, while still underway, is proving more difficult than anticipated.

PchG involved in pyochelin biosynthesis in *P. aeruginosa* was not obtained with sufficient purity and/or at a concentration high enough for protein crystallization in any of the clones. Therefore, we switched to the homologue, Irp3, in *Y. enterocolitica*. Irp3 was purified and crystallized very easily. A full, native x-ray diffraction data set has been collected and phasing experiments are underway. Heavy metal soaks for multiple isomorphous replacement (MIR) and single isomorphous replacement with anomalous scattering (SIRAS) are planned.

The three-dimensional structures of enzymes involved in the biosynthesis of siderophores are important for the rational design of inhibitors. The work provided in this chapter is a first step towards structure determination and ultimately the design of novel antibiotics targeting this very important pathway.

References

(1) Jancarik, J., and Kim, S.-H. (1991) Sparse matrix sampling: a screening method for crystallization of proteins. *J Appl. Cryst. 24*, 409-411.

(2) McPherson, A. (1999) *Crystallization of Biological Macromolecules*, Cold Spring Harbor Laboratory Press, Cold Spring Harbor.

(3) Carter, C. W. J. (1997) Response Surface Methods for Optimizing and Improving Reproducibility of Crystal Growth. *Methods Enzymol 276*, 74-99.

(4) Bergfors, T. (2003) Seeds to crystals. *J Struct Biol 142*, 66-76.

(5) Glusker, J. P., Lewis, M., and Rossi, M. (1994) *Crystal Structure Analysis for Chemists and Biologists*, Wiley-VCH, Inc., New York.

(6) Rhodes, G. (1993) *Crystallography Made Crystal Clear*, Second ed., Academic Press, San Diego.

(7) Petsko, G. A. (1985) Preparation of isomorphous heavy-atom derivatives. *Methods Enzymol 114*, 147-56.

(8) Visca, P., Serino, L., and Orsi, N. (1992) Isolation and characterization of *Pseudomonas aeruginosa* mutants blocked in the synthesis of pyoverdin. *J Bacteriol 174*, 5727-31.

(9) Visca, P., Ciervo, A., and Orsi, N. (1994) Cloning and nucleotide sequence of the *pvdA* gene encoding the pyoverdin biosynthetic enzyme L-ornithine N5-oxygenase in *Pseudomonas aeruginosa*. *J Bacteriol 176*, 1128-40.

(10) McMorran, B. J., Kumara, H. M., Sullivan, K., and Lamont, I. L. (2001) Involvement of a transformylase enzyme in siderophore synthesis in *Pseudomonas aeruginosa*. *Microbiology 147*, 1517-24.

(11) Reimmann, C., Patel, H. M., Serino, L., Barone, M., Walsh, C. T., and Haas, D. (2001) Essential PchG-dependent reduction in pyochelin biosynthesis of *Pseudomonas aeruginosa*. *J Bacteriol 183*, 813-20.

(12) Patel, H. M., and Walsh, C. T. (2001) In vitro reconstitution of the *Pseudomonas aeruginosa* nonribosomal peptide synthesis of pyochelin: characterization of backbone tailoring thiazoline reductase and N-methyltransferase activities. *Biochemistry 40*, 9023-31.

(13) Geoffroy, V. A., Fetherston, J. D., and Perry, R. D. (2000) *Yersinia pestis* YbtU and YbtT are involved in synthesis of the siderophore yersiniabactin but have different effects on regulation. *Infect Immun 68*, 4452-61.

(14) Fischbach, M. A., and Walsh, C. T. (2006) Assembly-line enzymology for polyketide and nonribosomal Peptide antibiotics: logic, machinery, and mechanisms. *Chem Rev 106*, 3468-96.

(15) Izaac, A., Schall, C. A., and Mueser, T. C. (2006) Assessment of a preliminary solubility screen to improve crystallization trials: uncoupling crystal condition searches. *Acta Crystallogr D Biol Crystallogr 62*, 833-42.

(16) Otwinowski, Z., and Minor, W. (1997) Processing of X-ray diffraction data collected in oscillation mode. *Methods Enzymol 276*, 307-326.

(17) (1994) The CCP4 suite: programs for protein crystallography. *Acta Crystallogr D Biol Crystallogr 50*, 760-3.

(18) McCoy, A. J., Grosse-Kunstleve, R. W., Storoni, L. C., and Read, R. J. (2005) Likelihood-enhanced fast translation functions. *Acta Crystallogr D Biol Crystallogr 61*, 458-64.

(19) Dauter, Z., Dauter, M., and Rajashankar, K. R. (2000) Novel approach to phasing proteins: derivatization by short cryo-soaking with halides. *Acta Crystallogr D Biol Crystallogr 56*, 232-7.

(20) Fields, J. D., and Kropp, P. J. (2000) Surface-mediated reactions. 9. Selective oxidation of primary and secondary amines to hydroxylamines. *J Org Chem 65*, 5937-41.

Chapter 5

Conclusion

Pathogenic bacteria require iron uptake systems for infection and colonization of the host organism. One of the most effective iron acquisition systems is the production of siderophores. Therefore, inhibition of the production, secretion, or import of siderophores is an attractive antimicrobial target for rational drug design. Several inhibitors of siderophore biosynthesis targets have been described including enzymes for the production of salicylate and dihyroxybenzoate, required for aryl-capped siderophores such as pyochelin and yersiniabactin, and enzymes containing aryl adenylation domains (*1-6*). However, many siderophores do not use salicylate and dihydroxybenzoate and thus are not inhibited by these compounds. The work described in this study is concerned with enzymes involved in pyoverdin and pyochelin production in *Pseudomonas aeruginosa* and Yersiniabactin production in *Yersinia enterocolitica*. However, the work does not relate to the production or adenylation of aryl compounds making these enzymes attractive targets for new antimicrobials.

Pyoverdin contains two derivitized ornithine groups that are required for effective chelation of the iron. The ornithine amino acid is derivitized by two enzymes, PvdA and PvdF. A detailed biochemical characterization of PvdA has led to insight into a new reaction mechanism for flavoproteins. The hydroxylated product formation assay has been miniaturized for use with 96 well plates and will be ideal for high throughput screening of potential inhibitors. For the rational design of new inhibitors, the structure of PvdA is needed. Crystallization studies are underway to determine the high-resolution structure of the enzyme for the rational design of inhibitors but no diffraction quality crystals have yet been obtained. However, using some initial bioinformatics data, some structural inferences can be made for PvdA.

Several putative functional homologues of PvdA have been identified, but only three have been characterized in detail and two homologues have had their structure determined (Figure 5-1). IucD, a lysine hydroxylase from *E. coli*, has 28% sequence identity (47% similarity) to PvdA, *p*-hydroxybenzoate hydroxylase (PHBH) from *P. fluorescens* has 21% sequence identity (34% similarity), and flavin-containing monooxygenase (FMO) has 19% sequence identity (37% similarity) to PvdA as aligned with the ALIGN algorithm (Genestream Search; CRBM Montepellier, France). The sequence similarities are scattered throughout the proteins and are not concentrated to areas of ligand binding. The sequence similarity of PHBH to FMO is 38% and the x-ray crystal structures of the two enzymes (Protein Data Bank accession numbers 1PBE and 1VQW respectively) differ such that multiple sequence alignments with PvdA are not informative. Therefore, a multiple sequence alignment of PvdA and IucD with PHBH, which shares the greatest biochemical characteristics to PvdA, was generated by ClustalW (7).

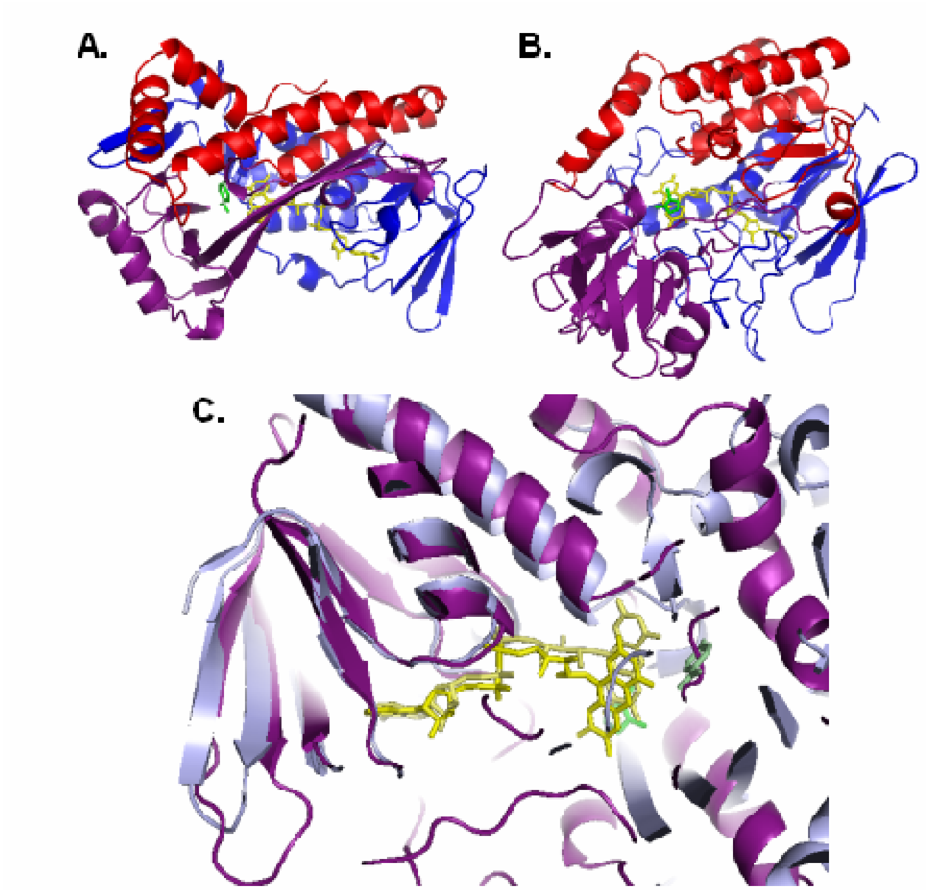

Figure 5-1: Proteins containing sequence homology to PvdA, (*A*) *p*-hydroxybenzoate hydroxylase (PHBH) from *Pseudomonas fluorescens* (PDB number 1PBE) and (*B*) flavin monooxygenase (FMO) from *Schizosaccharomyces pombe* (PDB number 1VQW). The domains are colored according to the PHBH structure with the N-terminal FAD binding domain (residues 1 – 174) in blue, the central substrate-binding domain (residues 175 – 295) in purple, and the C-terminal oligomerization domain (residues 296 – 394) in red with the corresponding domains in FMO labeled similarly. FAD in each structure is yellow with the substrates as green. An active site overlay of PHBH and FMO (*C*) shows the similarity between the two structures. The major divergence in the proteins is the position of the substrate and the surrounding loops. PHBH is labeled with light blue with a light yellow FAD molecule and the substrate, *p*-hydroxybenzoate, in light green. FMO is dark purple with FAD in dark yellow and the substrate, 1-methyl-1,3-dihydro-2h-imidazole-2-thione (methimazole), in dark green.

A significant decrease in the apparent sequence identity was observed compared to the pair-wise method calculated by Genestream. Therefore, starting with a multiple sequence alignment produced with the ALIGN algorithm, the previously determined substrate and cofactor binding information for PHBH and the hypothetical binding motifs for IucD, we further optimized the alignment by hand. This information included six binding motifs. The first binding motif was the flavin-binding motif, GXGXXG at the N-terminus of PHBH (*8*). The second motif incorporated was the flavin-binding motif at the N-terminus of IucD. This motif was initially hypothesized with the last conserved glycine as a proline (GXGXX**P**) (*9*), but was later modified to shift two amino acids toward the C-terminus to become GXGXX**N** (res. 11 – 16) (*10*). Third, in PHBH, the amino acids involved in NADPH binding have been defined by mutagenesis experiments (Arg33, Tyr38, Arg42, Arg44, Phe161, His162, Arg166, and Arg269) and are incorporated into the sequence alignment (*11-16*). A generic hydroxylase NADPH binding motif called the DG motif (residues 159-166) has been suggested (*15, 17*), and a model of interdomain NADPH binding has been developed (*13*). The fourth incorporated motif was a nucleotide-binding motif (GXGXXG) hypothesized for NADPH in IucD (residues 188 – 193) (*18*). The fifth binding motif incorporated into the sequence alignment was the amino acids involved in substrate-binding from the structure of PHBH (*19*). Finally, the sixth motif incorporated was the substrate-binding motif hypothesized for IucD (DXXXFATGYXXXXP, residues 224 – 237) (*18*). We reasoned these binding motifs would be areas of high conservation. This new alignment returned the sequence similarity to percentages similar to the Genestream calculation for the pair-wise alignments (26% identity, 46% similarity for PvdA/IucD and 18% identity, 34% similarity for PvdA/PHBH) (Figure 5-2).

An inspection of the alignment for PvdA shows the FAD binding motif at the N-terminus, with the GXGXXG of PHBH aligned with the GXGXXN in IucD and PvdA (Figure 5-2). This sequence (residues 17 – 22 in PvdA) corresponds to the N-terminus of an α-helix in the Rossman fold of PHBH as would be canonically expected for FAD binding, and is indeed involved in FAD binding in PHBH (*19*). The putative NADPH binding motif for IucD and PvdA, GXGXXA (PvdA residues 215-219) aligns with a modified sequence in PHBH, PXGXXG. While this alignment is initially promising, this putative binding motif is part of a β-strand in the predominantly β-conformation substrate-binding domain of PHBH, and is only solvent exposed at the extreme N-terminus (Pro182). No structures of PHBH have been determined with NADPH bound, but an interdomain model for binding has been proposed (*13*) based on extensive mutagenesis experiments (*11-17*). These amino acids are on the exterior of the protein, and NADPH binding in this region would be in close proximity to FAD for electron transfer. In this new alignment, many of these amino acids are conserved, indicating that a similar external interdomain binding is a more likely binding mode for NADPH in PvdA (and IucD). Finally, a substrate-binding motif (DXXXFATGYXXXXP, residues 224 – 237) for IucD with a

```
     |→ FAD binding
PvdA   MTQATATAVVHDLIGVGFGPSNIALAIALQERAQAQGALEVLFLDKQ-GDYRWHGNTLVSQ-SEL  63
IucD         MKKSVDFIGVGTGPFNLSIA-ALSHQIE---ELDCLFFDEHPHFSWHPGM-LVPD-CHM  53
PHBH           MKTQVAIIGAGPSGLLLGQLLHKAGI-----DNVILERQTPDYVL-GR--I-RAGVL  48
                   eeee  hhhhhhhhhhhhhhhh      eeeee  hhhhhhhhh       ee

PvdA   QISFLKDLVSLRNPTSPYSFVNYLHKHDRLVDFINLGTFYPCRMEFNDYLRWVASHFQEQSRYGE 128
IucD   QTVFLKDLVSAVAPTNPYSFVNYLVKHKKFYRFLTSRLRTVSREEFSDYLRWAAEDMNNL-YFSH 117
PHBH   E-QGMVDLLREAG-------VDRRMARDGLVHE-------GVEIAFAGQRRRIDLKRLSGGKT-V  97
       e hhhhhhhhhhh         hhhhhhheee        eeeeee  eeeeeehhhh      e

PvdA   EVLRIEPMLSAGQVEALRVISRNADGE--ELVRTT------RALVVSPGGTPRIPQVFRALKG-D 184
IucD   TV---ENID-FDKKRRLFLVQ-TSQGQ--YFARNI------CLGTGKQ---PYLPPCVKHMTQ-S 165
PHBH   TVY-GQTEVTRDLMEAREASGATTVYQAAEVRLHDLQGERPYVTFERDGERLRLDCDYIA--GCD 159
       ee   hhhhhhhhhhhhhhhh eeeee  eeeeee      eeeeeeeeeeeee  eeee

                 FAD binding ←|→ substrate binding
PvdA   GRVFHH-S-QYLEHMAKQPCSSGKPMKIAIIGGGQSAAEAFID-LNDSY-PSVQADMILRASALK 245
IucD   C--FHA-S-E---SNLRRPDLSG--LRITVVGGGQSGADLFLNALRGEWGEAAEINWVSRRNNFN 221
PHBH   G--FHGISRQSIP-AERL------KVFERVYPFGWLGLLAD------TP-P-V--------S--H 197
                               eeeeeeeeeeeeeeeee

PvdA   PADDSPFVNEVFAP-KFTDLIYSREHAERERLLREYHNTN----YS--VVDTDLIERIYG-VFYR 302
IucD   ALDEAAFADDYFTP-EYISGFSGLEEDIRHQLLDEQKMTS----DG--ITADSLLTIYRE-LYHR 278
PHBH   ---ELIYAN---HPRGF--ALCSQRSATRSRYYVQVPLTEKVEDWSDERFWTELKARLPAEVAEK 254
            eeee          eeeeeeee eeeeeeee          hhhhhhhhhhh  hhhhhh

                                      substrate binding ←|→ oligomerization
PvdA   QKV----S-GIPRHAFRCMTTVERATATAQ-GIELALRDA-GSGELSVETYDAVILATGYERQLH 360
IucD   FEVLRKPR-NIRLLPSRSVTTLES---SGP-GWKLLMEHHLDQGRESLES-DVVIFATGYRSALP 337
PHBH   L-VTG-PSLEKSIAPLRSFVVEPMQHGR----LFLAG-DA-AHIVPPTGA-KGLNLAASDVSTLY 310
       h       eeeeeeeeeeeeeee         eeee      eeee      hhhhhhhhhhhhh

PvdA   RQLLEPLAEYLGDHE-----IGRDYRLQTDER-CKVAIYAQGFSQASHGLSD-TLLSVLPVRAEE 418
IucD   -QILPSLMPLITMHDKNTFKVRDDFTLEWSGP-KENNIFVVNASMQTHGIAEPQLSLMAWRSARI 400
PHBH   RLLLKAYRE--GRGE-----LLEYRSAICLRRIWKAERFSWWMTSVLHRFPD-TD--AFSQRIQQ 365
       hhhhhhhhh               hhhhhhhhhhhhhhhhhhhhhhhh         hhhhhhhh

PvdA   ISGSLYQHLKPGTAARALHEHALAS      443
IucD   LNRVMGRDLFDLSMPPALIQWRSGT      425
PHBH   TELEYYLGSEAGLATIAENYVGLPYEEIE  394
       hhhhhhhhhhhhhhhhhhhhhh
```

Figure 5-2: Structure and binding motif based sequence alignment of PvdA with IucD (*E. coli*) and PHBH (*P. fluorescens*, PDB accession code: 1PBE). The domain structure of PHBH is noted above the sequence. The secondary structure elements of PHBH are indicated below the sequence: β-strand (e) or α-helix (h). The coenzyme and substrate binding motifs are labeled: FAD (highlighted in cyan, PHBH and IucD), canonical NADPH (highlighted in grey, IucD), and substrate (highlighted in red, IucD). Amino acids in PHBH involved in NADPH binding as determined by mutational analysis are highlighted in pink. The bold lettering highlighted in pink represents the DG sequence of the hydroxylase NADPH binding motif. Amino acids involved in substrate binding in the PHBH structure are highlighted in green. The cysteines implicated in PCMB inhibition are highlighted in yellow.

corresponding sequence in PvdA (DXXXLATGYXXXXH) has been hypothesized (*18*). This sequence has little correlation in PHBH with the hand-generated alignment (KXXXLAASDXXXXY) and is part of a long α-helix. Nevertheless, the loop just N-terminal to this helix in involved in substrate binding in PHBH (*19*).

PHBH has a cysteine near the putative NADPH binding site (Cys158) and spectral studies performed on IucD with FAD analogs indicate a cysteine in the FAD binding cavity which should be proximal to the NADPH binding site (*20*). This cysteine residue may be involved in the inhibition observed with mercurial compounds. With our alignment, both PvdA and IucD have cysteine residues that are near in sequence to Cys158 in PHBH and could be involved in mercury binding in an analogous manner. The IucD cysteine (Cys160) resides in a very similar position as the cysteine in PHBH, which could explain the similarities in inhibition by mercurial compounds and restoration by reducing agents. However, in PvdA, cysteine 202 is more distant from the proposed coenzyme binding sites but is still in a putative loop region involved in NADPH binding (Figure 5-2). This loop may be more solvent exposed, which could explain the strong inhibition seen upon addition of high concentrations of *p*-chloromercuribenzoate.

Based on this evidence, we predict PvdA and IucD will be distant structural homologues of PHBH, with an N-terminal Rossmann fold FAD binding domain, a central substrate-binding domain comprised of β-strands, and a C-terminal oligomerization domain. We propose that NADPH binding will be akin to the interdomain binding model proposed for PHBH, in contrast to the previously proposed GXGXX(G/A) motif in the substrate binding domain of PvdA and IucD. The substrate-binding site is predicted to reside in a cleft between the FAD and substrate binding domains, N-terminal to the previously hypothesized consensus motif for PvdA and IucD. However, the differences noted for the catalytic cycle argue for structural changes between PvdA and PHBH that may be more structurally characteristic of FMO.

The second enzyme involved in ornithine derivatization, PvdF shows sequence similarity to glycinamide ribonucleotide transformylase (GART) enzymes involved in the synthesis of purine residues (*21*). The GART protein from *Escherichia coli* shares 57% identity and 72% similarity to PvdF and an alignment between the two protein shows conservation of the three residues important in catalytic activity as well as the hydrophobic pocket important in cofactor binding (*21*). The structure of the *E. coli* GART protein has been solved (PDB accession number 1CDE) and contains a central core with a seven-stranded β-sheet surrounded by α-helices (Figure 5-3) (*22*). Protein crystals of PvdF are close to diffraction quality and the structure of PvdF is hypothesized to be very similar to the *E. coli* GART protein. Generation of the substrate for PvdF, hydroxyornithine, will be an essential next step for determining the biochemical characteristics of PvdF, crystal optimization for structure determination, and for the design of a high throughput assay for inhibitor screening.

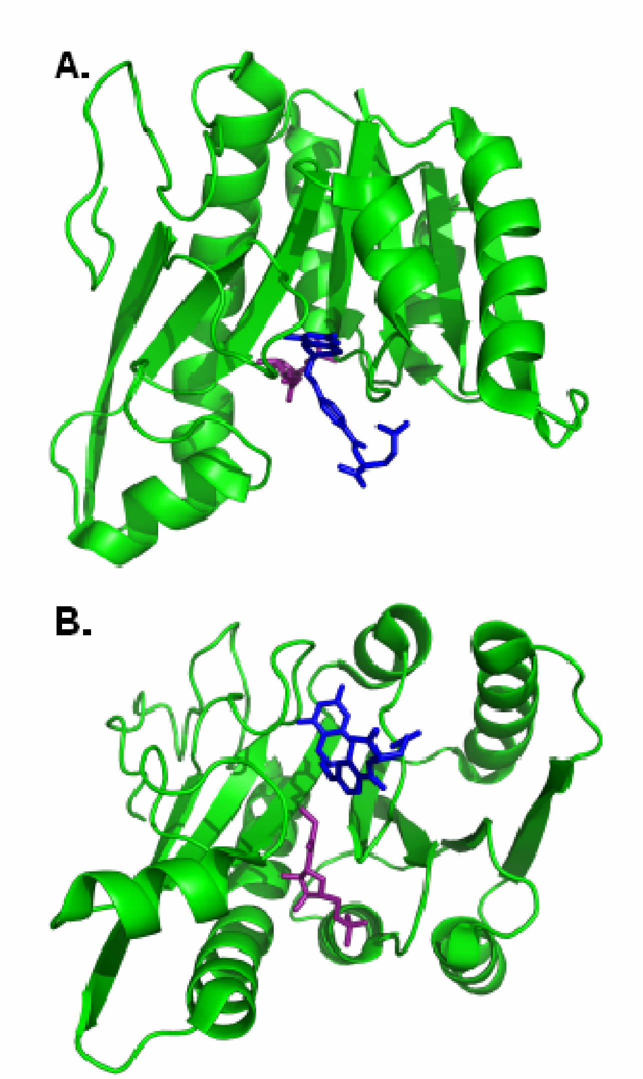

Figure 5-3: The structure of the PvdF homologue glycinamide ribonucleotide transformylase (GART) from *Escherichia coli* (PDB number 1CDE). (*A*) The *E. coli* GART protein shares 57% identity and 72% similarity to PvdF and consists of one domain (green) and is shown with the substrate, glycinamide ribonucleotide, in purple and an inhibitor, 5-deaza-5,6,7,8-tetrahydrofolate, in blue. (*B*) The *E. coli* GART protein rotated 90° around the x-axis.

A second siderophore in *P. aeruginosa*, pyochelin, is an aryl-capped siderophore. Inhibitors have been designed to the aryl adenylation domain, PchD, and the enzymes that convert chorismate into salicylate, PchA and PchB (*2-6*). However, work in this thesis has focused on PchG, an NADPH reductase required for the final steps in pyochelin production. No structures have been determined for functional homologues of PchG. The proteins with the most sequence similarity to PchG for which the structures have been determined have very low sequence similarity to PchG (< 45% similarity). These homologues are not structurally or functionally related to each other (or to PchG) and are most likely not structurally related to PchG either making none of them a good model for PchG. Solubility issues with a variety of different clones have complicated the determination of the PchG structure. Therefore, a functional homologue in *Yersinia enterocolitica*, Irp3, was pursued for structure determination. Diffraction data for the native Irp3 crystals has been collected and solving the phase problem is the last step for structure determination. An enzymatic assay for the NADPH reductase activity has not been optimized due to the complex, protein-bound substrate, which is attached to the previous protein in the pathway, PchF, thus making high throughput screening impossible. Therefore, designing new microbials to these targets might be more successful if based on the structure. However, an *in vitro* siderophore reconstitution assay using all of the biosynthetic enzymes in the pathway, the substrates, and cofactors has been optimized (*23*). Therefore, new inhibitors can be tested for effectiveness in blocking the siderophore pathway.

Because *P. aeruginosa* produces two unrelated siderophores, pyochelin and pyoverdin, an effective antimicrobial must inhibit both siderophore systems. The work described in this thesis has biochemically characterized the first step in ornithine derivitization and devised a high-throughput assay for determining new lead compounds for inhibition. This body of work has also described the reaction mechanism of this first step in ornithine modification to provide a broader understanding of how flavoproteins catalytically function. Until now, only two hydroxylase enzymes had been mechanistically understood, PHBH and FMO. PvdA has been described as having a third reaction mechanism and adds to our knowledge of how enzymes function. This thesis has also shown preliminary crystallization and structure determination of four enzymes involved in the synthesis of three siderophores. These enzymes have high sequence homology to enzymes in similar siderophore synthetic pathways. Therefore, the structures obtained from any of the four enzymes will aid in the understanding of siderophore biosynthesis and in the development of antimicrobials with a wide range of applications. Taken together, the work discussed in this thesis is a first step toward rationally designing new inhibitors to generate a cocktail antimicrobial for use in preventing *Pseudomonas* and other pathogenic bacterial infections.

References

(1) Miethke, M., and Marahiel, M. A. (2007) Siderophore-Based Iron Acquisition and Pathogen Control. *Microbiol Mol Biol Rev 71*, 413-451.

(2) Ferreras, J. A., Ryu, J. S., Di Lello, F., Tan, D. S., and Quadri, L. E. (2005) Small-molecule inhibition of siderophore biosynthesis in *Mycobacterium tuberculosis* and *Yersinia pestis*. *Nat Chem Biol 1*, 29-32.

(3) Bartlett, P. A., Nakamura, S., Johnson, C. R., Reich, S. H., and Luis, A. (1988) Chorismate Mutase Inhibitors: Synthesis and Evaluation of Some Potential Transition-State Analogs. *Journal of Organic Chemistry 53*, 3195-3210.

(4) Kozlowski, M. C., Tom, N. J., Seto, C. T., Sefler, A. M., and Bartlett, P. A. (1995) Chorismate-Utilizing Enzymes Isochorismate Synthase, Anthranilate Synthase, and *p*-Aminobenzoate Synthase: Mechanistic Insight through Inhibitor Design. *J Am Chem Soc 117*, 2128-2140.

(5) Payne, R. J., Kerbarh, O., Miguel, R. N., Abell, A. D., and Abell, C. (2005) Inhibition studies on salicylate synthase. *Org Biomol Chem 3*, 1825-7.

(6) Gaille, C., Kast, P., and Haas, D. (2002) Salicylate biosynthesis in *Pseudomonas aeruginosa*. Purification and characterization of PchB, a novel bifunctional enzyme displaying isochorismate pyruvate-lyase and chorismate mutase activities. *J Biol Chem 277*, 21768-75.

(7) Higgins, D., Thompson, J., and Gibson, T. (1994) CLUSTAL W: improving the sensitivity of progressive multiple sequence alignment through sequence weighting, position-specific gap penalties and weight matrix choice. *Nucleic Acids Res. 22*, 4673-4680.

(8) Hosokawa, K., and Stanier, R. Y. (1966) Crystallization and Properties of *p*-Hydroxybenzoate Hydroxylase from *Pseudomonas putida*. *Journal of Biological Chemistry 241*, 2453-2460.

(9) Thariath, A., Socha, D., Valvano, M. A., and Viswanatha, T. (1993) Construction and biochemical characterization of recombinant cytoplasmic forms of the IucD protein (lysine:N6-hydroxylase) encoded by the *pColV-K30* aerobactin gene cluster. *J Bacteriol 175*, 589-96.

(10) Stehr, M., Smau, L., Singh, M., Seth, O., Macheroux, P., Ghisla, S., and Diekmann, H. (1999) Studies with lysine N6-hydroxylase. Effect of a mutation in the assumed FAD binding site on coenzyme affinities and on lysine hydroxylating activity. *Biol Chem 380*, 47-54.

(11) Van Berkel, W. J., Muller, F., Jekel, P. A., Weijer, W. J., Schreuder, H. A., and Wierenga, R. K. (1988) Chemical modification of tyrosine-38 in *p*-hydroxybenzoate hydroxylase from *Pseudomonas fluorescens* by 5'-*p*-fluorosulfonylbenzoyladenosine: a probe for the elucidation of the NADPH binding site? Involvement in catalysis, assignment in sequence and fitting to the tertiary structure. *Eur J Biochem 176*, 449-59.

(12) Eppink, M. H., Schreuder, H. A., and Van Berkel, W. J. (1995) Structure and function of mutant Arg44Lys of *p*-hydroxybenzoate hydroxylase implications for NADPH binding. *Eur J Biochem 231*, 157-65.

(13) Eppink, M. H., Schreuder, H. A., and van Berkel, W. J. (1998) Interdomain binding of NADPH in *p*-hydroxybenzoate hydroxylase as suggested by kinetic, crystallographic and modeling studies of histidine 162 and arginine 269 variants. *J Biol Chem 273*, 21031-9.

(14) Eppink, M. H., Schreuder, H. A., and van Berkel, W. J. (1998) Lys42 and Ser42 variants of *p*-hydroxybenzoate hydroxylase from *Pseudomonas fluorescens* reveal that Arg42 is essential for NADPH binding. *Eur J Biochem 253*, 194-201.

(15) Eppink, M. H., Bunthol, C., Schreuder, H. A., and van Berkel, W. J. (1999) Phe161 and Arg166 variants of *p*-hydroxybenzoate hydroxylase. Implications for NADPH recognition and structural stability. *FEBS Lett 443*, 251-5.

(16) Eppink, M. H., Overkamp, K. M., Schreuder, H. A., and Van Berkel, W. J. (1999) Switch of coenzyme specificity of *p*-hydroxybenzoate hydroxylase. *J Mol Biol 292*, 87-96.

(17) Eppink, M. H., Schreuder, H. A., and Van Berkel, W. J. (1997) Identification of a novel conserved sequence motif in flavoprotein hydroxylases with a putative dual function in FAD/NAD(P)H binding. *Protein Sci 6*, 2454-8.

(18) Stehr, M., Diekmann, H., Smau, L., Seth, O., Ghisla, S., Singh, M., and Macheroux, P. (1998) A hydrophobic sequence motif common to N-hydroxylating enzymes. *Trends Biochem Sci 23*, 56-7.

(19) Schreuder, H. A., van der Laan, J. M., Hol, W. G., and Drenth, J. (1988) Crystal structure of *p*-hydroxybenzoate hydroxylase complexed with its reaction product 3,4-dihydroxybenzoate. *J Mol Biol 199*, 637-48.

(20) Macheroux, P., Plattner, H. J., Romaguera, A., and Diekmann, H. (1993) FAD and substrate analogs as probes for lysine N6-hydroxylase from *Escherichia coli* EN 222. *Eur J Biochem 213*, 995-1002.

(21) McMorran, B. J., Kumara, H. M., Sullivan, K., and Lamont, I. L. (2001) Involvement of a transformylase enzyme in siderophore synthesis in *Pseudomonas aeruginosa*. *Microbiology 147*, 1517-24.

(22) Almassy, R. J., Janson, C. A., Kan, C. C., and Hostomska, Z. (1992) Structures of apo and complexed *Escherichia coli* glycinamide ribonucleotide transformylase. *Proc Natl Acad Sci U S A 89*, 6114-8.

(23) Patel, H. M., and Walsh, C. T. (2001) In vitro reconstitution of the *Pseudomonas aeruginosa* nonribosomal peptide synthesis of pyochelin: characterization of backbone tailoring thiazoline reductase and N-methyltransferase activities. *Biochemistry 40*, 9023-31.